Channel Emulation for active characterization of MIMO communication systems

Nabil Arsalane

UNIVERSITE DE LIMOGES

ED n°521 Sciences et Ingénierie pour l'Information, Mathématiques

FACULTE DES SCIENCES ET TECHNIQUES

XLIM- Département Ondes et Systèmes Associés

Année : 2014 **Thèse N° [-----]**

Thèse

pour obtenir le grade de

DOCTEUR DE L'UNIVERSITÉ DE LIMOGES

Discipline : "Electronique des Hautes Fréquences, Optoélectronique"

Spécialité : "Télécommunications"

présentée et soutenue le 16/12/2014 par

Nabil ARSALANE

Channel Emulation for active characterization of MIMO communication systems

Thèse dirigée par Mr. Thierry MONEDIERE

JURY :

Rapporteurs

M. SANCHEZ-HERNANDEZ David	Professeur	Université polytechnique de Cartagena
M. PALADE Tudor	Professeur	Université technique de Cluj Napoca

Examinateurs

Mme. LIEBUS Stéphanie	Ingénieur	ANOV
M. CARSENAT David	Enseignant chercheur	3IL
M .DECROZE Cyril	Maitre de conférences (HDR)	Université de LIMOGES
M. MONEDIERE Thierry	Professeur	Université de LIMOGES.

Invité

M. MOUHAMADOU Moctar	Enseignant chercheur	3IL

This thesis was carried out in the XLIM laboratory of Limoges, OSA department (Waves and Associated Systems).

I would like to thank Mr. Thierry Monediere, Professor at the University of Limoges, for welcoming me in his team and providing the framework of my work. Many Thanks and Appreciations.

My sincere thanks to Mr. Carsenat David, Associate Professor, for supervising this thesis. His enthusiasm and support have contributed greatly in my research. I am pleased to have the opportunity to work with him in the last years.

I express my deep gratitude to Mr. Cyril Decroze, Associate Professor, for supervising this thesis and for participating to this Jury. His knowledge and advices were invaluable to the completion of this work. At the same time I also appreciate the confidence and the autonomy that he granted me, much appreciated.

I would like to thank the former member, Moctar Mouhamadou for their precious advices.

I sincerely thank Mr. David A. Sánchez-Hernández, Professor at the polytechnic University of Cartagena, and Mr. Tudor PALADE, Professor at the technical University of Cluj, for accepting to be part of the Jury and to perform the reporters' task.

I would like also to thank Mme. Stéphanie LIEBUS, Engineer at ANOVO Brive for doing me the honor in being part of this Jury.

A big thanks to M. Patricia Leroy, Secretary of the OSA department for her hard work and availability.

Finally I would like to thank my fellow OSA colleagues. They are too numerous to count. However I can mention M. A. Garcia Fernandez and I. Versman for sharing the office with me. Eric, Hassan, Aymen, Faycel, Thomas, Jamil, and Hussein for the good atmosphere.

General Introduction

In the space of twenty years, the use of mobile communication services has grown remarkably. This is illustrated in the evolution of the number of mobile subscribers in relation to the world's population: we count at the end of 2014 nearly 6 billion subscribers worldwide that represents 87% of the world population.

Originally designed to provide mobile phone service only, the mobile radio communications technologies have evolved considerably and allows providing a high speed connection in mobility. Mobile networks complete the residential access networks such as x-DSL (x Digital Subscriber Line) and FTTH (Fibre to the Home) for broadband internet access. Users of mobile devices can browse the web, use their favourite applications and services, check email, download videos, music, watching TV, share photos, all on the same terminal and in mobility.

History of mobile networks is marked by four main stages (the fifth is actually in development), called generation (abbreviated respectively 1G, 2G, 3G and 4G). These four generations differ mainly in the techniques used to access the radio resource.

The evolution of these techniques has been guided by the desire to increase the capacity and the throughput offered by the system in a restricted frequency band.

The orientation to the 4G-LTE (Long Term Evolution) which has been considered since November 2004 as long-term evolution of UMTS, during a workshop organized by the 3GPP (3rd Generation Partnership Project) called future evolution workshop. Works on this new standard began in 3GPP in January 2005 with a feasibility study, which ended in September 2006 with the definition of major principles of LTE.

The LTE is related to a combination of technical and industrial factors, such as capacity, throughputs, adaptation to available spectrum, ease of exploitation of networks.

The evolution of communications standards have made necessary the development of tools to characterize these wireless communication systems and their propagation environment. This is where the Multiple-Input Multiple-Output (MIMO) Over The Air (OTA) characterization methods make their appearance. Since one of the major features of wireless communications remains the environments in which the electromagnetic waves propagate. Indeed, these environments are most often of multipath type, and affect the quality of the received signal (fading, inter-symbol interference …)

Thus, there is a strong desire of operators and mobile phone manufacturers to evaluate by standardized measurements, the performances of wireless communication systems. This evaluation must be performed in realistic environments. However, the standardisation of this kind of measurements in real conditions cannot be envisaged. This is why; the emulation in controlled environment of multipath propagation channels that represent equivalent conditions to realistic environments has to be investigated.

The work presented in this thesis focuses on channel emulation in reverberation chamber in order to propose real time and non real time characterization test beds for LTE mobiles, able to extract figure of merits of these devices.

This work was conducted within “Signals & Multiple Antenna Systems” team of waves and associated systems department at XLIM research institute.

This thesis report is divided into three chapters that detail the evolution of the performed work.

The first chapter presents the context of the study. First of all a bibliographic study for MIMO OTA methods will be drawn. Then, a MIMO channel model description necessary to carry out our study will be presented. This will lead us to the presentation of the MIMO OTA platforms, based on MSRC (Mode-Stirred Reverberation Chambers) method selected to evaluate the performances of a wireless communication system in controlled multipath environment.

Among the different possibilities, the Mode stirred reverberation chamber has been proposed to 3GPP (in Technical Report 37.976) as one of the candidate methodologies for conformance testing of MIMO OTA performance. MSRC are able to reproduce a rich multipath environment with a controlled delay spread of the channel. Nevertheless, this last point needs a long calibration procedure to be efficiently implemented.

The second chapter is therefore dedicated to the development of a simulator, using Matlab, modelling a mode stirred reverberation chamber in order to estimate the channel delay spread of the propagation channel generated in the chamber. This simulator will be developed based on a circuit approach to achieve a flexible and preferment simulation tool. Firstly, the theory of reverberation chambers is studied in order to identify and understand the mechanisms governing the functioning of these metallic cavities. Assumptions considered for this model will be selected and implemented to guarantee best possible performance

The elaboration of an analytical model able to predicting the value of Delay spread, taking into account the antennas, losses and stirrers; has made possible the emulation of different channel models in the MSRC and subsequently the performance evaluation of wireless communication systems and real mobile terminals in these channels. These will be discussed in detail in the third chapter.

Based on the results obtained in simulation, the third chapter will be devoted to the experimental establishment of a characterization test bed for wireless communications systems in controlled environment. The characterization process of these systems will be divided into three parts. The first part is intended to analyze the dependence of the diversity gain of a wireless communication system versus root mean square (RMS) delay spread, by the use of an OTA communication system with QPSK modulation. For this, several channels having different RMS delay spread are emulated.

The second part will be devoted to assessing the performance of a multi antennas communication system, in controlled multi paths propagation channel models. These channel models will be emulated following channel models predefined in the literature. The last step will be dedicated to assessing the performance of LTE mobile terminals in real time.

This manuscript is concluded with a retrospective of work and by proposing some research perspectives.

Chapter I: Over The Air Methodologies For Multiple Antennas Systems Characterization

1. Introduction

Wireless devices; need pass some evaluations showing that their performances reaches the minimum requirements considered to address a specific market. For this reason, various experiment methods to which wireless devices are subjected before reaching the final consumer and several measurements techniques proposed for the characterization and qualification of MIMO systems are necessary. Those methods are called Over The Air (OTA) methodologies.

Among factors that have an impact on the performance limits of any communication system, there is the wireless channel. Indeed, one of the major features of wireless communications remains the environments in which the electromagnetic waves propagate. Indeed, these environments are usually of multipath type because of reflection, diffraction phenomena, caused by scaterers in the propagation environment, which can affect the quality of communications. To reduce such phenomena, MIMO technology has been proposed. The MIMO technique uses multiple antennas at both transmitter and receiver ends of a communications system to increase the link performance by exploiting the multipath propagation. In the beginnings of cellular communications, fading and path loss of the narrowband channel were the key parameters. For broadband modern communications, the frequency selectivity of the channel presents a great interest.

The performance measurements of wireless terminals in a real environment are expensive and difficult to implement.

Hence the need to establish the experimental OTA tests methodologies capable of emulating these types of environments and giving access to the factors of merit of the device under test (DUT). This chapter aims to introduce and describe these methods.

2. Over the Air methodologies for MIMO devices testing

2.1. Overview

In a wireless communication, the transmitter and the receiver have one or several antennas. The wireless communications are distinguished in four different cases according to the antennas number in transmitting and receiving side.

At this point it is necessary to clarify the terminology used in description of the four different cases of radio link structure, namely SISO, SIMO, MISO and MIMO.

- Single Input – Single Output (SISO) transmission is the traditional radio link structure that is used with both transmitter and receiver having single antenna. Examples of this structure would be existing cellular standards e.g. Global System for Mobile Communications (GSM) and Universal Mobile Telecommunications System (UMTS). Only one spatial stream is transmitted.

- Multiple Input – Multiple Output (MIMO) transmission requires both transmitter and receiver to have multiple antennas. The important feature of MIMO transmission is it exploits the spatial aspects of the channel. Multiple spatial streams are transmitted in this case. In scatter-rich environment, multiple signal streams can be assigned to different spatial streams in order to achieve higher throughput.

- Single Input – Multiple Output (SIMO) and Multiple Input – Single Output (MISO) are degenerate cases of MIMO with transmitter or receiver (respectively) having only a single antenna. Although it is not possible in this case to transmit multiple signal streams, it is still possible to exploit the multi-path channel for better transmission reliability. In these cases, radio systems can implement different techniques to improve signal quality e.g. switching, selecting, combining and in MISO case, also Transmit Diversity (TD).

Over-The-Air (OTA) measurement platforms give a highly accurate and effective method for measuring MIMO systems performance [1, 2]. OTA testing solutions create an environment where signals are transmitted to verify the performance of a product and accurately distinguish a poorly performing device from a good device. OTA test methods evaluate the wireless device end-to-end.

If the device has a single antenna mode, it can be evaluated using traditional Single-Input Single-Output SISO OTA measurement methods [2]. In all other cases, new test methodologies and metrics are required to correctly characterize the device under test.

2.1.1. Single-Input-Single-Output (SISO) tests

For devices supporting only SISO transmission, traditional OTA measurement focuses on the radiation efficiency of the antenna. Parameters to be reported are Total Radiated Power

(TRP) for uplink and Total Isotropic Sensitivity (TIS) for downlink transmission. TRP and TIS measurements can be performed in either anechoic chambers or reverberation chambers.

- TIS can be defined as an approximation of the reciprocal average of Equivalent Isotropic Sensitivity (EIS). For each Angle of Arrival (AOA), EIS is defined as the power that would have been received by a terminal with an ideal isotropic antenna under the same test conditions.
- TRP is a measure of how much power the device under test (DUT) actually radiates. The TRP is defined as the integral of the power transmitted in different direction over the entire radiation sphere [77].

$$TRP = \frac{1}{4\pi}\oint\left(EIRP_{\theta}(\Omega; f) + EIRP_{\varphi}(\Omega; f)\right)d\Omega$$

$$TIS = \frac{4\pi}{\oint\left[\frac{1}{EIS_{\theta}(\Omega; f)} + \frac{1}{EIS_{\varphi}(\Omega; f)}\right]d\Omega}$$

$EIRP_{\theta}$ and $EIRP_{\varphi}$ are the actually transmitted power-levels in corresponding polarizations.

Where the effective isotropic sensitivity (EIS) is defined as the power available at the antenna output such as the sensitivity threshold is achieved for each polarization. Ω is the solid angle describing the direction, *f* is frequency. θ and φ are the orthogonal polarizations.

The anechoic chamber is principally selected as the environment for SISO OTA testing, as depicted on figures I.1 and I.2. Two types of anechoic chamber structures are presented in standard SISO OTA measurements [3]. One Type has a dual polarized test antenna fixed in the chamber. The DUT is mounted on a dual-axis positioner as illustrated in Figure.I.1. The other type has the dual polarized test antenna mounted on a one-axis boom positioner, making it possible to move along a vertical circle. The device is mounted on a platform which is capable to turn around the Z-axis as given in Figure.I.2.

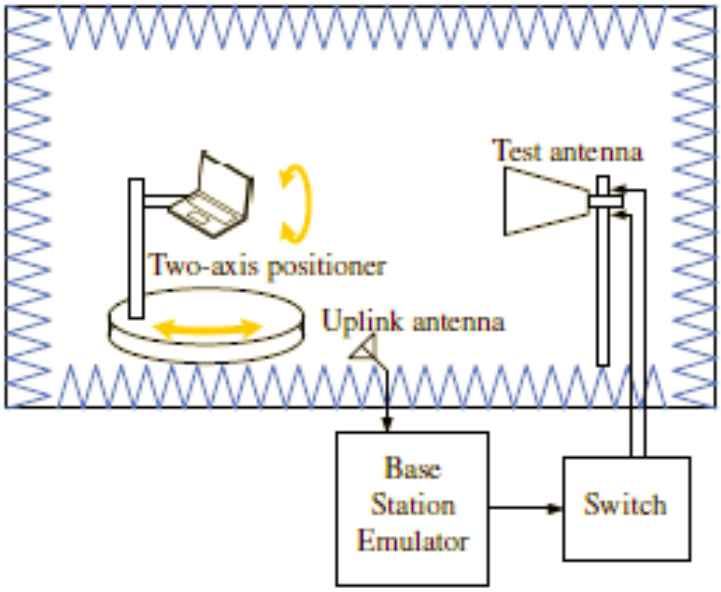

Figure I.1: Standardized anechoic chamber with a combined axis structure as introduced in [3]

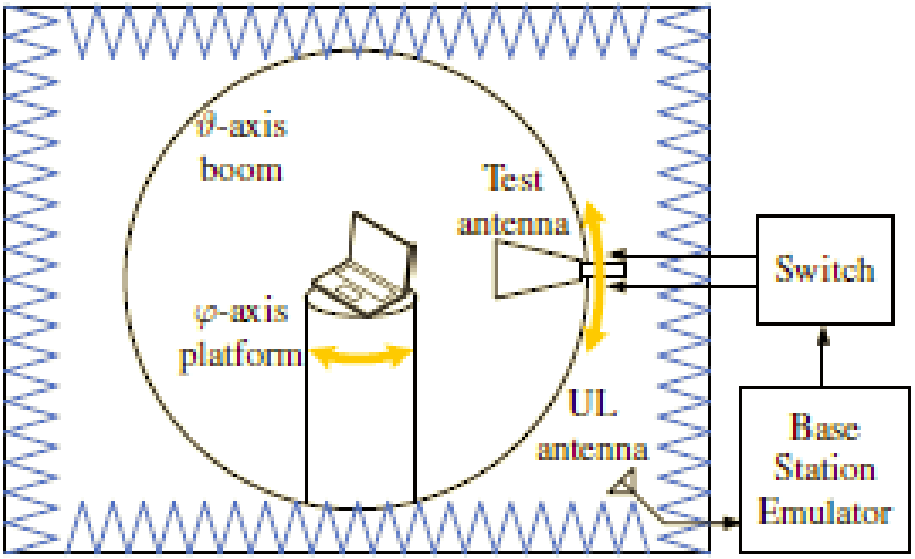

Figure I.2: Standardized anechoic chamber with distributed axis structure as introduced in [3]

In order to reach all possible orientations of the device under test (DUT) in the measurements, both presented test bed allow to the test antenna to move freely around the DUT.

2.1.2. Multiple-Input-Multiple-Output (MIMO) tests

User equipment (UE) with multiple antennas can be used to optimize the SNR in the presence of fading (use of reception combining, or space-time coding). Or it can be used to increase the throughput, and in this case we take advantage of the wealth of the canal in

MIMO transmission modes (space multiplexing techniques (e.g. BLAST)). SISO OTA measurements are insufficient to evaluate this aspect without implementation of spatial diversity in the measurement testbed. Although the antennas of a MIMO terminal can be quantified separately, comparable to what is done in a SISO OTA test; the relations between their radiation patterns would be rejected. MIMO antenna terminals represent strong coupling between ports and cannot be handled as a collection of separate antennas. The goal of a MIMO OTA test is to quantify UE with respect to in-the-field performance for different MIMO transmission modes and an almost infinite choice of multi-path channel conditions.

An additional important necessity is to design low complexity platforms, since tests are to be performed for a large number of frequency bands, which could lead to increase measurements time significantly [4].

3GPP (3rd Generation Partnership Project), CTIA (Cellular Telecommunications Industry Association) and COSTs (European Cooperation in Science and Technology) define the list of factors of merit (FOM) commonly used to evaluate the performance of MIMO terminals and methodologies referenced in Table I.1 [18].

Category	**I**	**II**	**III**	**IV**	**V**
FOMs	MIMO Throughput CQI	TRP TRS	Gain Imbalance Spatial correlation MIMO Capacity	Antenna Efficiency MEG (Mean Effective Gain)	MIMO Throughput
Type	OTA	OTA	MIMO antennas	MIMO antennas	OTA
Methodology	Active (with fading)	Active (with fading)	Passive/Active (with fading)	Passive/Active (without fading)	Active (with fading)

Table I.1: Categories of factors of merit

These figures of merit are classified into two categories depending on the measurement methodology: active measurement (active FOM) and passive measurement (passive FOM). The passive method uses a vector network analyzer to evaluate the effectiveness and performance of antenna diversity techniques such as diversity gain, correlation and MIMO capacity in a controlled (referenced) multipath channel. It therefore does not require a base station emulator (BS).Concerning the active measurements aims to

assess the parameters of MIMO system such as throughput, channel quality indicator (CQI), EVM (error Vector Magnitude), BLER (Block Error Rate), total radiated power (TRP), or total radiated sensitivity (TRS) by establishing a real-time communication between the User Equipment (UE) or terminal and base station (BS) emulator.

The CQI is used for measuring the transmission quality in the downlink (DL). It indicates the modulation scheme and the coding rate for which the BLER in the channel does not exceed 5%. Mobile terminal can measure it and transmit it in uplink (UL) to the BS. In response, the BS adapts the transmission of signal in DL. These performance parameters and methodology are being standardized by the 3GPP [18].

The process of the standardization is being performed by the 3GPP organization in collaboration with CTIA, in order to choose a common methodology in terms of complexity and cost efficiency that can emulate realistic multi paths propagation channel to evaluate the performance of the wireless communication systems [5, 6].

Many propositions have been done during the last few years. The result is synthesized in the 3GPP document [7], and a lot of important points still not standardized.

Several candidates for MIMO OTA methods have emerged from the work of the 3GPP, European Cooperation in Science and Technology (COST): COST2100, and COST IC1004. These candidates can be grouped in three main categories: Two-Stages Methods, Anechoic Chamber Method, and Mode Stirred Reverberation Chamber Method.

2.2. Two-Stages Method

The MIMO OTA testing using the two stage method is based on the theory that the far field antenna pattern of multiple antennas can completely capture the mutual coupling of the multiple antennas and their influence. This method is divided in two stages.

Stage 1: The MIMO antenna radiation pattern is measured inside an anechoic chamber. Thus, to perform the antenna pattern measurement, the chamber is set up as showed in [8, 9, and 10], where the UE is placed inside a chamber and each antenna element's far zone pattern is measured. The chamber is equipped with a positioner, that makes it possible to carry out full 3-D far zone pattern measurements for both Rx and Tx radiated performance. The measurement antenna should be able to measure two orthogonal polarizations.

Stage 2: Combining the antenna patterns measured in stage 1 to desired MIMO channel model, emulate the MIMO channel model with the measured antenna patterns incorporated in a commercial channel emulator and perform the OTA test in wired approach. The MIMO OTA method based on the two-stage method is illustrated in Figure I.3. The integrated channel model with both MIMO antenna effect and the multipath channel effect can be emulated with a commercial MIMO channel emulator. The BS emulator is connected to the MIMO channel emulator and then to the MIMO device's. These ports are the standard ones provided for conducted conformance tests. By controlling the power settings of the channel emulator and also the integrated channel model, the end-to-end throughput with the MIMO antenna radiation influence can be measured. In the following two different approaches are presented in order to combine the antenna patterns with MIMO propagation channel model.

a) Apply antenna patterns to Ray-based channel models.

b) Apply antenna patterns to correlation-based channel models. The correlation matrix and the UE and the antenna imbalance can be calculated and then generated by the channel emulator.

Using this method it can be possible to determine the following figure of merit:

1) Throughput.
2) TRP and TRS.
3) CQI, BLER.
4) Antenna efficiency and mean effective gain (MEG).
5) Antenna correlation, MIMO channels capacity.

During antennas pattern measurement stage the coupling between the UE antenna and internal spurious emission of the UE might be characterized by lowering down the signal power.

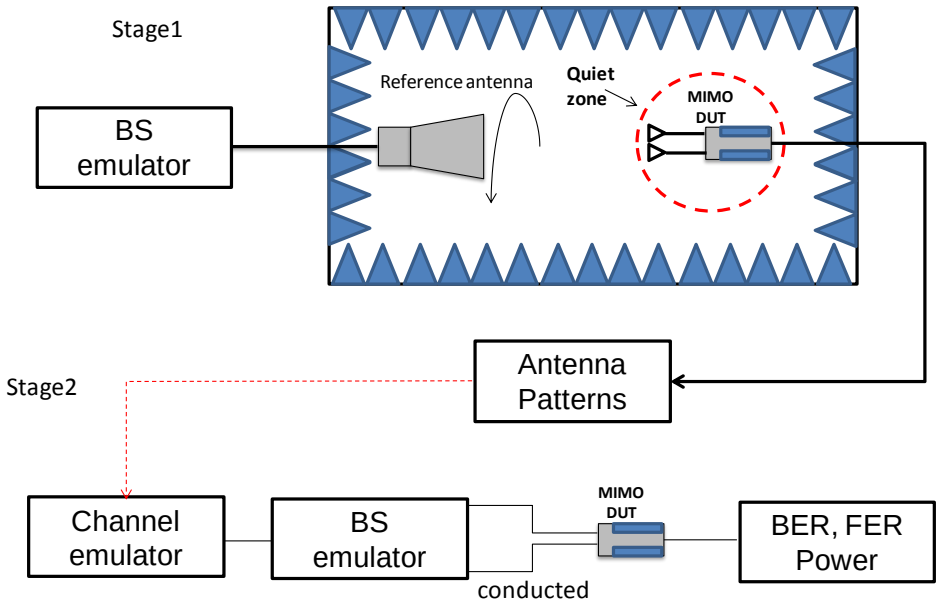

Figure I.3: Proposed two stage test methodology for MIMO OTA test [11]

2.3. Anechoic chamber based method

In this case, the MIMO OTA test bed is composed of an anechoic chamber, a fading emulator, a number of OTA chamber antennas, a Base Station emulator and the device under test (DUT) [12, 13]. The figure below represents an example of the OTA model. The principle of the figure is not to restrict the implementation, but rather to clarify the general idea of the MIMO OTA concept.

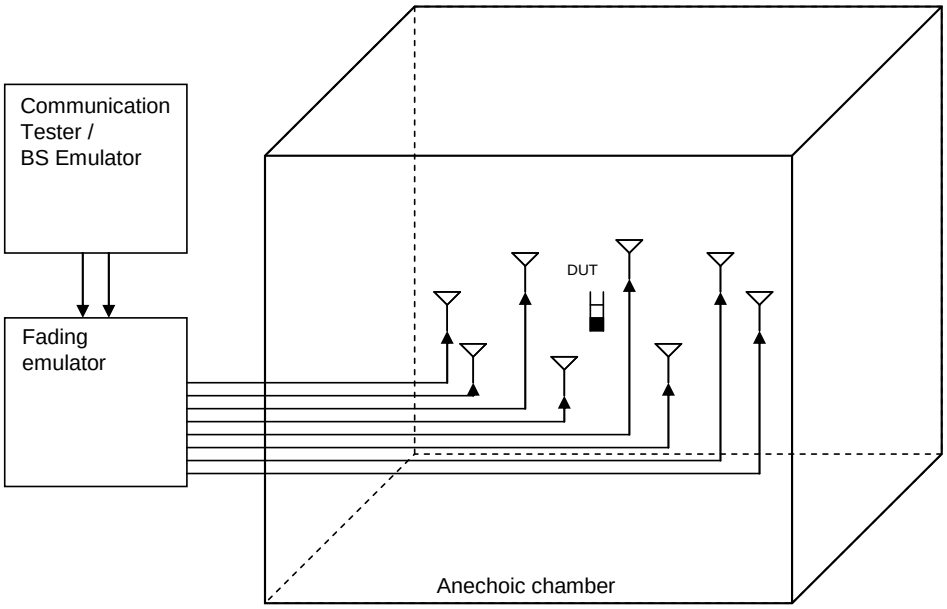

Figure I.4: Anechoic chamber methodology for MIMO OTA test [14]

The DUT is located at the centre of the anechoic chamber. This configuration gives the possibility to create a radio channel environment where the signal can arrive from different probable directions simultaneously to the DUT [12]. Transmitting antennas are positioned around the UE in a way that to be possible to modify the receiving spatial profile of Angle of Arrival (AoA) and therefore the Angle Spread (AS) at the UE location. Others characteristics, like correlation, delay, fading profile or Doppler shift can be implemented using a fading emulator [15].

The important challenge is to emulate realistic polarization and angular behaviour inside the anechoic chamber. The geometry-based stochastic channel models (GSCM) family is well appropriate for MIMO OTA testing. The GSCM include 3GPP Spatial Channel Model (SCM), Spatial Channel Model Extended (SCME) and WINNER channel models. This polarization and angular behaviour creates suitable correlation at the DUT antennas. The correlation is defined implicitly via the per-path angle of arrival and real antennas. Correlation matrix based model is not suitable for this, because it includes the antenna information in the model itself.

This test methodology gives flexibility in the number of transmitting antennas. The important question is how the channel model is emulated accurately. Based on the quiet zone discussion, it was proposed to use 8 antennas in the case of single polarization and 16 antennas (or 8 bipolarized) in the case of dual polarization. In general, the softest configurations necessitate the higher number of transmitting antennas.

As an advantage, this method shows a flexibility to generate most of parameters that characterize a propagation channel model (Angle Of Arrival (AoA), Angle Of Departure (AoD), Doppler shift, polarization and delay).

On the other hand, the major disadvantage of this methodology is the cost and complexity when the number of probe antennas increases, compared to the other solutions.

2.4.Mode Stirred Reverberation Chamber based method

The reverberation chamber (RC) is a metallic cavity with reflecting walls providing a full isolation with the outside, which can generate an isotropic multi-path propagation environment with metallic stirrers that can produce a random variation in time of the field with a uniform angular distribution over all directions. This isotropic multi-path environment represents a reference environment for systems designed to work during fading. The idea is then to be able to compare the performances of various devices in a simple way. The Rayleigh

or rice environment emulated in a reverberation chamber is well known as a good reference for urban and indoor environments, but does not well represent rural and suburban environments [16, 17].

Nevertheless, for a Multi-antenna OTA measurement it is important to have a fast and reproducible test method to qualify and compare wireless devices in the environments and under the worse conditions where they going to be work. The great majority of calls/data connections with mobile phones are made in indoors and in urban zones that can be represented in the reverberation chamber.

Mechanical stirrers and switching between different fixed wall-mounted antennas allow emulating a dynamic Rayleigh fading inside the chamber for each antenna of the terminal.

The measurements begins by sending the transmitting signals inside the RC through the use of transmitting antennas facing the wall in order to reproduce a NLOS (Non Line Of Sight) propagation channel [18]. Several UE metrics can be measured: throughput, TRP TIS, etc

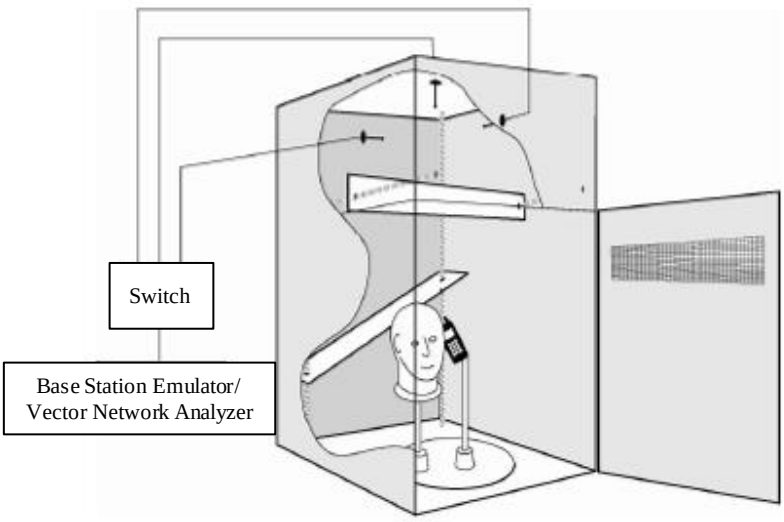

Figure I.5: Reverberation chamber methodology for MIMO OTA test

In [19] and [20] the authors have shown the possibility to generate a Rayleigh and Rice non-isotropic fading environment inside the reverberation chamber. Indeed, this measurements system has some advantages since it's able to assure the angular spread of multi paths of receiving antenna. However, it has also disadvantages which are represented by the inability to control the angle of arrivals of different paths at receiving side.

The reverberation chamber has a limited range of channel modelling capabilities. Particularly,

- The power delay profile is limited to a single decaying exponential.
- The Doppler spectrum and maximum Doppler is limited by the relatively slow motion of the stirrers.
- It is difficult to impart a specific, repeatable MIMO fading correlation on the downlink waveform.

These limitations can be surmount when a MIMO channel emulator and reverberation chamber are cascaded [66, 67].

The reverberation chamber based method for MIMO OTA represents several advantages:

-Cost effective solution: the number of probe antennas used in a MSC is lower than in other solutions.

- Measurement time: the capability of MSC to emulate a 3-D environment involves that the measurement time with this method is lower than in other techniques.

After a detailed study of various MIMO OTA test methodologies covering their advantages and disadvantages, the choice of the Mode Stirred Chamber based method was retained for this thesis. A study concerning MIMO OTA performance evaluation using MSC will be detailed later in this chapter.
Knowledge of the environment in which the mobile terminal is going to work remains important. For this, the following section is more focused on the definition of the propagation channel, its mathematical representation, the parameters characterizing the radio channel and classification of MIMO channel models.

3. The MIMO propagation channel model.

3.1.Multipath propagation channel

In a real environment, the transmission of a signal is usually done by superposing in addition to a possible direct path, other propagation paths. These paths have a variable number and undergo different effects depending on the nature of the interaction between the wave and elements of the environment. The signal obtained at the receiving antenna corresponds to recombination of these waves, which have undergone a different weakening

and phase rotation, and which arrive at the receiver with a delay due to the length of the propagation path [21, 22]. The presence of multiple propagation paths can lead to a significant distortion of received signal. On the other hand, especially inside buildings, a line of sight (LOS) path is not always available. In this case, no line of sight (NLOS) paths, enabling radio communication [23]. The Figure I.6 below illustrates the concept of multipath, and the main propagation phenomena.

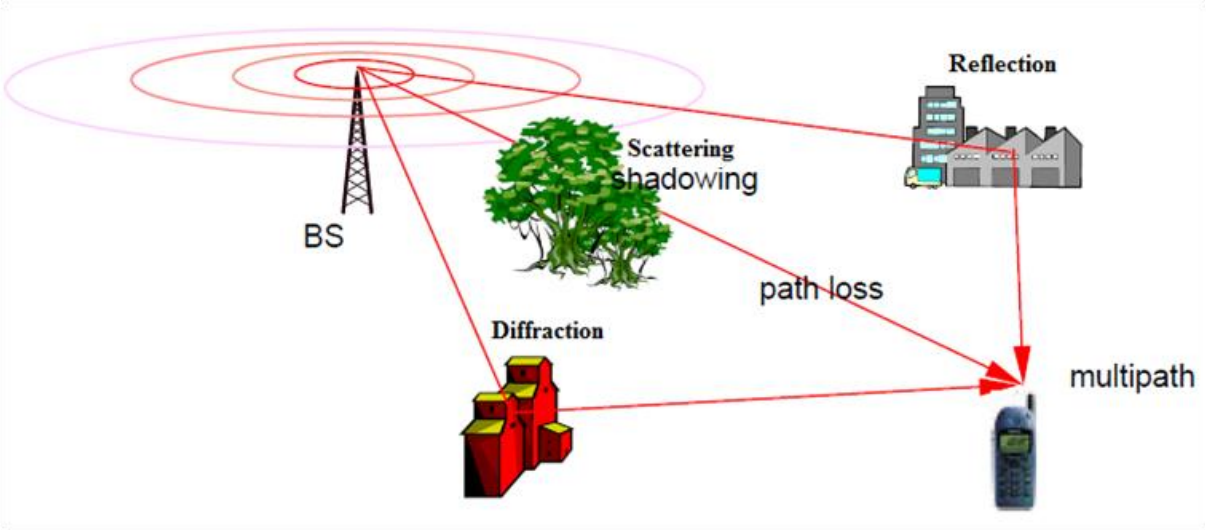

Figure I.6: main propagation mechanisms [24]

Due to the different interactions of radio waves and their propagation environment, significant variations of the channel characteristics are observed at different scales. In addition to the propagation loss in free space, the phenomena of large-scale variation are mainly due to the masking effect (shadowing). In fact, many obstructions in the environment generate additional attenuation for the transmitted wave. Generally, this attenuation is a function of the distance d between the transmitter and the receiver, and is characterized by the propagation loss coefficient N_d, the received signal power decreasing in proportion to d^{-Nd}. The parameter value N_d is 2 in free space, and varies between 2 and 5 in NLOS configuration. In visibility, wave guiding effects may lead to a value of N_d less than 2. The deviations of the order 1dB of the received power compared to the trend of d^{-Nd} are due to punctual masking and are called slow variations or shadowing effect. The small fluctuations are a direct effect of multipath propagation. Indeed, the recombination of multiple versions of a signal having different attenuation and a phase shift causes significant rapid fluctuations, which may reach several tens of dB. If the system bandwidth is large, this involves the consideration of the arrival time of paths: what is known as “wide-band channels”.

- *Narrowband channel*

The phenomenon of spatial selectivity depends on the phase difference between each path and therefore the frequency of the transmitted signal. When the frequency band is narrow, all the frequency components of the signal undergo similar phase changes, and then the power density remains constant over the entire considered band. The term flat fading is sometimes used to describe the frequency behaviour of such a narrow band signal. When the mobile terminal move a power fluctuation (flat fading) linked to the multipath recombination is observed. To fight against, diversity techniques such recombination or space-time coding which can improve the average SNR are used. It is also possible to use the advantage of the de-correlation in multi-antenna channels through spatial multiplexing techniques.

- *Wideband channel*

For signals occupying a wider frequency band, the various frequency components can be affected in different ways, so that the received signal has some distortion compared to the transmitted signal. This is called frequency selectivity fading, which manifested in a variation of the received power as a function of frequency. The bandwidth in which the spectral components of the signal are affected in the same way is called coherence band or correlation band.

We can then apply advanced techniques in reception, such as channel equalization, to retrieve the maximum energy of multipath [25, 26, 27], and Orthogonal Frequency Division Multiplexing (OFDM). As it is known OFDM signal gives better performance than using mono-carrier signal.

3.2.MIMO channel models

The MIMO propagation channel can be characterized by its impulse response $h(\tau)$, which is a function of delay. If both transmitter and receiver antennas and the elements that cause multipath reflections are static, then the channel impulse response is static. However, the usual case is that both the antennas and surrounding objects are moving, and therefore the impulse response is time-variant ($h(t, \tau)$) [28].

MIMO channel describes the relationship between the transmitter (Tx) and receiver (Rx). Figure I.7 shows a 2x2 MIMO system with the channel matrix (H) and the scattering environment around.

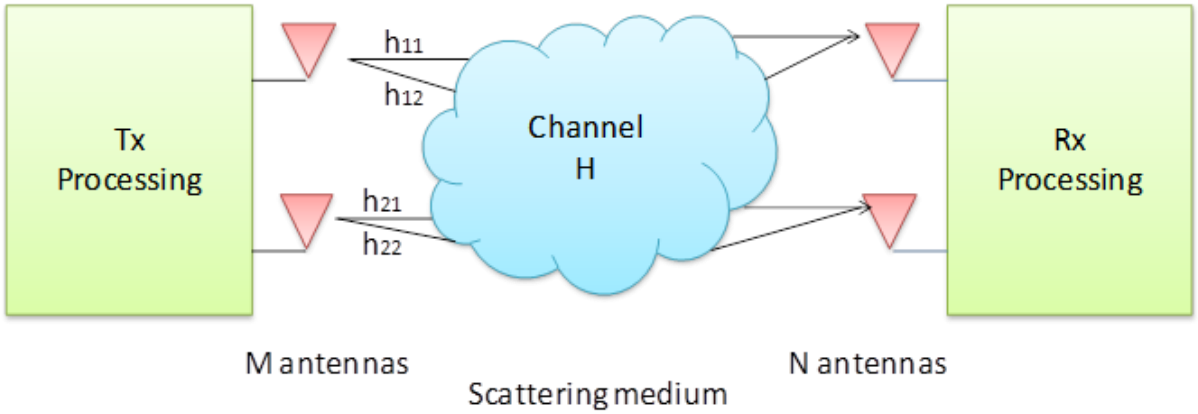

Figure.I.7: MIMO channel representation

For a 2x2 MIMO system the channel matrix is:

$$H(\tau) \in C^{MxN} \Rightarrow H = \begin{bmatrix} h_{11} & h_{12} \\ h_{21} & h_{22} \end{bmatrix} \qquad (I.1)$$

The channel (H) matrix entirely illustrates the propagation channel between transmitters and receivers. Before arriving to channel matrix H there has to be some additional properties included, such as power delay, spatial correlation functions and impact of fading.

The MIMO channel matrix (H) without noise can be expressed as:

$$H(t,\tau) = \sum_{l=1}^{L} H_l \delta(t, \tau - \tau_l) \qquad (I.2)$$

Where L is the number of taps of the channel model, H (t,τ) is the 2x2 matrix of the channel.

$H_l = \left[\alpha_{MN}^{l} \right]_{2x2}$ is a complex matrix which illustrates the linear transformation.

Between two considered antenna arrays at delay τ_l and α^{l}_{MN} is the complex transmission coefficient from antenna M at the transmitter to antenna N at the receiver.

A study on different channel models is showed in [29]. Based on this study, channel models can be distinguish on two major categories.

- *Physical channel model:* describe the propagation environment from an electromagnetic approach. The bidirectional propagation channel that connects the positions of the transmitter and receiver is described, by propagation theory of electromagnetic waves. Thus, they are quantified parameters intrinsic to the physical channel as the AoA, the Delay Spread (DS), complex amplitude, or AoD. This channel

models type is independent of parameters such as antenna radiation pattern, number of antennas. Channel models based on ray tracing are examples of this type of models.

- *Analytical channel model*: Analytical channel models characterize the impulse response (equivalently, the transfer function) of the channel between the individual transmit and receive antennas in a mathematical/analytical way without explicitly accounting for wave propagation. The individual impulse responses are subsumed in a (MIMO) channel matrix. Analytical models are very popular for synthesizing MIMO matrices in the context of system and algorithm development and verification. Analytical models can be further subdivided into *propagation-motivated models* and *correlation-based models*. The first subclass models the channel matrix via propagation parameters [30]. Examples are the finite scattered model, the maximum entropy model, and the virtual channel representation. Correlation-based models characterize the MIMO channel matrix statistically in terms of the correlations between the matrix entries. Popular correlation-based analytical channel models are the Kronecker model and the Weichselberger model [31, 32].

Apart from the models listed in the above categories, some international organizations have proposed a number of channel models for the purpose of comparing different wireless systems in order to define some reproducible conditions. These types of models are called empirical channel models. These models are based on field measurements made in real environments such as streets, indoors and rural environments [33, 34, 35 and 36].

3.3. Standardized channel models

3.3.1. 3GPP spatial channel model (SCM)

In order to satisfy the need of channel models, serving as reference for outdoor measurements, the 3GPP has developed the spatial channel models (SCM) family. Three scenarios are distinguished to reproduce the use conditions of use that are experienced under real situations [33].

- "Urban macro cell" corresponds to the scenario where user equipment is located in a reflective (urban) environment, with a certain distance to the BS.
- "Suburban macro cell" corresponds to the case where user equipment is located in a non-reflective (suburban or rural) scenario, with presence of line of sight components.

- "Urban microcell" corresponds to the case where user equipment is located in a reflective scenario and is being serviced by a BS located within walking distance of it.

3.3.2. Extended spatial channel model (SCME)

The SCME model [37] suggests the extension of some of the parameters proposed by the SCM model, maintaining the basic idea of the original models. With the arrival of the LTE standards, an extension of the bandwidth of the channel applicability is essential to the channel model. The SCME model proposes to add intra-path DS following a one-sided exponential function. This approach is based in the methodology proposed by Saleh and Valenzuela for the modelling of indoor environments.

Scenario		Suburban Macro		Urban Macro				Urban Micro	
Power-delay parameters: relative path power (dB) / delay (μs)	1	0	0	0		0		0	0
	2	-2.6682	0.1408	-2.2204		0.3600		-1.2661	0.2840
	3	-6.2147	0.0626	-1.7184		0.2527		-2.7201	0.2047
	4	-10.4132	0.4015	-5.1896		1.0387		-4.2973	0.6623
	5	-16.4735	1.3820	-9.0516		2.7300		-6.0140	0.8066
	6	-22.1898	2.8280	-12.5013		4.5977		-8.4306	0.9227
Resulting total DS (μs)		0.231		0.841				0.294	
Path AS at BS, MS (deg)		2, 35		2, 35				5, 35	
Angular parameters: AoA (deg) / AoD (deg)	1	156.1507	-101.3376	65.7489	81.9720	76.4750	-127.2788	0.6966	6.6100
	2	-137.2020	-100.8629	45.6454	80.5354	-11.8704	-129.9678	-13.2268	14.1360
	3	39.3383	-110.9587	143.1863	79.6210	-14.5707	-136.8071	146.0669	50.8297
	4	115.1626	-112.9888	32.5131	98.6319	17.7089	-96.2155	-30.5485	38.3972
	5	91.1897	-115.5088	-91.0551	102.1308	167.6567	-159.5999	-11.4412	6.6690
	6	4.6769	-118.0681	-19.1657	107.0643	139.0774	173.1860	-1.0587	40.2849
Resulting total AS at BS,MS (deg)		4.70, 64.78		7.87, 62.35		15.76, 62.19		18.21, 67.80	

Table I.2: Parameters of SCME scenarios (3GPP document TR 37.976)

3.3.3. Winner channel models

The winner channel model [34, 35] results a series of extended channel models (3GPP-SCM) for “outdoor” environments and IEEE 802.11 TGn for “indoor” environments. It’s considered in the literature as the most successful channel model. This model is born from the desire to have a MIMO geometric stochastic channel model representing several “indoor” and “outdoor” environments (cf. Table I.3) for bandwidth higher than 20MHz. Eighteen typical scenarios were studied (measured and modelled) for frequencies between 2GHz and 6GHz and a bandwidth that can reach 100MHz.

As mentioned before, the WINNER channel model belongs to the family of geometric and stochastic models, describing the propagation channel as a source of paths grouped in clusters.

Each cluster contains a paths group which has a similar propagation features. In the terminology of WINNER mode, it's possible to provide a geometrical interpretation to the concept of cluster. Indeed, each cluster contains all the rays that interact with obstacles in spreading zone. As well, the propagation channel is composed of a large number of clusters that varies according to the scenario considered. Each cluster is characterized by its delay, its power, and the angles of departure and angles of arrivals of each path in the cluster.

The WINNER channel model is generally built using the result obtained from measurements. The advent of MIMO technologies, involves a very important demand on the efficient ways to evaluate the performances of diversity wireless communication systems.

Modified Winner II Outdoor-to-Indoor								
Cluster #	**Delay [ns]**			**Power [dB]**			**AoD [°]**	**AoA [°]**
1	0	5	10	-3	-5.2	-7	0	0
2	0			-8.7			32	101.5
3	5			-3.7			-21	66.2
4	10			-11.9			37	-118.7
5	35			-16.2			-43	138.5
6	35			-6.9			28	-90.4
7	65	70	75	-3.9	-6.1	-7.9	-49	32.7
8	120			-10.3			-34	10.5
9	125			-20.7			-49	156.6
10	195			-16.0			43	137.7
11	250			-21.0			49	-157.7
12	305			-22.9			51	-164.7
Delay spread [ns]								40.5
Cluster AS AoD / AS AoA [°]								5 / 25
Cluster PAS shape								Laplacian
Total AS AoD / AS AoA [°]								28.6 / 56
Mobile speed [km/h] / Direction of travel [°]								3 / 120
XPR NOTE: V & H components based on assumed BS antennas								9dB
Mid-paths Share Cluster parameter values for:								AoD, AoA, AS, XPR_V and XPR_H

Table I.3: Parameters of WINNER II scenarios (3GPP document TR 37.976)

The MIMO OTA based MSRC is retained to be the MIMO OTA test methodology used during this thesis. A complete description of this methodology and the measurements aspects related to it are presented below.

4. MIMO OTA performance evaluation using MSRC.

4.1.Overview of the Mode Stirred Reverberation Chamber

A reverberation chamber is a closed metallic cavity with dimensions higher than a few wavelengths [44]. A MSRC is characterized by, the density of modes D_n [modes/Hz], that means the number of modes present per Hz, is given by [45]:

$$D_n = \frac{8\pi abdf^2}{c^3} \qquad (I.3)$$

And the total number of modes in a frequency band Δf is given by:

$$N_n \approx \frac{8\pi Vf^2}{c^3}\Delta f \qquad (I.4)$$

Where a, b and c are respectively the dimensions of the MSC along the x, y, and z axis. A modal representation of the electromagnetic field is represented in the Appendix1.

The electromagnetic fields inside the MSRC present a statistical uniformity in all measurement points, in all directions and all radiation source positions. This uniformity is obtained using mechanical stirrer (s) rotating inside the chamber. In recent years, an increasing interest has developed inside the scientific community to use reverberation chamber as test tool for the wireless communication system. The main reason is that one of the most important characteristics of reverberation chamber is that electric field amplitude along a giving polarization is distributed according to a Rayleigh distribution. This distribution is also used to model fading in a wireless communication channel. It's this characteristic that many studies are based on to compare the channel in reverberation chamber and the classical environment (indoor or outdoor).

These characteristics make the MSRC an ideal solution for diversity system qualification. In the last few years some researches have been performed on the measurement capabilities of MSRC's. Parameters such as antenna efficiency, MIMO capacity, or diversity gain have successfully measured using MSRC. Different propagation channels have been emulated, by taking into account the delay spread.

4.2. MSRC characterization parameters

4.2.1. Impulse response and Power Delay Profile (PDP)

An example of impulse response measured in the reverberation chamber is shown in figure I.8-a. It shows clearly that h(t, τ) varies very rapidly with delay. This is due to the reflective

nature of the RC. For a given position of mechanical stirrer, some delays correspond to a sum of constructive rays while further delays correspond to a sum of destructive rays [38, 39].

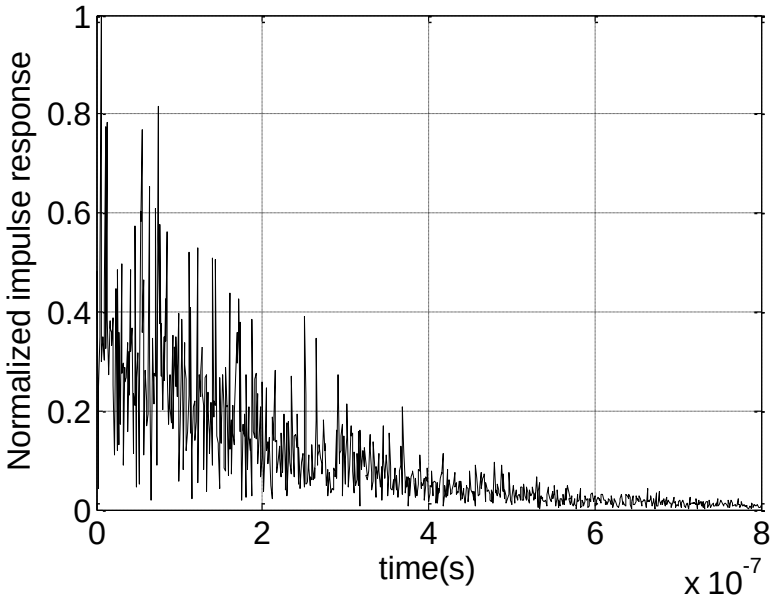

Figure I.8-a: example of impulse response measured inside reverberation chamber

If we average these amplitudes, we obtain the PDP. An example of PDP (figure I.8.b) with a bandwidth of 1GHz around 3.5GHz is given in figure I.8. This PDP is characterized by a delay spread of 300ns.

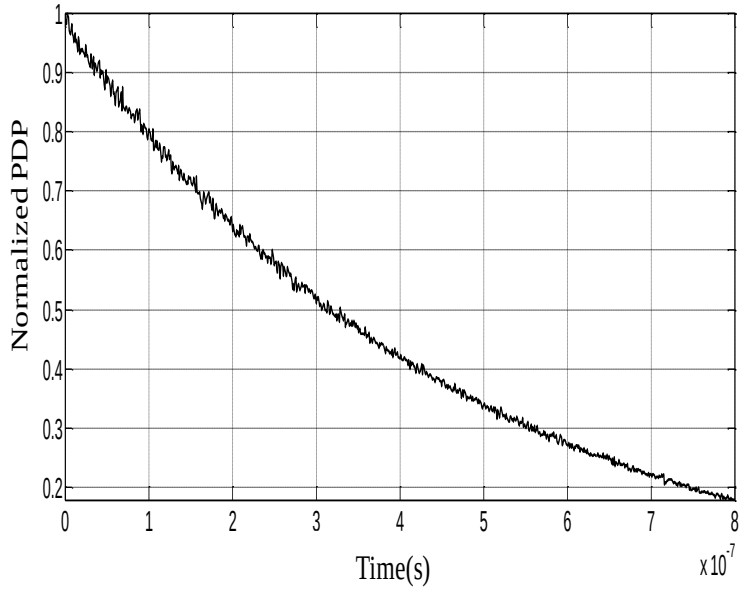

Figure I.8-b: example of PDP measured inside reverberation chamber

To characterize the Power Delay Profile, different times can be calculated. The most used is the normalized second moment also called RMS delay spread [40], given by:

$$\tau_{RMS} = \sqrt{\frac{\int_{-\infty}^{+\infty} P(\tau).\tau^2 d\tau}{\int_{-\infty}^{+\infty} P(\tau).d\tau} - \left(\frac{\int_{-\infty}^{+\infty} P(\tau).\tau d\tau}{\int_{-\infty}^{+\infty} P(\tau).d\tau}\right)^2} \qquad (I.5)$$

Where $P(\tau) = \left\langle |h(t,\tau)|^2 \right\rangle$

4.2.2. Fading signal strength distribution

The fading statistical behaviour qualified by an electromagnetic signal in real environments represents an interesting tool for quantifying and designing wireless systems. In a propagation environment with limited noise, the system behaviour is determined by the received field strength. The field strength has a stochastic behaviour, and therefore must be analysed in statistical terms. Thus the power density function (PDF), both in the field amplitude, and phase, is important parameter when characterizing the environment fading. The most used distributions are: Rayleigh, Rice and Nakagami.

- Rayleigh distribution

  In this case, the complex received signal consists of large number of indirect paths (NLOS) having random amplitudes and phases, independent and uniformly distributed. The envelope of this signal follows a Rayleigh law defined by the following equation [40]:

$$p(r) = \frac{r}{\sigma^2} e^{\left(-\frac{r^2}{2\sigma^2}\right)}, r \geq 0 \qquad (I.6)$$

σ is the standard deviation of the real part or of the imaginary part of the received signal

r is the complex envelope of the received signal

- Rice distribution

  In other situations, a propagation channel is characterized by indirect multi paths and a direct path (LOS). Therefore, the probability density of the

envelope of the received complex signal follows the Rice distribution defined as [41]:

$$p(r)=\frac{r}{\sigma^2}e^{\left(-\frac{r^2+r_d^2}{2\sigma^2}\right)}I_0\left(\frac{rr_d}{\sigma^2}\right), r\ and\ r_d \geq 0 \qquad (I.7)$$

Where r_d is the amplitude of the direct path and I_0 the modified Bessel function of the first kind and zero order.

- ❖ Nakagami distribution

In most cases, Rayleigh and Rice distributions are sufficient to characterize the fading distribution of received signals in a mobile radio channel. However, some channels are not characterized either Rayleigh or by Rice. For example, if the channel is characterized by two paths with comparable power and stronger than the other paths, the statistical expression of the received signal cannot be approximated by the Rice distribution.

An alternative distribution to model this case of scenario is provided by M.Nakagami [42]. this distribution is referred to as to the Nakagami distribution, whose the probability density is given by:

$$p(r)=\frac{2}{\Gamma(m)}\left(\frac{m}{\Omega}\right)^m r^{2m-1}e^{\left(-\frac{m}{\Omega}r^2\right)}, r\geq 0 and\ m\geq 0.5 \qquad (I.8)$$

Where:

Γ (.) is the gamma function, $\Omega = E\left\{r^2\right\}$ is the mean square value and $m=\frac{E^2\left\{r^2\right\}}{Var\left\{r^2\right\}}$ is the fading parameter.

4.2.3. Envelope correlation coefficient

The advantage of using diversity techniques is to receive multiple versions of the same signal to rebuild as better as possible the signal transmitted to the receiver. The antenna diversity system must be optimized to receive independents signals. One of these characteristics is the independence of the complex radiation pattern of the antennas of the receiving system [52]. The envelope correlation can be deduced in isotropic Rayleigh channel from S-parameters, following this equation [53]:

$$\rho_e = \frac{\left|S_{11}^* S_{12} + S_{21}^* S_{22}\right|^2}{\left(1-\left(\left|S_{11}\right|^2+\left|S_{12}\right|^2\right)\right).\left(1-\left(\left|S_{21}\right|^2+\left|S_{22}\right|^2\right)\right)} \qquad (I.9)$$

It sufficient that this coefficient is less than 0.5 for that received signals by antennas system are considered as un-correlated.

4.2.4. Diversity Gain

The diversity gain (DG) is one of the most significant parameters to evaluate the performances of diversity system. DG can be defined as the improvement of the signal to noise ratio (SNR) obtained by combining the fading signals received from a multi antenna system, relative to SNR received from one reference antenna [54, 55]. Transformation of received signals to one signal with higher quality, in order to resist to multi paths effects, is made through the use of combining techniques. Four different techniques are used to combine signals coming from the different receiving antennas. These techniques are selection combining, switching combining, Equal gain combining (EGC) and Maximum Ratio combining (MRC). The DG is can be expressed as:

$$DG = \frac{P_{div}}{P_{ref}} \qquad (I.10)$$

Where P_{div} is the power of the combining signal , and P_{ref} is the power of the reference antenna. Both power levels must be read it from a cumulative density function (CDF) representing the probability that an arbitrary power sample is smaller than a certain power level. In Figure I.9 it is shown an example of a DG measurement.

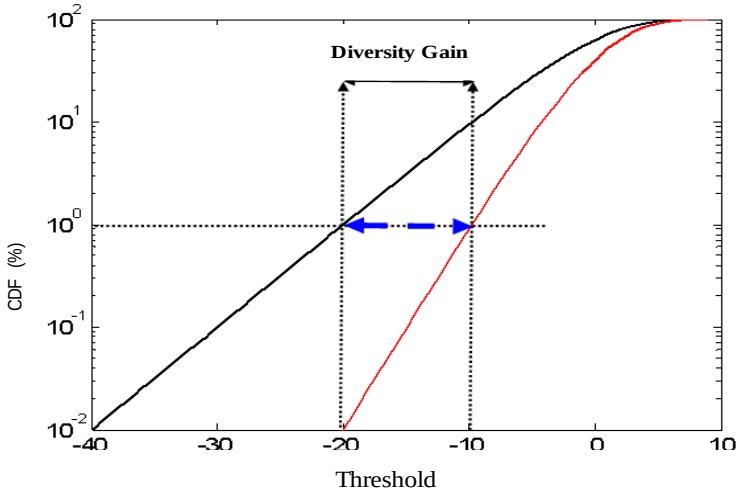

Figure I.9: DG of a given dual antenna for calculated at 99% signal level reliability

4.2.5. Reverberation chamber quality factor Q: theoretical approach

The quality factor is defined in [46] by:

$$Q = \omega \frac{U_s}{P_d} \qquad (I.11)$$

Where U_s [J] is the electromagnetic energy stored in the chamber, ω is pulsation and P_d is the dissipated power. In steady state, the energy stored by the reverberation chamber is given by the integral of the energy density, w [J.m^{-3}] over the cavity volume, V [m^3]:

$$U_s = \int_v w dV \qquad (I.12)$$

$$= \bar{w} V \qquad (I.13)$$

And $\bar{w}$ is the spatially averaged power density, defined as

$$\bar{w} = \frac{1}{V} \int w dV \qquad (I.14)$$

Through the assumption of ergodicity, this spatial average is equivalent to an average over all realizations (positions of mechanical stirrers), w=<w>. The most specific aspect of reverberation chambers appears here clearly since the energy density <w> is an average over all achievements of the channel. Finally, note that the average density of power flow $\langle S_c \rangle$ [W.m^{-2}] is given by:

$$\langle S_c \rangle = c \langle w \rangle \qquad (I.15)$$

To calculate the quality factor of a reverberation chamber, the mechanisms of power dissipation must be identified. There are four mechanisms [45]: the power dissipated in the walls, in the objects in the chamber, in the load impedance of the antenna, and the power loss optionally present in the apertures. The total power dissipated is the sum of the powers dissipated by each mechanism. Each mechanism of power dissipation can be associated to one quality factor Q_i and the global Q factor is given by [46]:

$$Q^{-1} = Q_1^{-1} + Q_2^{-1} + Q_3^{-1} + Q_4^{-1} \qquad (I.16)$$

Developing the calculation of magnetic energy and the power dissipated in the walls [47], we have:

$$Q_{wall} = 2\pi f \frac{2\frac{\mu}{4}\int_V \left|\vec{H}\right|^2 dV}{\frac{R_s}{2}\int_S \left|\vec{H}_t\right|^2 dS} \approx \frac{2V}{\delta S} \qquad (I.17)$$

Where R_s is the surface resistance, H_t is the magnetic field tangent to the wall and δ is the skin depth. The integral in the numerator is proportional to volume although the exact value depends on mode type and the chamber size. Similarly, the integral in denominator is proportional to the surface walls. This value of Q_{wall} factor takes into account only the conduction losses in walls.

4.2.6. Delay spread and its relationship with reverberation chamber quality factor

Let us consider a reverberation chamber whose source is a transmitting antenna located inside the cavity. In steady state, the radiated power P_t compensates exactly the total power dissipated in the reverberation chamber. [46]

$$P_t = P_d \qquad (I.18)$$

Using (I.18), (I.22) and (I.25), the average density of power flow $\langle S_c \rangle$ is given by:

$$\langle S_c \rangle = \frac{\lambda Q P_t}{2\pi V} \qquad (I.19)$$

The average power received by a matched antenna located in the reverberation chamber is given by the product of the equivalent surface of an antenna immersed [48] in an isotropic spectrum, and the average density of the power flow $\langle S_c \rangle$:

$$\langle P_r \rangle = \frac{\lambda^2}{8\pi}\frac{\lambda Q P_t}{2\pi V} \qquad (I.20)$$

Finally, the Q factor is obtained rearranging the equation (I.27)

$$Q = \frac{16\pi^2 V}{\lambda^3}\frac{\langle P_r \rangle}{P_t} \qquad (I.21)$$

This Q factor relationship has the advantage of being based on the measured average received power, and therefore includes all dissipation mechanisms present in the reverberation chamber [49].

Consider the case of a reverberation chamber in steady state including a sinusoidal source. This source is suddenly switched off, leading to a decrease of electric and magnetic fields in the chamber. Matching the variation of energy in the cavity to the power dissipated during an interval of time dt, we obtain [46]:

$$dU = -P_d dt \qquad (I.22)$$

Using (I.18) and assuming that this relationship is valid for each moment, we obtain

$$dU = -\frac{\omega U}{Q} dt \qquad (I.23)$$

The resolution of this first order differential equation is obtained through the initial condition $U = U_s$ at t=0, the solution is then:

$$U = U_s e^{-t/(Q/\omega)},\ t > 0 \qquad (I.24)$$

And the delay spread becomes: $\tau_{RMS} = \frac{Q}{2\pi f}$

The parameters described before allow the characterization of measurements performed inside the MSRC. These measurement evaluations are different depending on the desired results.

4.3.OTA measurement procedure

In this section, the MIMO OTA performance evaluation using RC method will be classified in two types of measurement methodologies. The first type is the ***passive measurement*** and the second is the ***active measurement***. Regarding active measurements, two aspects will be distinguished *not real-time active measurements*, and *real-time active measurements*.

4.3.1. Passive measurements

Passive measurements are based on the use of a Vector Network Analyser (VNA). The transmission coefficients (Sij) are then collected in order to evaluate performances of the terminal under test, taking into account only antennas, in terms of diversity parameters such

as: envelope correlation coefficient and diversity gain. In this case several works which carry an interest in the control of fading [50], and the characterization of diversity systems through the use of passive techniques were performed [51]. An example of MIMO OTA passive measurement test bed is shown in figure I.10.

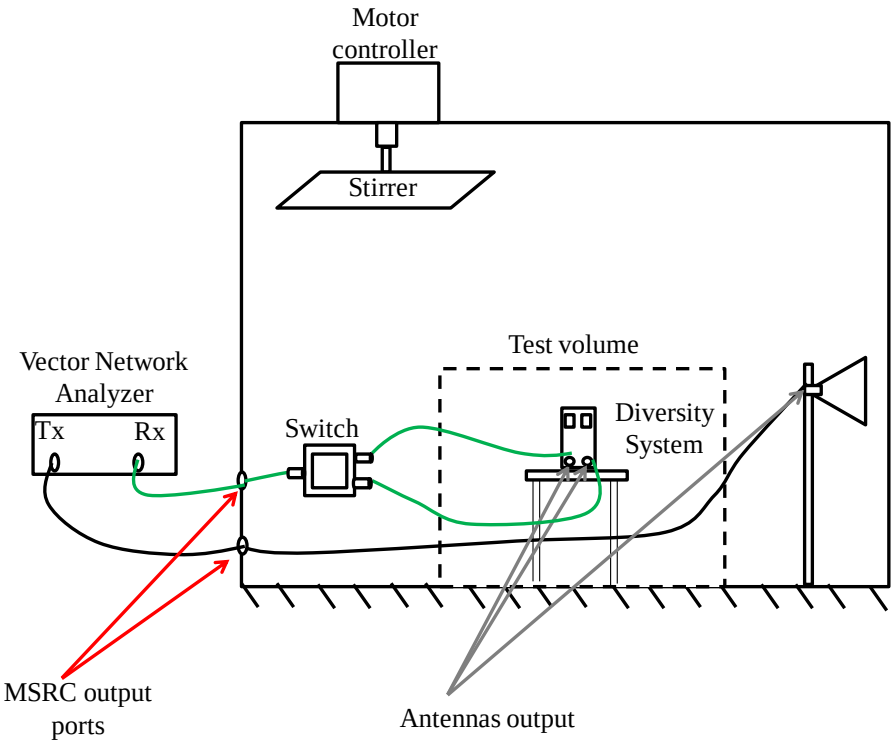

Figure I.10: overview of MIMO OTA passive measurements test bed

Mobile communication systems use antenna diversity. Methods for Characterisation of antenna diversity performance are therefore of interest. Some works has demonstrated diversity performance measurements in typical indoor and outdoor environments [59]. A characterisation method using a mode stirred chamber, with several advantages over passive techniques, is proposed [60]. The repeatability of the method, and the fact that the chamber represents a controlled environment, makes it suitable as a standard test method for diversity characterisation.

The cellular phones performance or wireless terminals operating in multipath propagation environment can be greatly improved by introducing different diversity schemes. The improvement is qualified in terms of a diversity gain. An effective diversity gain is defined in [61]. This is an absolute measure of diversity gain and can therefore be used to compare different diversity antennas. The research studies performed in [62 and 63] also show how the diversity gain can be measured in a mode stirred reverberation chamber.

There is an increasing need to test the operation and functionality of wireless devices in different multipath environments, ranging from line-of-sight environment to a pure Rayleigh environment. Studies in [19, 64, 65 and 66] discuss how a reverberation chamber can be used to simulate a controllable Rician and No-isotropic radio environment. By changing the antenna configurations in the chamber and/or the characteristics of the MSRC, any desired Rician K-factor can be reached. Experimental results are presented in [64, 67 and 68] to illustrate how the reverberation chamber can be used to simulate different multipath environments, and to show the realization of a controlled K-factor test facility.

Reverberation chamber measurements suffer from fluctuations in the average power of a measured sequence. The standard deviation of these fluctuations depends on the independent samples number in the sequence. A common method to estimate this number of independent sample is based on a sample selection technique [69]. With the sample-selection technique, the study [70] has demonstrated the ability of MSCs to accurately emulate Rician-fading distributions. This has been done without any hardware alteration within the MSC for the first time. The obtained data set is composed of unmodified measured samples conforming to a Rician-fading statistical ensemble. The sample-selection technique can further enhance the capabilities of MSCs for MIMO OTA measurements. The technique is patent-protected by EMITE Ing.

4.3.2. Active measurements

Regarding the MIMO OTA active methodology it serves to emulate realistic multi paths propagation channels by considering the fast fading, and the frequency selectivity due to channel delay spread [56, 57, 58]. The performances of the terminal under test are subsequently evaluated, taking into account the antennas and the full transmission chain, SNR, bit error rate (BER), symbol error rate (SER), and frame error rate (FER).

4.3.2.1.Not-real time active measurements

The evaluation of wireless devices in term of BER, FER and SNR does not need to realize measurements in real time. Figure I.11 shows an overview of the test bed that can be used to retrieve the desired figures of merit. As it can be seen, this test bed consists of a generator that allows generating a modulated frame and a receiver that ensures synchronization and

demodulation. So it can be possible to evaluate the performance of the antenna system but also the processing algorithms in reception.

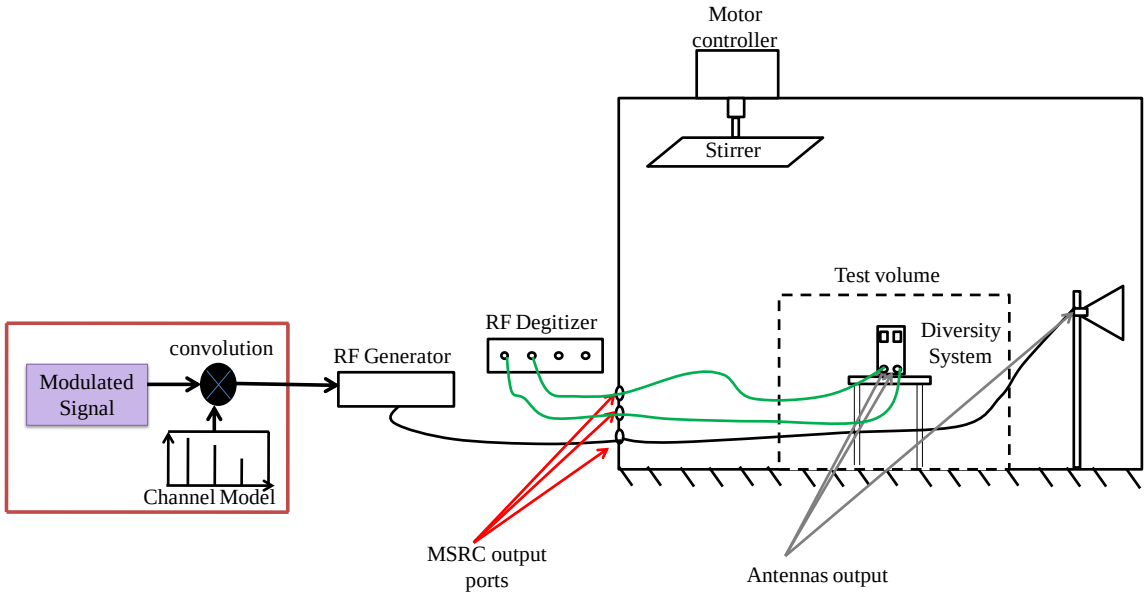

Figure I.11: overview of MIMO OTA No-real time active measurement test bed

Studies taken an interest on this type of measurements were made (it is mentioned here the contribution of Xlim and NIST research institutes). These contributions [71 and 72] show the use of the reverberation chamber to emulate wireless propagation environments including effects such as Doppler spread and narrowband fading. These effects have a significant impact on the wireless channel quality and the capability of a receiver to decode a modulated signal. Different channel characteristics such as power delay profile and RMS delay spread are modified inside the MSRC by introducing different amounts of losses. The studies shown in [71 and 72] illustrate the impact of the chamber configuration on the quality of a wireless communication channel, bit error rate measurements are performed inside the reverberation chamber for different loadings, symbol rates, and paddle speeds.

These studies showed experimentally that loading the chamber decreases the RMS delay spread value. The quality factor of the chamber was measured for different amounts of absorber material, and it is shown that, for a number of absorbers used in measurements, the field uniformity characteristics of the chamber were maintained. RMS delay spread was presented as a function of losses.

These studies showed also that the BER, changed significantly when the chamber is loaded or the paddle speed was changed. Thus, the BER is a function of the channel delay spread [71 and 73]. Using the BER as an indicator, it showed that it is possible to simulate many desired

wireless channel properties. The results achieved in the reverberation chamber were compared to PDP measurements in outdoor. BER measurements inside the chamber were also compared to those made in a low multipath office environment.

4.3.2.2.Real time active measurements

Figures of merit like TIS, TRP and throughput need a real time measurement to be achieved. The test setup (Figure I.12) for testing UE receiver diversity performance is composed of a base station emulator, channel emulator and a reverberation chamber. For these tests a real communication is established between the base station and the user equipment (mobile terminal). The base station generates a modulated signal that will be sent to the channel emulator in order to convolve it with the desired channel model. After the convolution, the signal is sent inside the MSRC through transmitting antenna. The Up-link (UL) signal is recovered by the base station, in order to evaluate the performance parameters of the wireless device.

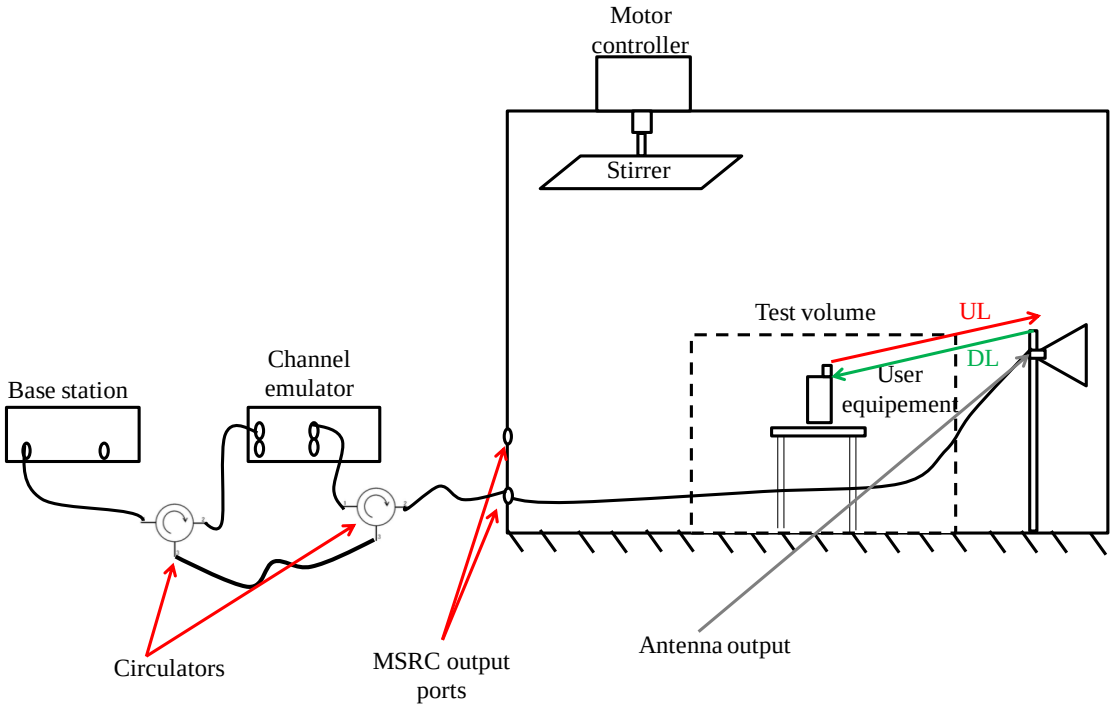

Figure I.12: overview of MIMO OTA real time active measurement test bed

The total isotropic sensitivity (TIS) and throughput are important parameters for the mobile phone, and should be measured by manufacturers and developers.

The measurements of TIS and throughput would take a long time based on the stepping test technique of the Cellular Telecommunications & Internet Association (CTIA).

The authors in [75 and 76] explain two methods to measure receive performance of active mobile terminals by using a reverberation chamber, referred to as total isotropic sensitivity (TIS) and average fading sensitivity. The latter is a new method which can be measured very fast in a reverberation chamber. It is also more representative of the actual performance of a terminal in a real environment than the former. Based on measured results, they conclude that the average fading sensitivity is a promising alternative to TIS measurements for qualification of performance of mobile terminals. The reverberation chamber is well suited for both these measurements. Average fading sensitivity measurements can be done faster than TIS and give similar relative results.

Other study that takes an interest to the throughput evaluation is presented in [76]. This study presents a theoretical model for the throughput data rate of a wireless LTE device. This model includes the improvements of data rate due to the use of the Orthogonal Frequency Division Multiplexing (OFDM) and MIMO techniques under frequency selective fading. The model is based on defining an ideal threshold receiver for the line-of-sight (LOS) case, corresponding to reception with advanced error-correcting codes. The theoretical throughput model is in agreement with measurements in the MSRC of a commercial LTE terminal for the 1 × 2 SIMO case, both regarding diversity and MIMO array gains, and it can therefore be used to complement measured results in performance evaluation of LTE devices.

5. Conclusion

This chapter provides an introduction to MIMO OTA standardization, and describes the different test methodologies under consideration by 3GPP/CTIA. Many different MIMO OTA test methods have been proposed, which vary widely in their propagation channel characteristics, size, and cost. In this chapter, it has been shown that the test methodology adopted in this thesis is the MIMO OTA test methodology based on MSRC. This choice is made for several reasons: the ability to emulate a variety of fading scenarios and the cost effectiveness.

This chapter have shown that the measurement methodologies based on MSRC are classified in two types of measurements. The first type is the passive measurement and the second is the active measurement. Regarding active measurements, two aspects will be distinguished not real-time active measurements, and real-time active measurements.

In the MSRC, the emulation of a channel model encounters two major problems: the first is the control of the delay spread and the second is the control of the spatial parameters. For the second, it can be solved by the emulation of an isotropic environment.

Our first contribution to us in this thesis is manifested in the implementation of a method able to control the delay spread of an emulated channel in the MSRC.

The channel delay spread is strongly linked to the quality factor of the chamber. The first to explore is to control this parameter experimentally, but this solution will be costly in terms of time. A second solution that will make the goal of the second chapter is to control this parameter analytically. This means to develop an analytical model allowing the estimation of the channel delay spread value.

References

[1] Propagation (EuCAP), 2010 Proceedings of the Fourth European Conference on , vol., no., pp.1,5, 12-16 April 2010

[2] Roberto Verdone & Alberto Zanella, Pervasive Mobile and Ambient Wireless Communications, COST Action 2100, Part I, chapter 5 "OTA" Test Methods for Multiantenna Terminals, Springer, 2012.

[3]RP-080766. (2008, Sep.) LS on status of radiated testing methods for MIMO/multiple receive antenna terminals. [Online]. Available: www.3gpp.org/LiaisonsDocs/Outgoing LSs/Rp-41-meeting.htm

[4]M. Rumney, "Efficacy criteria of MIMO OTA test," in COST 2100, 9th MCM, Vienna, Austria, Sep. 2009, TD(09)925. [Online]. Available: www.cost2100.org.

[5] J. Krogerus, P. Makikyro and P. Vainikainen, "Towards an applicable OTA test method for multi-antenna terminals", COST 2100 TD (08)671, Oct 6-8 2008, Lille, France. M. Feogelle, "Over The Air performance testing of wireless devices with multiple antennas", RF Design, February 2006, pp. 44-52.

[6] D. Kurita, Y. Okano, S. Nakamatshu and T.Okada, "Experimental Comparison of MIMO OTA Testing Methodologies", NIT DOCOMO INC, EUCAP 2010, Barcelona, Spain.

[7] J. R. FOERSTER, « The effects of multipath interference on the performance of UWB systems in an indoor wireless channel », in IEEE Vehicular Technology Conference, VTC Spring, Rhodes, Greece, vol. 2, pages 1176–1180, mai 2001.

[8] a Jing, Xu Zhao, Hongwei Kong, Steve Duffy, and Moray Rumney, "Two-Stage Over-the-Air (OTA) Test Method for LTE MIMO Device Performance Evaluation," International Journal of Antennas and Propagation, vol. 2012, Article ID 572419, 6 pages, 2012

[9] Ya Jing ; Zhu Wen ; Hongwei Kong ; Duffy, S. ; Rumney, M.," Two-stage over the air (OTA) test method for MIMO device performance evaluation", International Symposium on Antennas and Propagation (APSURSI), Publication Year: 2011 , Page(s): 71 - 74

[10] 3GPP TSG-RAN WG4, Tdoc R4-093094, Agilent Technologies, "Performance Analysis of Two-Stage MIMO OTA Method versus SCM Approximation Method", ShenZhen, China, August 24–28, August 200

[11]3GPP TSG-RAN WG4, Tdoc R4-093095, Agilent Technologies, "Experimental validation of two-stage MIMO OTA method versus SCM approximation method," ShenZhen, China, August 24–28, August 200

[12] M. Gurumurthy and M. McKernan,"MIMO-OTA Device Testing With Anechoic Chambers", MICROWAVE JOURNAL, MARCH 14, 2011

[13] Pekka Kyösti, Tommi Jämsä, and Jukka-Pekka Nuutinen, "Channel Modelling for Multiprobe Over-the-Air MIMO Testing," International Journal of Antennas and Propagation, vol. 2012, Article ID 615954, 11 pages, 2012

[14] Foged, L.J.; Scannavini, A.; Gross, N.; Estrada, J., "MIMO OTA testing using a multiprobe system approach," Antennas and Propagation (EuCAP), 2013 7th European Conference on , vol., no., pp.1673,1677, 8-12 April 2013

[15] Rudant, L.; D'Errico, R., "Wideband Over-The-Air test-bed reproducing channel delay dispersion characteristics," Antennas and Propagation (EuCAP), 2010 Proceedings of the Fourth European Conference on , vol., no., pp.1,5, 12-16 April 2010

[16] Genender, E.; Holloway, C.L.; Remley, K.A.; Ladbury, J.; Koepke, G.; Garbe, H., "Use of reverberation chamber to simulate the power delay profile of a wireless environment," Electromagnetic Compatibility - EMC Europe, 2008 International Symposium on , vol., no., pp.1,6, 8-12 Sept. 2008

[17] Xiaoming Chen; Kildal, P- S., "Theoretical derivation and measurements of the relationship between coherence bandwidth and RMS delay spread in reverberation chamber," Antennas and Propagation, 2009. EuCAP 2009. 3rd European Conference on , vol., no., pp.2687,2690, 23-27 March 2009

[18]3GPP TR 37.976, Measurement of radiated performance for MIMO and multi-antenna reception for HSPA and LTE terminals (Release 10), version 1.1.0, May 2010.

[19] J. D. Sanchez-Heredia, J. F. Valenzuela-Vald`es, A. M. Martinez-Gonzalez, and D. A. Sanchez-Hernandez, "Emulation of MIMO rician fading environments with mode-stirred reverberation chambers," IEEE Transactions on Antennas and Propagation, vol. 59, no. 2, pp. 654–660, 2011.

[20] J. F. Valenzuela-Vald`es, A. M. Martinez-Gonzalez, and D. A.Sanchez-Hernandez, "Diversity gain and MIMO capacity for non isotropic environments using a reverberation chamber," Antennas and Wireless Propagation Letters, IEEE, vol. 8, pp. 112–115, 2009.

[21] R. COSQUER, Conception d'un sondeur de canal MIMO - Caractérisation du canal de propagation d'un point de vue directionnel et doublement directionnel, Thèse de Doctorat, Institut National des Sciences Appliquées de Rennes, France, 2004.

[22] J. D. PARSONS, The Mobile Radio Propagation Channel, Chichester : Wiley, 2000.

[23] A. AFFANDI, Caractérisation et modélisation de la propagation à l'intérieur des bâtiments dans les bandes de 450 - 900 - 1800 - 2400 – 5800 MHz, Thèse de Doctorat, Institut National des Sciences Appliquées de Rennes, France, 2000.

[24] W. C. JAKES, Microwave Mobile Communications, New York : IEEE Press, 1993.

[25] R. J. M. CRAMER, M. Z. WIN, et R. A. SCHOLTZ, « Impulse radio multipath characteristics and diversity reception », in IEEE International Conference on Communications, Atlanta, GA, USA, vol. 3, pages 1650–1654, juin 1998.

[26] J. R. FOERSTER, « The effects of multipath interference on the performance of UWB systems in an indoor wireless channel », in IEEE Vehicular Technology Conference, VTC Spring, Rhodes, Greece, vol. 2, pages 1176–1180, mai 2001.

[27] S. GAUR et A. ANNAMALAI, « Improving the range of ultrawideband transmission using RAKE receivers », in IEEE Vehicular Technology Conference, VTC Fall, Orlando, FL, USA, vol. 1, pages 597–601, octobre 2003.

[28] Robert W. Stewart and Ian A. Glover Faisal Darbari, MIMO Channel Modelling, Signal Processing, Available from: http://www.intechopen.com/articles/show/title/mimo-channel-modelling ed., ISBN: 978-953-7619-91-6 Sebastian Miron (Ed.), Ed.: InTech, 2010.

[29]P. Almers et al., "Survey of channel and radio propagation models for wireless mimo systems," EURASIP Journal on Wireless Communications and Networking, Volume 2007.

[30] L. Schumacher, K. I. Pedersen, P. E. Mogensen, and F. Frederiksen, J. P. Kermoal, "A stochastic MIMO radio channel model with experimental validation," IEEE Journal on Selected Areas in Communications, vol. 20, no. 6, pp. 1211-1226, 2002.

[31] W. Weichselberger, M. Herdin, H. Ozcelik, and E. Bonek, "A stochastic MIMO channel model with joint correlation of both link ends," IEEE Transactions on Wireless Communications, vol. 5, no. 1, pp. 90-99, 2006.

[32] 3rd Generation Partnership Project 3GPP, "Spatial channel model for Multiple Input Multiple Output (MIMO) simulations (Release 9)," TR 25.996, Technical Specification Group Radio Access Network 2009.

[33]D.S. Baum, J. Hansen, and J. Salo, "An interim channel model for beyond-3G systems: extending the 3GPP spatial channel model (SCM)," in Vehicular Technology Conference, 2005. VTC 2005-Spring. 2005 IEEE 61st , 30 May-1 June 2005 , pp. 3132 - 3136 Vol. 5.

[34] H. El-Sallabi, et al. IST-WINNER D5.4 D.S. Baum, "Final report on link and system level channel models," ver 1.4. Oct.2005.

[35] Kyösti et al., "WINNER II Channel Models," IST-WINNER D1.1.2 p., ver 1.1, Sept. 2007.

[36] K. Bakowski and K. Wesolowski, "Change the Channel ," Vehicular Technology Magazine, IEEE, vol. 6, no. 2, pp. 82-91, June 2011.

[37] COST 231, "Urban transmission loss models for mobile radio in the 900- and 1800 MHz bands," TD(90)119 Rev. 2, Sep 1991[21] H.El-Sallabi, et al. IST-WINNER D5.4 D.S. Baum, “Final report on link and system level channel models,” ver 1.4 Oct.2005.

[38] W. C. JAKES, Microwave Mobile Communications, New York : IEEE Press, 1993.

[39] O. Delangre et al., "Modeling in-Vehicle Wideband Wireless Channels Using Reverberation Chamber Theory," in Proc. IEEE Vehic. Tech. Conf., Sept. 2007, pp. 2149-2153.

[40] Xiaoming Chen; Kildal, P- S., "Theoretical derivation and measurements of the relationship between coherence bandwidth and RMS delay spread in reverberation chamber," Antennas and Propagation, 2009. EuCAP 2009. 3rd European Conference on , vol., no., pp.2687,2690, 23-27 March 2009

[41] Andreas F. Molisch, Wireless Communciations, 2nd ed.: John Wiley and Sons, 2011.

[42] S. O. Rice, "Statistical properties of a sine wave plus random noise," Bell Syst. Tech. J., vol. 27, pp. 109-157, Jan. 1948.

[43] M. Nakagami, "The m-distribution-A general formula of intensity distribution of rapid fading," Statistical Methods in Radio Wave Propagation, pp. 3-36, 1960.

[44] P. Corona, G. Latmiral, E. Paolini, and L. Piccioli, "Use of a reverberating enclosure for measurements of radiated power in the microwave range," Electromagnetic Compatibility, IEEE Transactions on, vol. EMC 18, no. 2, pp. 54–59, May 1976.

[45] A. Richter, "Estimation of radio channel parameters : Models and Algorithms," Ph.D. dissertation, Royal Institute of Technology, KTH, Stockholm, 2005.

[46] D. Hill, M. Ma, A. Ondrejka, B. Riddle, M. Crawford, and R. Johnk,"Aperture excitation of electrically large, lossy cavities," Electromagnetic Compatibility, IEEE Transactions on, vol. 36, no. 3, pp. 169–178, Aug 1994.

[47] U. S. Inan and A. S. Inan, Electromagnetic Waves. Prentice Hall, 2000.

[48] C. Tai, "On the definition of the effective aperture of antennas," Antennas and Propagation, IEEE Transactions on, vol. 9, no. 2, pp. 224–225, Mar 1961.

[49] P. Hallbjorner, "A model for the number of independent samples in reverberation chambers," Microwave and optical technology letters, vol. 33, no. 1, pp. 25–28, 2002.

[50] Hill, D.A., "Probability Density Function of Power Received in a Reverberation Chamber," Electromagnetic Compatibility, IEEE Transactions on , vol.50, no.4, pp.1019,1019, Nov. 2008

[51] Valenzuela-Valdes, J.F.; Martinez-Gonzalez, A.M.; Sanchez-Hernandez, D.A., "Diversity Gain and MIMO Capacity for Nonisotropic Environments Using a Reverberation Chamber," Antennas and Wireless Propagation Letters, IEEE , vol.8, no., pp.112,115, 2009

[52] Z.Ying, "Characterization of multi-channel antenna performance for mobile terminal by using near field and far field parameters", COST 273 TD (04) (095) Goteborg, Sweden, June 2004.

[53] F. Adachi, M.T. Feeney, A.G. Willianson, J.D. Parsons, "Cross correlation between the envelopes of 900 MHZ Signals received at a mobile radio base station site", IEEE Proceedings Radar and Signal Processing, Vol.133, No.6 Part F, pp 506-512, October 1986.

[54] R.G. Vaughan, J. Bach Andersen, "Channels, Propagation and Antennas for Mobile Communications", The institution of Electrical Engineers, Electromagnetic wave series 50, London, United Kingdom, 2003.

[55] R. Janaswamy, "RadioWave Propagation and Smart Antennas for Wireless Communications", Kluwer Academic Publishers, 2001.

[56] Orlenius, C.; Kildal, P- S.; Poilasne, G., "Measurements of total isotropic sensitivity and average fading sensitivity of CDMA phones in reverberation chamber," Antennas and Propagation Society International Symposium, 2005 IEEE , vol.1A, no., pp.409,412 Vol. 1A, 3-8 July 2005

[57] Franzen, M.; Orlenius, C.; Kildal, P- S.; Nilsson, G., "Realized diversity gain of active DECT phones in talk position measured in reverberation chamber," Antennas and Propagation Society International Symposium 2006, IEEE , vol., no., pp.3565,3568, 9-14 July 2006

[58] Kildal, P- S., "Overview of 6 Years R&D on Characterizing Wireless Devices in Rayleigh Fading Using Reverberation Chambers," Antenna Technology: Small and Smart Antennas Metamaterials and Applications, 2007. IWAT '07. International Workshop on , vol., no., pp.162,165, 21-23 March 2007

[59] P. Hallbjörner and K. Madsén, "Terminal Antenna Diversity Characterisation using Mode Stirred Chamber", Electronics Letters, Vol.37, No.5, 1st March 2001.

[60] M. Mouhamadou, M. Koubeissi, C. Tounou et al., "Multiband diversity antenna performances evaluation for multistandard compact wireless terminal," in Proceedings of the 3rd European Conference on Antennas and Propagation (EuCAP'09), Berlin, Germany, March 2009.

[61] Kildal, P.-S., Rosengren, K., Byun, J. and Lee, J, "Definition of effective diversity gain and how to measure it in a reverberation chamber." Microw. Opt. Technol. Lett., 34: 56–59. 2002

[62]Joonho Byun; Donghwan Kim; Juhyung Lee; Kildal, P- S., "Actual diversity gain measured in the reverberation chamber," *Antennas and Propagation Society International Symposium, 2002. IEEE* , vol.3, no., pp.718,, 16-21 June 2002

[63] Kildal, P- S.; Rosengren, K., "Electromagnetic analysis of effective and apparent diversity gain of two parallel dipoles," Antennas and Wireless Propagation Letters, IEEE , vol.2, no.1, pp.9,13, 2003

[64] Holloway, C.L.; Hill, D.A.; Ladbury, J.M.; Wilson, P.F.; Koepke, G.; Coder, J., "On the Use of Reverberation Chambers to Simulate a Rician Radio Environment for the Testing of Wireless Devices," *Antennas and Propagation, IEEE Transactions on* , vol.54, no.11, pp.3167,3177, Nov. 2006

[65] Lemoine, C.; Amador, E.; Besnier, P., "Improved estimation of the K-factor for Rician channels emulation in a reverberation chamber," Antennas and Propagation (EuCAP), 2010 Proceedings of the Fourth European Conference on , vol., no., pp.1,5, 12-16 April 2010

[66] Valenzuela-Valdes, J.F.; Martinez-Gonzalez, A.M.; Sanchez-Hernandez, D.A., "Diversity Gain and MIMO Capacity for Non isotropic Environments Using a Reverberation Chamber," *Antennas and Wireless Propagation Letters, IEEE* , vol.8, no., pp.112,115, 2009

[67] Valenzuela-Valdes, J.F.; Garcia-Ferndndez, M.A.; Martinez-Gonzalez, A.M.; Sanchez-Hernandez, D., "Non-Isotropic Scattering Environments with Reverberation Chambers,"

Antennas and Propagation, 2007. EuCAP 2007. The Second European Conference on , vol., no., pp.1,4, 11-16 Nov. 2007

[68] Valenzuela-Valdes, J.F.; Martinez-Gonzalez, A.M.; Sanchez-Hernandez, D.A., "Emulation of MIMO Nonisotropic Fading Environments With Reverberation Chambers," *Antennas and Wireless Propagation Letters, IEEE* , vol.7, no., pp.325,328, 2008

[69] Sanchez-Heredia, J.D.; Gruden, M.; Valenzuela-Valdes, J.F.; Sanchez-Hernandez, D.A., "Sample-Selection Method for Arbitrary Fading Emulation Using Mode-Stirred Chambers," Antennas and Wireless Propagation Letters, IEEE , vol.9, no., pp.409,412, 2010

[70] Marin-Soler, A.; Gruden, M.; Sanchez-Heredia, J.D.; Hallbjorner, P.; Martinez-Gonzalez, A.M.; Rydberg, A.; Sanchez-Hernandez, D.A., "Sample Selection Algorithms for Enhanced MIMO Antenna Measurements Using Mode-Stirred Reverberation Chambers," Antennas and Propagation, IEEE Transactions on , vol.60, no.8, pp.3892,3900, Aug. 2012

[71] Floris, S.J.; Remley, K.A.; Holloway, C.L., "Bit Error Rate Measurements in Reverberation Chambers Using Real-Time Vector Receivers," Antennas and Wireless Propagation Letters, IEEE , vol.9, no., pp.619,622, 2010

[72] Genender, E.; Holloway, C.L.; Remley, K.A.; Ladbury, J.M.; Koepke, G.; Garbe, H., "Simulating the Multipath Channel With a Reverberation Chamber: Application to Bit Error Rate Measurements," Electromagnetic Compatibility, IEEE Transactions on , vol.52, no.4, pp.766,777, Nov. 2010

[73] Garcia Fernandez M. A., Arsalane N., Mouhamadou M., Carsenat D., Decroze C., Monédière T, "Analysis of antenna diversity performance dependence on multi-antenna channel delay spread in reverberation chamber". Antennas and Propagation (EUCAP), 2012 6th European Conference - EuCAP 2012: the 6th European Conference on Antennas and Propagation, Congress Centre in, Tchèque, République (2012).

[74] Orlenius, C.; Patane, C.L.; Skarbratt, A.; Asberg, J.; Franzen, M., "Analysis of MIMO OTA measurements for LTE terminals performed in reverberation chamber," Antennas and Propagation (EUCAP), 2012 6th European Conference on , vol., no., pp.1934,1938, 26-30 March 2012

[75] Kildal, Per-Simon; Carlsson, Jan, "New approach to OTA testing: RIMP and pure-LOS reference environments & a hypothesis," Antennas and Propagation (EuCAP), 2013 7th European Conference on , vol., no., pp.315,318, 8-12 April 2013

[76] Kildal, P- S.; Hussain, A.; Xiaoming Chen; Orlenius, C.; Skarbratt, A.; Asberg, J.; Svensson, T.; Eriksson, T., "Threshold Receiver Model for Throughput of Wireless Devices With MIMO and Frequency Diversity Measured in Reverberation Chamber," Antennas and Wireless Propagation Letters, IEEE , vol.10, no., pp.1201,1204, 2011

[77]3GPP TS 34.114, Technical Specification Group Radio Access Network; User Equipment (UE) / Mobile Station (MS) Over The Air (OTA) antenna performance; Conformance testing (Release 11), version 11.3.0, 2012.

Chapter II: Channel delay spread estimation in RC based on circuit approach

1. Introduction

In the literature it has been shown that the channel delay spread in RC may be controlled experimentally in RC by adding losses in the chamber. The disadvantage of this method is evident in the measurement time required before obtaining the desired value of the delay spread. Since, the amount of losses to be introduced into the chamber is not known in advance.

An alternative to the experimental approach is to develop an analytical solution able to estimate the delay spread in RC by computing the channel transfer function.

Several methods have been proposed in the literature to model a MSRC. These methods will be described later in this chapter. During this thesis, the choice of a solution based on a circuit approach is done. This solution represents as advantages, the flexibility and the simple implementation.

This chapter aims to develop an analytical model equivalent to the MSRC, based on a circuit approach. This approach takes into account the antennas, losses and stirrers. The analytical model to implement aims to extract the channel transfer function. Knowledge of the channel transfer function will allow retrieving the value of Delay Spread by Inverse Fourier Transform, and by using the equation shown in Chapter I (eq I.5). This analytical simulator will be developed with Matlab©.

This chapter is organized as follows, in section 2, MSRC functioning principle, and brief revue of simulation methods applied to MSRC modelling are shown.

In section 3, working hypotheses and description of the electrical circuit model chosen to estimate the channel transfer function are presented. Losses and stirrer effect modelling are also introduced in this part. Comparisons of simulations results with experimental measurements will be presented in this chapter to check the operation of the implemented Matlab simulator. Finally, a conclusion summarizing the work and representing prospects close this chapter.

2. Functioning principle of mode stirred reverberation chamber

The mode stirred reverberation chamber (MSRC) is composed of a parallelepiped-shaped metal cavity with a high quality factor and large dimensions compared to the wavelength. The MSRC functioning is based on the properties of the resonant cavities. These properties are

described in this part. The resonance conditions of the cavity are changed by rotating a metallic stirrer. This disturbance acts also on the field distribution inside the cavity.

2.1. Modes concept applied to reverberation chamber

The MSRC described in the figure below, is a metallic enclosure containing antennas and stirrer.

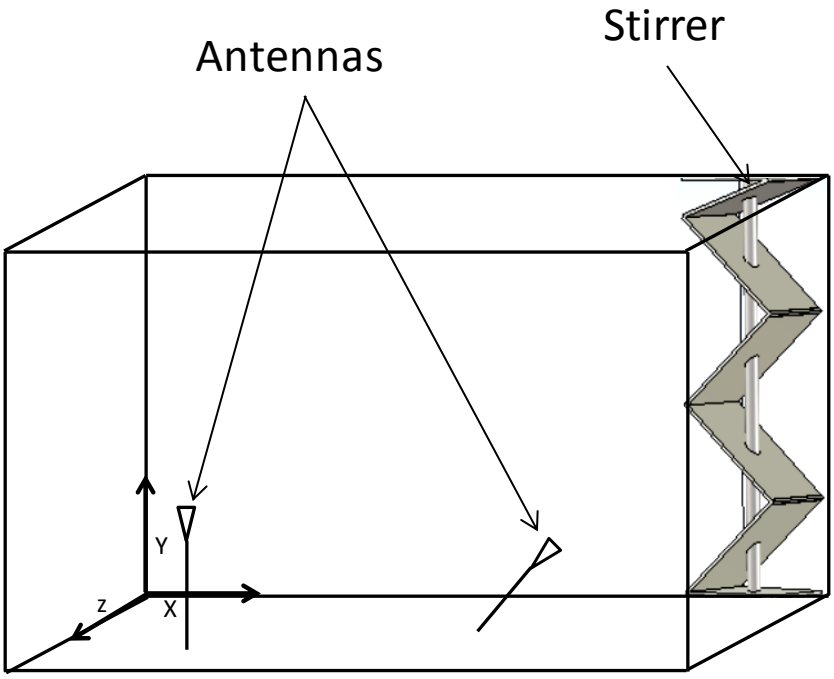

Figure II.1: Modes stirred reverberation chamber overview

Let us consider a parallelepiped metal cavity of dimensions *X*, *Y*, *Z* (Figure II.1). This cavity may be associated to resonant frequencies (I.1) characterized by Eigen modes identified by an integer triplet (*m*, *n*, *p*).

$$f_{mnp} = \frac{c}{2}\sqrt{\left(\frac{m}{X}\right)^2 + \left(\frac{n}{Y}\right)^2 + \left(\frac{p}{Z}\right)^2} \qquad (II.1)$$

Each mode is characterized by a field distribution law determined by Maxwell equations (Appendix I). The modes order m, n, p imply the TE polarization or TM polarization and the existence of modes (Table II.1).

Order	Polarization	No evanescent components
m≥1 n≥1 p≥1	TM	$E_x\ E_y\ E_z\ H_y\ H_z$
m≥1 n≥1 p≥1	TE	$E_y\ E_z\ H_x\ H_y\ H_z$
m≥1 n≥1 p=0	TE	$E_z\ H_x\ H_y$
m≥1 n=0 p≥1	TE	$E_y\ H_x\ H_z$
m=0 n≥1 p≥1	TM	$E_x\ H_y\ H_z$

Table II.1: classification of resonance mode of a cavity

The number of modes and the density of modes are crucial concepts for reverberation chambers functioning. Mathematical developments in [1] provided analytical solutions for the estimation of the evolution of the number of modes N_E (II.2), included in the frequency band lower than the frequency f_{mnp} and the mode density n_E (II.3) according to the frequency f_{mnp}.

$$N_E = \frac{8\pi XYZ}{3c^3} f^3 - \frac{X+Y+Z}{c} f + \frac{1}{2} \qquad (II.2)$$

$$n_E = \frac{dN_E}{df} = \frac{8\pi XYZ}{c^3} f^2 - \frac{X+Y+Z}{c} \qquad (II.3)$$

At high frequencies, the asymptotic behaviour of n_E is similar to the law of Weyl encountered in statistical physics [2]. The density of modes then takes a new expression presented here versus the volume V of the cavity.

$$n_E = \frac{8\pi V f^2}{c^3} \qquad (II.4)$$

This relationship allows estimating again the number of modes N_E (II.5) contained in a frequency band Δf centred around Eigen frequencies that is supposed, according to this interpretation, continuously distributed. This relationship is valid if and only if $\Delta f << f$ [3].

$$N_E \approx \frac{8\pi V f^2}{c^3} \Delta f \qquad (II.5)$$

This formulation indicates that the number of modes N_E contained in a band Δf changes in proportion to the square of the frequency. In fact, an accurate determination of N_E involves a digital counting of modes. This shows that when the frequency is higher, the number of modes which are inserted in Δf band is more important. This property has important consequences for modes stirring.

Under the condition that Δf is very small compared to f, the frequency interval is connected to f (II.6) by the global quality coefficient Q_G of the cavity [4]. In an ideal cavity the global quality factor is infinite. In other hand, the presence of losses in the cavity reduces the quality coefficient and extends the Δf band. Number of available modes N_E is then expressed in terms of the global quality coefficient (II.7).

$$\Delta f = \frac{f}{Q_G} \qquad (II.6)$$

$$N_n = \frac{8\pi V}{c^3 Q_G} f^3 \qquad (II.7)$$

The global quality factor Q_G can be expressed by the power ratio defined by (II.8), where W_{EM} represents the electromagnetic energy stored in the cavity and the P_d the power dissipated in the elements present in the cavity (walls, antennas, DUT, stirrer, ...) [5].

$$Q_G = \frac{2\pi f W_{EM}}{P_d} \qquad (II.8)$$

Another definition (II.9) consist to introduce in equation (II.8) the total electric field E, the permittivity in vacuum ε_0 and the power P_{inj} injected into the emission antenna, supposed well matched over all the frequency band [6].

$$Q_G = \frac{\pi f V \varepsilon_0 |E|^2}{P_{inj}} \qquad (II.9)$$

Antennas, objects located inside the chamber and the dissipation of energy on the walls affect the finale value of the global quality factor. It can possible to associate for each of these absorbing elements a quality factor Q_i. In lower frequencies, the global quality coefficient is dominated by the quality factor related to antennas. In high frequencies, the walls or object located inside the RC that dominate the Q_G [7]. It is easy to show [7] that Q_G is defined by equation (II.10).

$$Q_G = \sum_i \frac{1}{Q_i} \qquad (II.10)$$

2.2. Modes stirring in rectangular metallic cavity

Let ‘us consider a punctual probe located inside the cavity. The amplitude and polarization of the received field at a point is a function of frequency and geometry criteria [8]. Geometric criteria means dimensions of the cavity and the presence of metallic and dielectric objects.

If the cavity is undersized, that means under a frequency equal or near to the first resonance cavity mode, the probability to obtain a field of maximum amplitude for a specific polarization is very low.

At higher frequency, for oversized cavity, this probability is greatly increased because the wavelength is very small compared to dimensions. Thus, for a randomly selected frequency, the probability of exciting the cavity on an Eigen mode is much higher. However, this condition is not sufficient for the observation point to be subjected to the maximum field in the desired polarization.

The following discussion describes the physical principle of modes stirring.

2.2.1. Cavity modes perturbation

The stirrer consists of metal blades fixed to a pivot axis. By changing the angle of the stirrer, a modification of the boundary conditions that can shift the resonance frequencies of the modes is applied. Thus, when the mode density is sufficiently high, the cavity can be coupled whatever the excitation frequency.

The stirring method that gives until now the best test reproducibility seems to be the mechanical stirring method [9]. Mechanical stirring is efficient when excursion engendered on the resonant frequencies allow an overlap between modes. This overlap is easier to obtain at high frequencies, where the modes density is high. By cons, at low frequencies, the excursion caused by the rotation of the stirrer is insufficient. The use of MSRC is therefore submitted to limits at low frequencies, depending on the modes density and therefore the size of the chamber.

The dimensions of the chamber must be in an irrational ratio to avoid a modal degeneration. Indeed, consider the example where two dimensions (X and Y) of the chamber are equal. In this case, the modes with order (m, n, p) and (m', n', p') have the same resonant frequency when $m = n'$ and $n = m'$. The modes are called degenerated and have the effect of reducing the modes density and thus increase the low frequency limit [8].

The quality factor of the cavity plays an important role in the effectiveness of stirring. A low quality factor reduces the amplitude of the available fields. Conversely too large quality coefficient provides high levels of fields, but can affect the efficiency of stirring, particularly in the frequency range where the modes density is low. The number of available modes N_E is reduced.

Modal stirring has other consequences, like when rotating the stirrer, the field distribution in the cavity is disrupted. The variation law of the field amplitude becomes quasi random.

2.2.2. Field distribution inside mode stirred reverberation chamber

To approach these variations laws in simple statistical laws, this analogy imposes certain conditions that are identified. These conditions define the limits of use of MSRC as a test tool.

Consider the case where the wavelength is small compared with dimensions of the chamber (Condition 1). Several modes are excited. The field at a point of the chamber is the vector sum of the contributions of all these modes. By changing the orientation of the stirrer, the way how energy is distributed over each mode is changed. The energy provided to one mode behaves as a random variable towards the orientation of the stirrer.

The basic assumption is that the action of the mode stirrer can applied on DUT maximum amplitude for all polarizations. However, this condition is not strictly satisfied in the extent that it lives an area of uncertainty whose assessment escapes all determinism. Several physical reasons exist.

The principal raison is linked to the recovery of modes. Indeed, the cavity has a quality factor that depends on the power dissipated in the chamber. When the excitation frequency coincides with an Eigen mode, other modes are also excited but with a lower amplitude. Through assumptions derived from the statistical properties of the electromagnetic field, it can be shown that the field is similar to a random variable which distribution is derives from Gauss's law [10].

Cartesian components of the electric field *Ex*, *Ey* and *Ez* are expressed according to equations (II.11) in which *r* and *i* correspond respectively to the real and imaginary components of the complex field.

$$\begin{aligned} E_x &= E_{xr} + jE_{xi} \\ E_y &= E_{yr} + jE_{yi} \\ E_z &= E_{zr} + jE_{zi} \end{aligned} \qquad (II.11)$$

Each of these six complex components is the sum of several random variables.

$$E_x = \sum E_x^{mnp}; E_y = \sum E_y^{mnp}; E_z = \sum E_z^{mnp}; \qquad (II.12)$$

By the central limit theorem, each of these components follows a normal distribution law. This distribution law is centred if there is no direct coupling between the transmitting antenna and the point of measurement [6]. Therefore, the transmitting antenna must be directed to a corner of the room or to the stirrer (Condition 2). The probability density function f (x) of each component is expressed by function (II.13) in accordance with the standard deviations of the variable x, which is associated with each of the complex components.

$$f(x) = \frac{1}{\sigma\sqrt{2\pi}} e^{\frac{x^2}{2\sigma^2}} \qquad (II.13)$$

From this expression, we can define the probability density function of squared amplitude of a cartesian component of field (II.14). This variable is the sum of the squares of two random variables that follow a normal distribution. Its distribution law follows a law of χ^2 with two degrees of freedom [11]. The expression of the probability density of the squared amplitude is given for cartesian component *Ex* by equation (II.15), but it can be extended to Cartesian components *Ey* and *Ez*.

$$|E_x|^2 = E_{xr}^2 + E_{xi}^2 \qquad (II.14)$$

$$f(|E_x|^2) = \frac{1}{2\sigma^2} e^{\frac{|E_x|^2}{2\sigma^2}} \qquad (II.15)$$

The quadratic amplitude of the total field (II.16) also follows a known distribution: the law of χ^2 with 6 degrees of freedom (II.17).

$$|E|^2 = E_{xr}^2 + E_{xi}^2 + E_{yr}^2 + E_{yi}^2 + E_{zr}^2 + E_{zi}^2 \qquad (II.16)$$

$$f(|E|^2) = \frac{|E|^4}{16\sigma^2} e^{\frac{|E|^2}{2\sigma^2}} \qquad (II.17)$$

If the distribution law of a component is centred, the average amplitude component is equal to zero (II.18).

$$\langle E_{xr} \rangle = \langle E_{xi} \rangle = \langle E_{yr} \rangle = \langle E_{yi} \rangle = \langle E_{zr} \rangle = \langle E_{zi} \rangle = 0 \qquad (II.18)$$

The assumption of a completely disordered field implies that these variables are independent and follow the same distribution law provided that the measuring point is sufficiently far from the metal walls. Indeed, near the walls, the tangential component of the electric field becomes zero and the field components then have different mean square amplitude. By cons, in an area called useful test volume, the mean square amplitude of each component is identical (II.19) and is equal to (II.20). This useful volume is placed at a certain distance from the walls (Condition 3).

$$\langle E_{xr}^2 \rangle + \langle E_{xi}^2 \rangle + \langle E_{yr}^2 \rangle + \langle E_{yi}^2 \rangle + \langle E_{zr}^2 \rangle + \langle E_{zi}^2 \rangle = E_0^2 \qquad (II.19)$$

$$\langle E_{xr}^2 \rangle = \langle E_{xi}^2 \rangle = \langle E_{yr}^2 \rangle = \langle E_{yi}^2 \rangle = \langle E_{zr}^2 \rangle = \langle E_{zi}^2 \rangle = \frac{E_0^2}{6} = \sigma^2 \qquad (II.20)$$

These components have the same law of distribution and the same variance σ^2, they produce the same statistical dispersion of their maximum amplitude.

These relationships reveal two essential properties of modes stirred reverberation chamber: isotropy and uniformity of the field on a revolution of stirrer. Components have the same mean-square amplitude, the same maximum value and the same law of distribution over a revolution of stirrer. The field that illuminates the DUT is isotropic. DUT is subject to all its faces to the same maximum amplitude over a revolution of stirrer. Components observe the same amplitude and the same distribution regardless the point of observation, provided that this point is within the useful volume. The field in the working volume is uniform over a stirrer tour. The DUT can be placed anywhere in the useful volume.

In this part, a presentation of the behaviour of EM fields in the MSRC was made. It was mentioned that the mechanical stirring is an effective tool to install the isotropy and uniformity in the chamber. Mechanical stirring represents the type of stirring adopted during experimental works carried out in this thesis. It was also mentioned that we can assimilate the stirring operation at a change in the dimensions of the cavity.

The reverberation chamber is a statistical tool which may require many samples for some measurements. From a pragmatic point of view, modelling allows the simulation of experiments and measurements that can be long when the number of stirrer positions, the number of excitation frequencies and even the number of the source position in the room increased. A model allows the study of chamber under conditions where the measurements may be difficult: at low frequency, near the walls, etc. As the MSRC can be used to simulate the propagation channels, modelling can help to deduce the channel parameters.

Deterministic models, as models of statistical nature have their own limits and the field of investigation is still important. Between these two options, it is interesting to develop simple physical models, integrating physical parameters to describe the statistical behaviour of a reverberation chamber as faithful as possible. Physical simulation of a reverberation chamber allows understanding physical functioning by giving meaning to the observations achieved through measurement campaigns. In addition, physical models allow measure the influence of physical parameters on the behaviour of the chamber and so make theoretical assumptions about the physical functioning of a reverberation chamber. In the following an overview of MSRC modelling methods that exists is shown.

2.3. Brief revue of simulation methods applied to MSRC modelling

The simulation of the electromagnetic field inside a MSRC is a complex problem because of the large number of variables involved. Many methods have been proven. These methods can be distinguished into two categories, deterministic and statistical methods. For deterministic methods there are finite differences method and method of moments, which solve Maxwell's equations. These methods require the implementation of powerful computers but provide an accurate representation of the electromagnetic environment. On the other hand methods based on statistics, as the superposition of plane waves were used. These methods easier to implement, do not allow an accurate characterization of the intrinsic environment of reverberation chambers. The choice of the method will depend on the desired application.

2.3.1. Finite difference method in time domain

The FDTD (Finite Differences in Time Domain) method aims to simulate by finite difference in time domain the propagation of the electrical and magnetic fields from the Maxwell equations. Using Fourier transform, the results can be transposed into the frequency domain. The geometry of the object is discretized by parallelepiped mesh. The mesh is called improper because it does not correctly follow the geometry of the object. The dimensions of meshes are inversely proportional to the maximum study frequency. Frequency study requires a fine mesh of the object and therefore increases of the computation time.

The excitation of the chamber by a pulse type signal provides an answer on a wide frequency band and thus a modal analysis of the chamber [12]. In addition, this method allows the calculation of the quality factor.

However, for a resonant structure as is currently the case, the calculation time must be very long to reach a convergence of the results.

The simulation of the stirrer rotation is possible. The mechanical stirrer can be represented, but rudely if the stirrer has a particular shape, to not prohibitively increase the computation time. In addition, an overall calculation can be performed for each stirrer position. The researchers, who have used the FDTD method to simulate the rotation of the stirrer, have made calculations for a small number of stirrer positions (8 simulation positions used by L. Bail in [13]).

The FDTD method allows calculation of the fields only on the grid discretization. So the field cannot be calculated anywhere in the cavity unless if we use interpolation methods. In addition, the number of points where the field is calculated is limited by the storage capacity of used computers.

2.3.2. Transmission line method

TLM (Transmission Line Matrix) method is a space-time discretization of Maxwell's equations. The propagation of electromagnetic waves is supported by a dummy network of orthogonal transmission lines. The junctions between the transmission lines are characterized by S matrix.

The mesh is non-compliant and its dimensions are inversely proportional to the maximum of study frequency. The modelling of reverberation chambers were represented either by two dimensions to simulate mechanical stirring [14], or three-dimensional to simulate an electronic stirring [15].

2.3.3. Finite elements method

The Finite Element Method (FEM) requires discretization of the study domain by volume elements, generally tetrahedral form. The method aims to solve at each node relative to the elements of discretization, the propagation equation (II.1) resulting from Maxwell's equations.

$$\nabla * \left(\frac{1}{\mu} \nabla * E_{(x,y,z,t)} - k_0^2 \varepsilon E_{(x,y,z,t)} \right) = 0 \qquad (II.21)$$

Where: μ: permeability

ε: permittivity

k_0: wave vector in the vacuum

$E_{(x, y, z, t)}$: Electric field

This method is a volumetric method and therefore requires the discretization of study volume in its entirety. The internal volume of the reverberation chamber must be meshed. By cons, the mesh by non-rectangular elements can be according to the geometry of the object. The dimensions of the elements are inversely proportional to the frequency study.

FEM method is a frequency method used to simulate reverberation chambers. An overall calculation must be performed for each frequency. It does not conduct to a broadband study. In the case of cavities, usually frequency calculation doesn't coincide with a resonant frequency [16].

2.3.4. Boundary finite elements method

The BEM (Boundary Element Method) method is an adaptation of the finite element boundary method in the frequency domain, taken from the method of moments. It requires discretization of the structure studied by surface elements, usually form triangular. This method is based on the integral formulation of the radiated field. This frequency method doesn't allow broadband frequency exploration of the response of the chamber. Calculations are performed globally at discrete frequencies. Except using interpolation or derivation methods, this method can't access to direct calculation of the quality factor.

One advantage of this method, excluding modelling of reverberation chambers is taking into account the radiation problems intrinsically, that means without approached conditions to truncate the spatial domain of study around the studied object, as this is done in FDTD, TLM

and FEM methods. In addition, the field can be calculated everywhere at infinity or near the surfaces of the structure.

A major advantage of this method is in its surface character allowing lightens mesh manipulation and description of complex objects. The action of mechanical stirrer is simulated, but it requires rather long calculations. Some developments of the method, such as partial assembly, are used to simulate the stirrer rotation for more reasonable computing time.

2.3.5. Ray tracing method

Ray Tracing Approach (RTA) aims to consider that the field at a point is the sum of the field directly obtained from the source and field of the rays reflected from the walls. The field reflected by a wall is calculated by the image theory. This same field is mitigated by the reflection coefficient assigned to the wall.

The Walls of the chamber have a high conductivity and therefore a reflection coefficient near to 1. The number of images required to reach the convergence is very important. It is therefore recommended to reduce strongly the reflection coefficient [17] or limit arbitrary the number of reflections on the walls, which is equivalent to introduce "numeric losses" [18].

This method can only be used in high frequency, because the advantage of this theory appears when the conditions of geometrical optics are satisfied. This is an advantage in that the methods mentioned above do not allow simulations at high frequencies. This method is complementary to the previous as it is hardly applicable to the simulation of reverberation chambers for the first resonance modes.

Nevertheless, the calculations are performed at discrete frequencies. Calculation of cavity relaxation time, by combining images number and propagation time of waves, allows determining the constant of time τ. This constant is used to evaluate (II.2) directly the quality factor Q [17]. But to get the value of the quality factor, it's necessary to calculate a large number of images and thus increase the computation time.

$$\tau = \frac{Q}{\omega} \qquad (II.22)$$

A global calculation for each stirrer position is necessary to simulate the rotation of the stirrer. The computation time also becomes very long.

2.3.6. Plane wave spectrum method

The Plane Wave Spectrum (PWS) method means Spectrum or Overlaying planes waves. Its principle aims to assume that the field at a point in the reverberation chamber is represented by a summation of plane waves. The amplitude and phase of each plane wave are considered as random variables that depend on the position of the stirrer.

The calculations are performed at discrete frequencies. A development of this method allows access to the quality factor of the chamber [19]. It is based on the Kern theory calculated from S matrix (Scattering Matrix). Each S matrix is associated to a plane wave with a given incidence and polarization [10]. It is particularly suitable to the calculation of coupling on the receiving antenna or for the equipment under test [20, 21].

The PWS method to be representative of reverberation chambers, considers that the field is perfectly uniform and isotropic. This implies that the density of modes is high. It is devoted exclusively to high frequencies. This method alone can therefore not be interested in the operating limits of the reverberation chamber at low frequencies.

The statistical hypothesis requires that the coupling calculations cannot be performed only in terms of mean values. The maximum values can only be obtained from estimates. The PWS method providing the distribution law of the field or the current on the antennas, these estimates are made through the determination of PDF (Probability Density Function).

But the estimates of the maximum field values from PDF conclude that, if the number of samples of field converges to infinity, then the maximum field also converges to infinity.

Therefore it cannot be possible to obtain an exact value of the maximum values of coupling based only on statistical principles. However, if this method is based on experimental results, the determination of the maximum values is possible. In addition, a major advantage of this method is that, as statistics, it does not require large calculation. The computation times compared to a deterministic method are greatly reduced [20].

2.3.7. Image theory method

This modelling method is based upon image theory [22]. In [23], a representation of a rectangular waveguide through image theory is given. This model is an adaptation of this model of a waveguide to the geometry of a rectangular cavity. It consists in closing the waveguide by adding two boundary conditions. In the model, an elementary current is placed in the cavity. The positions and the angular orientations of image-current created by the

reflective walls must be determined. This very straightforward model does not directly involve Maxwell's equations or a spatial discretization of the environment. It fits the simple geometry of a shielded cavity. It only uses the far-field and free-space radiation approximation of millions of elementary currents to represent a complex interaction between elementary current and electrical conductor boundaries.

The core of the simulation is an impulse response. By convolving the impulse response with a chosen waveform, the model is able to simulate the behaviour of the RC with a particular waveform. By applying a Fourier transform on the impulse response, we can explore the frequency domain. The rough representation of the RC by a rectangular shielded cavity without a mode stirrer is too elementary to obtain deterministic results. But it has been shown that source stirring is equivalent to mechanical stirring [24]–[25] and so from a statistical point of view taking randomly N receiver positions is equivalent to taking N stirrer positions. In our model, the stirrer is not described but its absence will not affect the statistics of the results as long as the receiver positions are taken randomly.

The modelling methods presented above show a certain degree of complexity to implement. This complexity is reflected in the time required to complete these simulations (since the number of needed mesh cells is in the order of 10^6). Because of this we thought of setting up a new flexible, simple method, based on a circuit approach.

The objective is to implement an analytical model, with reduced calculation time, that takes into account the metallic cavity, losses, antennas, and the statistical aspect of the stirrers.

3. Mode stirred reverberation chamber modelling based on circuit approach

In this section, we propose a frequency domain model of reverberation chamber. The aim of this model based on a circuit approach is to allow simulating (under matlab) the behaviour of metallic cavity in order to determine the channel transfer function. After the introduction of this model, results of different configurations are presented and compared to simulations made with the CST Microwave Studio software, and measurements. The figure II.2 below represents the MSRC to model.

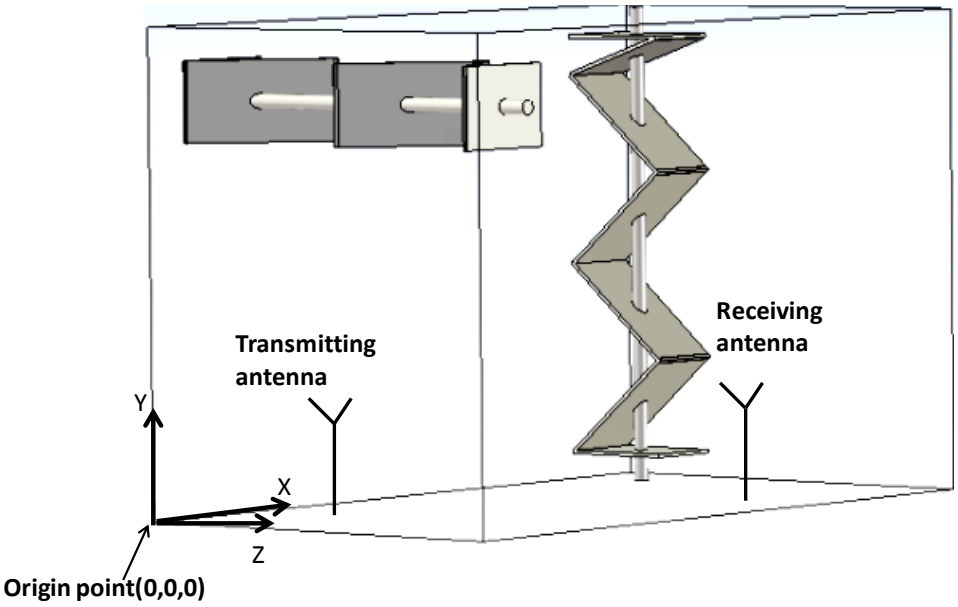

Figure II.2: Overview of the system to be modelled

3.1. Circuit model description

This section aims to obtain an equivalent circuit model of the cavity and set up an analytical method allowing the determination of the equivalent circuit elements.

Several modes can be excited in an oversized cavity. Thus, in order to understand the functioning principle of cavities from a circuit approach, it will be interesting to start by studying the equivalent circuit model for a single resonance mode.

3.1.1. Equivalent circuit model for one resonance mode

In our circuit approach, the resonators can be modelled in discrete elements, such as an LC circuit.

This circuit resonates at a frequency: $f_0 = \frac{1}{2\pi\sqrt{LC}}$ (*II*.23)

At this frequency, the electric energy stored in the capacitor C is equal to the magnetic energy stored in the inductor L.

Taking into account losses in the resonator, this cavity is equivalent to *R*, *L*, *C* circuit distributed in a series or parallel.

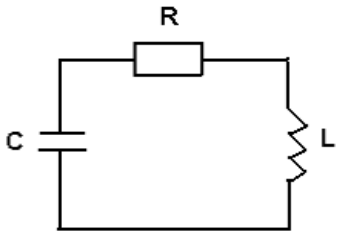

Figure II.3: Equivalent circuit for resonator with losses

This equivalent circuit present the same resonant frequency and the same quality factor namely:

$$\begin{cases} LC\omega_0^2 = 1 \\ \dfrac{L\omega_0}{R} = Q_0 \end{cases} \qquad (II.24)$$

During this study, a choice of setting the parameter *C* is done. The value *C* can be expressed by:

$$C = \frac{XY}{4\mu_0 c^2} \cdot \frac{1}{Z} \quad [26] \qquad (II.25)$$

X, Y and Z *are* the dimensions of the cavity.

μ_0 is the vaccum permeability.

c is speed of light.

The writing of equations (II.24) and (II.25) lead to the determination of the three parameters *R, L,* and *C* constituting the equivalent circuit of a single mode. The resonant frequency and the quality factor can be analytically calculated using the equations (II.1) and (II.26).

$$Q_0 = \frac{3V}{2S\sqrt{\dfrac{2}{\mu\omega\sigma_w}}} \qquad (II.26)$$

Where:

V is the volume; *S* is the surface, μ the permeability, and σ_w the conductivity of walls.

In our case, the cavity is coupled by transmitting antenna and the receiving antenna that are positioned inside the metallic cavity. In Figure II.4, the transformer of access 1 represents the

coupling between the transmitting antenna and the excited mode inside the cavity. At the access 2, the second transformer represents the coupling between the excited mode in the cavity and the receiving antenna.

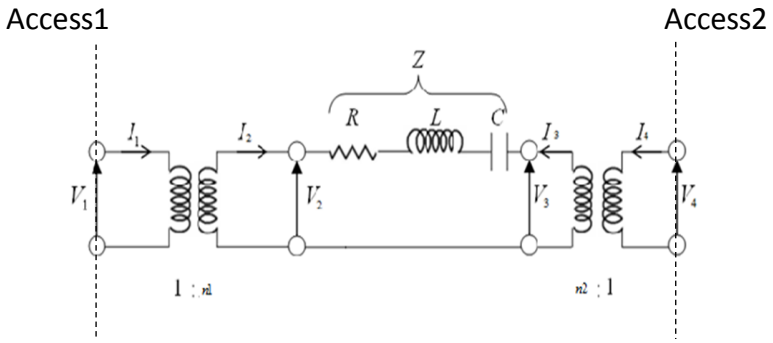

Figure II.4: Equivalent model for a single coupled mode

In order to solve this problem, the model above will be used, with *n1* the transformation ratio at access1 and *n2* at access 2.

The application of the Kirchhoff's law allows drawing the following equations:

$$\frac{V_1}{V_2}=\frac{1}{n_1}\ ;\ \frac{I_1}{I_2}=n_1\ ;\frac{V_3}{V_4}=n_2\ ;\ \frac{I_3}{I_4}=\frac{1}{n_2};\qquad (II.27)$$

$$\begin{Bmatrix} V_2=n_1V_1 \\ I_1=n_1I_2 \\ V_3=n_2V_4 \\ I_4=n_2I \end{Bmatrix}\ ;\ \text{Then:}\ \begin{Bmatrix} V_3=V_2+ZI_3 \\ I_2=I_3 \end{Bmatrix}$$

The use of these two systems of equations aims to express *V4* and *I4* versus *V1* and *I1*.

$$I_1=n_1I_2=n_1I_3\ ;\ I_4=n_2I_3=n_2\frac{I_1}{n_1}\qquad (II.28)$$

$$V_4=\frac{V_3}{n_2}=\frac{1}{n_2}(V_2+ZI_3)=\frac{1}{n_2}(n_1V_1+Z\frac{I_4}{n_2})\qquad (II.29)$$

From (II.28) and (II.29), the characteristics relationships of the model are [27]:

$$\rightarrow V_4=\frac{1}{n_2}(n_1V_1+Z\frac{n_2}{n_1n_2}I_1)=\frac{1}{n_2}(n_1V_1+Z\frac{I_1}{n_1})\ \rightarrow\begin{Bmatrix} V_4=\frac{1}{n_2}(n_1V_1+Z\frac{I_1}{n_1}) \\ I_4=n_2\frac{I_1}{n_1} \end{Bmatrix}\qquad (II.30)$$

A. Channel transfer function expression for one coupled mode

The transmission coefficient can be estimated by calculating S-parameters. All of the currents and voltages must be normalized to the characteristic impedance Zc.

$$v1 = \frac{V_1}{\sqrt{Z_0}} \; ; \; i_1 = \sqrt{Z_0} I_1 \; ; \; v_4 = \frac{V_4}{\sqrt{Z_0}} \; ; \; i_4 = \sqrt{Z_0} I_4; \qquad (II.31)$$

v and i are normalized voltage and current.

S-parameters connect the reflected waves and the incident waves.

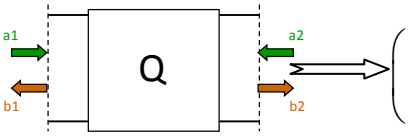

$$\begin{pmatrix} b_1 \\ b_2 \end{pmatrix} = \begin{pmatrix} S_{11} & S_{12} \\ S_{21} & S_{22} \end{pmatrix} \begin{pmatrix} a_1 \\ a_2 \end{pmatrix} \qquad (II.32)$$

They can be expressed in terms of voltages and currents, by following relations:

$$\left\{ \begin{matrix} v_1 = a_1 + b_1; v_4 = b_2 + a_2 \\ i_1 = a_1 - b_1; i_4 = b_2 - a_2 \end{matrix} \right\} \qquad (II.33)$$

To obtain the S parameters, it is necessary to express *b1* and *b2* versus *a1* and *a2*.

After normalization of voltages and currents, and replacing of voltage and current by the incident and reflected waves, the equation system (II.30) becomes.

$$\left\{ \begin{matrix} b_2 + a_2 = \frac{n_1}{n_2}(a_1 + b_1) + \frac{z}{n_1 n_2}(a_1 - b_1) \\ b_2 - a_2 = \frac{n_2}{n_1}(a_1 - b_1) \end{matrix} \right\} \qquad (II.34)$$

By developing the system of equations expressed in (II.34), the transfer function becomes

$$S_{12} = \frac{2n_1 n_2}{n^2{}_1 - z + n^2{}_2} \rightarrow S_{21} = \frac{2n_1 n_2}{n^2{}_1 + n^2{}_2 + z} \qquad (II.35)$$

Writing the expression of normalized impedance z of the equivalent resonant mode, and introducing the coupling coefficients (on transmission side and reception side) which are expressed by:

$$\alpha_1 = \frac{Q_0}{Q_{e1}} = \frac{n^2{}_1 Z_c}{R} \qquad (II.36) \; ; \quad \alpha_2 = \frac{Q_0}{Q_{e2}} = \frac{n^2{}_2 Z_c}{R}; \qquad (II.37)$$

Where Q_{e1} and Q_{e2} present the extern quality factors related to the coupling.

The global quality factor is:

$$\begin{cases} \frac{1}{Q_L} = \frac{1}{Q_0} + \frac{1}{Q_{e1}} + \frac{1}{Q_{e2}} = \frac{1}{Q_0} + \frac{\alpha_1}{Q_0} + \frac{\alpha_2}{Q_0} \\ Q_L = \frac{Q_0}{1+\alpha_1+\alpha_2} \end{cases}; \qquad (II.38)$$

The frequency evolution of the channel transfer function becomes:

$$S_{21} = \frac{2n_1 n_2 \frac{z_c}{R}}{\frac{z_c}{R} n^2{}_1 + \frac{z_c}{R} n^2{}_2 + (1 + 2jQ_0 \frac{\Delta f}{f_0})} = \frac{2\sqrt{\alpha_1 \alpha_2}}{1+\alpha_1+\alpha_2} * \frac{1}{1+2jQ_L \frac{\Delta f}{f_0}} \qquad (II.39)$$

B. Determination of transformation ratio

The estimation of the channel transfer function is insolvent, as the determination of the transformation ratios is not made. The following part will be devoted to the implementation of an analytical method capable of determining these transformation ratios.

The model circuit shown in Figure (II.4) can be assimilated to the schematic below. This schematic shows the nature of the problem to be solved.

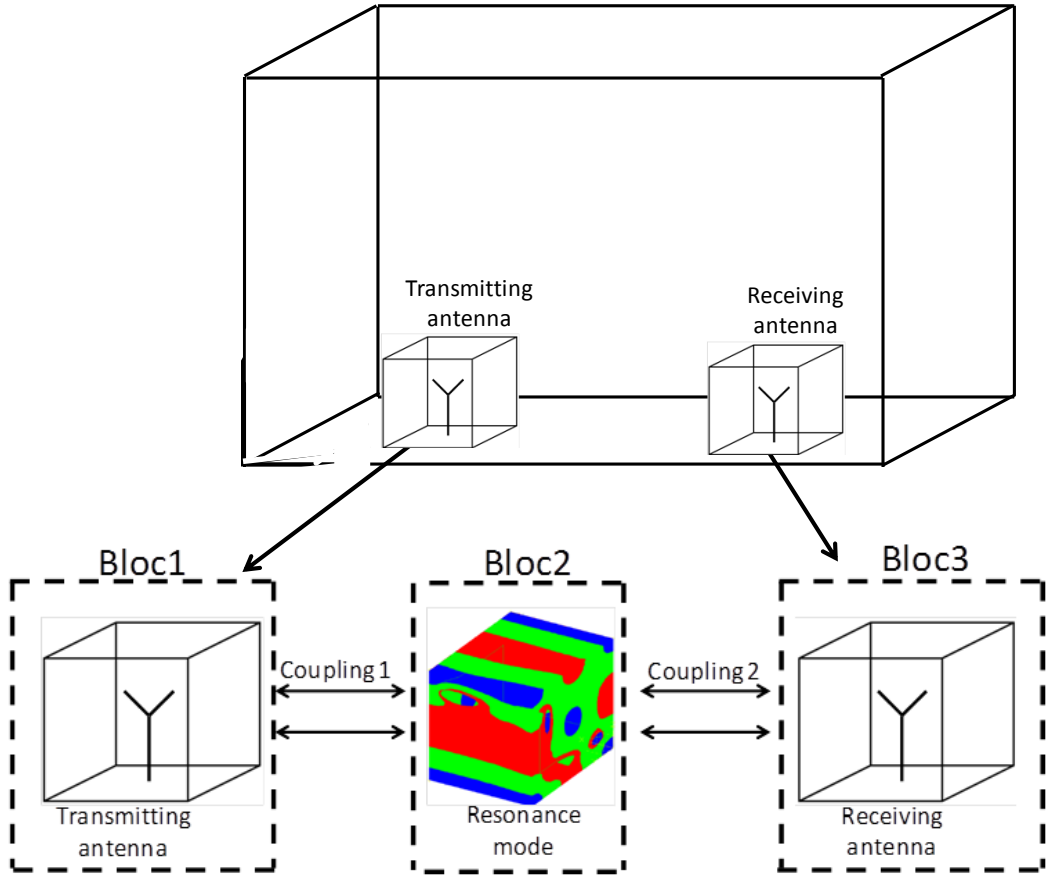

Figure II.5: Concept of the study

The determination of the transformation ratios is the main part of the analytical calculation method to implement. Since this determination in principle allows to calculate the coupling whatever the type of used antenna.

The interaction between the antenna and the mode excited inside the MSRC is expressed by a coupling (figure II.5). Coupling1 and coupling2 in Figure II.5 can be explained physically by transformers. These transformers possess a transformation ratios *n1* and *n2* (as showed in figure II.4).
Before introducing the calculation method of the transformation ratios, it can be noted that this method needs the achievement of two previous steps.

- ***Step1***

  This step (figure II.6) concerns the simulation of antenna used in the MSRC. The simulation is carried out under CST Microwave studio in a small volume, with a very fast simulation time.

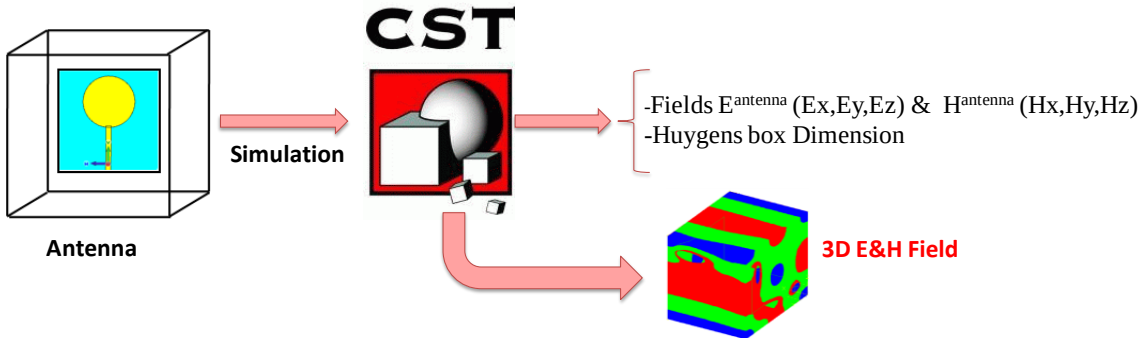

Figure II.6: Antenna simulated under CST Microwave Studio

This simulation allows extracting the values of near fields (E and H) across a volume that surrounds the antenna (Huygens box). This volume is discretized in several meshes; each mesh contains the three Cartesian components of electric field $E^{antenna}$ and magnetic field $H^{antenna}$. The calculation volume of the antenna (Huygens box) should, of course, not exceed the volume of calculation of the metallic cavity.

To optimize the calculation time, the Huygens-Fresnel theorem is applied. The principle formulated by Huygens and Fresnel is that the field at any point in space can be derived from equivalent sources around the radiation sources. The near fields calculated in the antenna volume can be then replaced by surface currents J_e and *Jm* as follow:

$\vec{J}_e = (\vec{n} \wedge \vec{H}^{antenna}).ds;\ \vec{J}_m = -(\vec{n} \wedge \vec{E}^{antenna}).ds;$

Where $\vec{J}_e$ and $\vec{J}_m$ present the electric and magnetic currents. ds is a surface element

- ***Step 2***

This step aims to determine the modal distributions inside the mode stirred reverberation chamber. Concerning modes distributions, they are obtained from analytical calculation performed with Matlab©. As depicted in (Figure II.7) to perform this calculation, the Matlab simulator needs to know the resonance frequencies and the cavity dimensions.

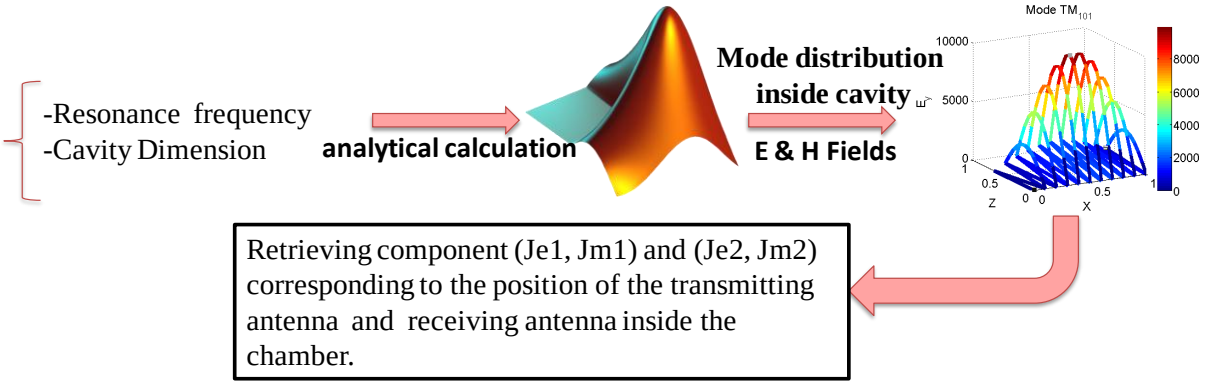

Figure II.7: Resonance mode calculated analytically

At first, the field distribution of the resonance mode excited in the cavity is calculated. After, a calculation volume corresponds to the positions of the transmitting and receiving antennas are recovered. This calculation volume should be similar in size to that of the antenna simulated under CST Microwave Studio.

To reduce the calculation time, the Huygens theorem is applied another time. The field distribution of the resonance mode at position 1 (transmitting antenna) and position 2 (receiving antenna) can be then replaced successively by surface currents couples (J_{m1},J_{e1}) and (J_{m2},J_{e2}).

- **Principle of calculation method**

In this section, we will introduce a calculation method of the transformation ratios. This method is based on the reciprocity theorem. The calculation volumes obtained previously are discretized to several meshes.

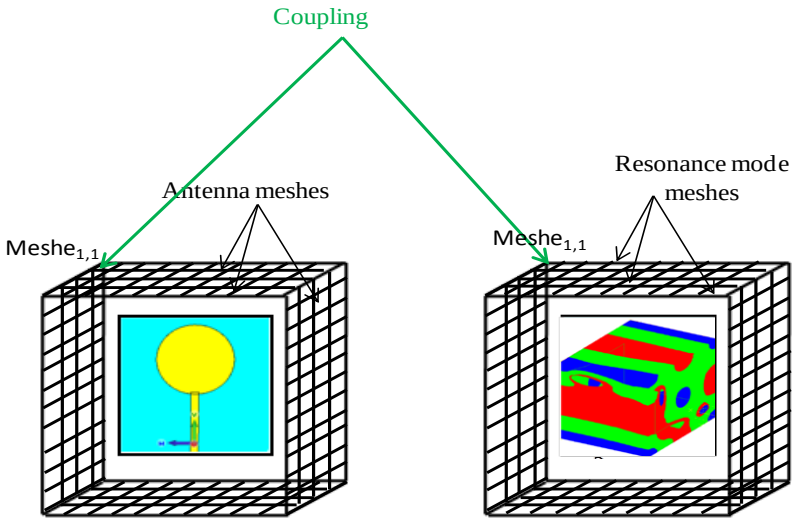

Figure II.8: coupling method

Firstly the transformation ratios calculation is performed between each corresponding meshes of the discretized antenna volume and the discretized resonance mode volume (figure II.8). The final transformation ratio will be the sum of transformation ratios calculated over all meshes. The transformation ratio calculation principle is based on reciprocity theorem.

The generalization of Reciprocity theorem to all linear and passive systems based on electromagnetism, other than single circuits, establishes some relationships between concepts that involve, by definition, reciprocity. This applies in particular to the transmission and reception of information in transmission systems using antennas.

The figure below shows the principle scheme of coupling between block 1 or 3 and block 2, while making use of the reciprocity theorem.

Block 1, Block 2 and Block 3 depicted in figure II.5 represent successively the transmitting antenna, the receiving antenna and the resonance mode.

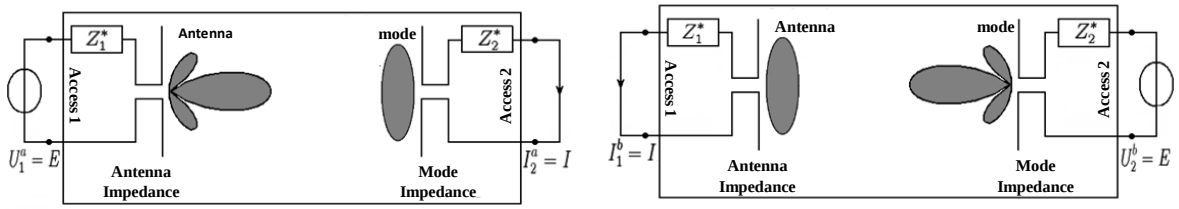

(a) (b)

Figure II.9: Equivalent quadruple

The two situations described above, where a complete transmission system with antennas is treated as an equivalent quadruple, shows the role of each one of the elements (antenna or

mode) in transmission or reception, that can be reversed by simply swapping the two accesses.

The reciprocity theorem implies the following relation

$$\sum_{k=1}^{N} U_k^a . I_k^b - U_k^b . I_k^a = 0$$

$$U_1^a . I_1^b + U_2^a . I_2^b - U_1^b . I_1^a - U_2^b . I_2^a = 0 \qquad (II.40)$$

$$U_1^a . I_1^b + U_2^a . I_2^b = U_1^b . I_1^a + U_2^b . I_2^a \qquad (II.41)$$

U_1^a voltage that appears at access 1 when the antenna radiates to the resonant mode.

U_2^a voltage that appears at access 2 when the antenna radiates to the resonant mode.

U_1^b voltage that appears at access 1 when the resonance mode radiates to the antenna.

U_2^b voltage that appears at access 2 when the resonance mode radiates to the antenna.

By analogy, the equation II.41 can be expressed in electromagnetic domain.

The correspondence can be made between the Voltage (*U*) and the electric field (E), and between the current (*I*) and the magnetic field (*H*).

Taking into an account the vector nature of the values of Electric and magnetic fields of antennas and Mode, equation (II.41) becomes:

$$\left(\vec{E}_1^a \wedge \vec{H}_1^b\right) + \left(\vec{E}_2^a \wedge \vec{H}_2^b\right) = \left(\vec{E}_1^b \wedge \vec{H}_1^a\right) + \left(\vec{E}_2^b \wedge \vec{H}_2^a\right) \qquad (II.42)$$

Equation (II.28) defines the coupling coefficient (transformation ratio) as a voltages ratio. Similarly, we set the new definition of coupling coefficient as, the square root of the ratio between received power and available power:

$$n = \frac{\left(\vec{E}_1^a \wedge \vec{H}_1^b\right) + \left(\vec{E}_2^a \wedge \vec{H}_2^b\right)}{\sqrt{P}} = \frac{\left(\vec{E}_1^b \wedge \vec{H}_1^a\right) + \left(\vec{E}_2^b \wedge \vec{H}_2^a\right)}{\sqrt{P}} \qquad (II.43)$$

By introducing the values of E and H fields of the antenna and the Mode, the equation (II.43) that present the transformation ratio for one mesh becomes:

$$n = \frac{\left(\vec{E}^{mode} \wedge \vec{H}^{antenna}\right) + \left(\vec{E}^{antenna} \wedge \vec{H}^{mode}\right)}{\sqrt{P}} \qquad (II.44)$$

Where P can be expressed by: $P = \left| \frac{1}{2} \left(\vec{E}^{mode} \wedge \vec{H}^{mode}\right) . \left(\vec{E}^{antenna} \wedge \vec{H}^{antenna}\right) \right|$ (II.45)

$\vec{E}^{mode}$ and $\vec{H}^{mode}$ represents the field distribution of the mode at the antenna position.

$\vec{E}^{antenna}$ and $\vec{H}^{antenna}$ represents the radiated field of antenna.

This implies that the final transformation ratio is nothing other than the surface integral of transformation ratios in each mesh.

$$N = \iint \frac{\left(\vec{E}^{mode} \wedge \vec{H}^{antenna}\right) + \left(\vec{E}^{antenna} \wedge \vec{H}^{mode}\right)}{\sqrt{P}} ds \qquad (II.46)$$

To simplify the calculation, the *E* and *H* fields will be replaced by electric current and magnetic current (*Je*,*Jm*) obtained by applying the Huygens principle.

By determining the different values of the elements of equivalences model, we will be able to estimate the transmission coefficient between the transmitting and the receiving antennas positioned inside a metal cavity.

C. Simulations results

In a first approach, a comparison of the simulations results for one mode carried out under the Electromagnetic Simulator CST Microwave studio and the semi-analytical method is made. For the case presented below, two dipoles (of 10mm length) are placed in a small cavity of 20x20x10 cm3.The objective of this simulation is to validate the calculation of coupling: for this we consider a cavity without intrinsic losses (Perfect conductor).

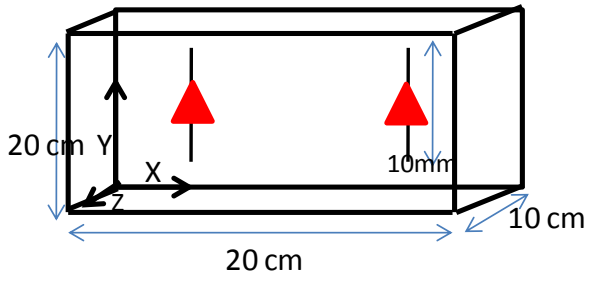

Cavity Dimension		(20x20x10)cm³
Antennas Position (cm)	Antenna1 (X1,Y1,Z1)	(5,5,5)
	Antenna2 (X2,Y2,Z2)	(15,5,5)

Figure II.10: Simulation configuration

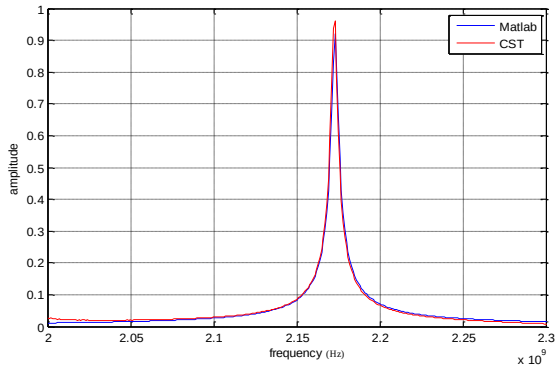

Figure II.11.a: S21 magnitude

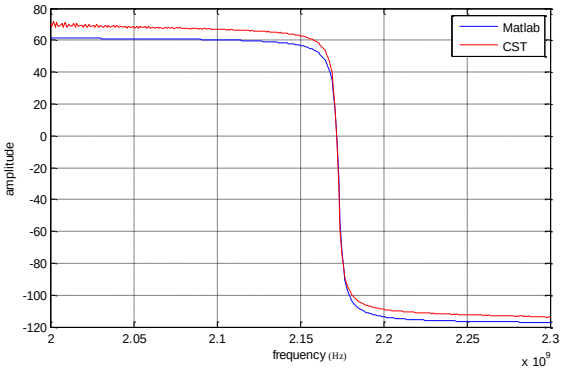

Figure II.11.b: S21 phase

The comparison of the modulus of S21 between electromagnetic simulation and analytical method shows a very good agreement in terms of amplitude and quality factor (figure II.11.a). This validates the good estimation of the coupling at the input and output ports.

Regarding the phase (figure II.11.b), the two curves show a great similarity. This leads to confirm the validity of the implemented calculation method.

3.1.2. Equivalent circuit model for several resonance mode

The equivalent model circuit shown in Figure II.4 can be assimilated to a quadruple Q1.

The model depicted in (figure II.12) aims modelling infinity of modes that can be excited in a frequency band, within a cavity.

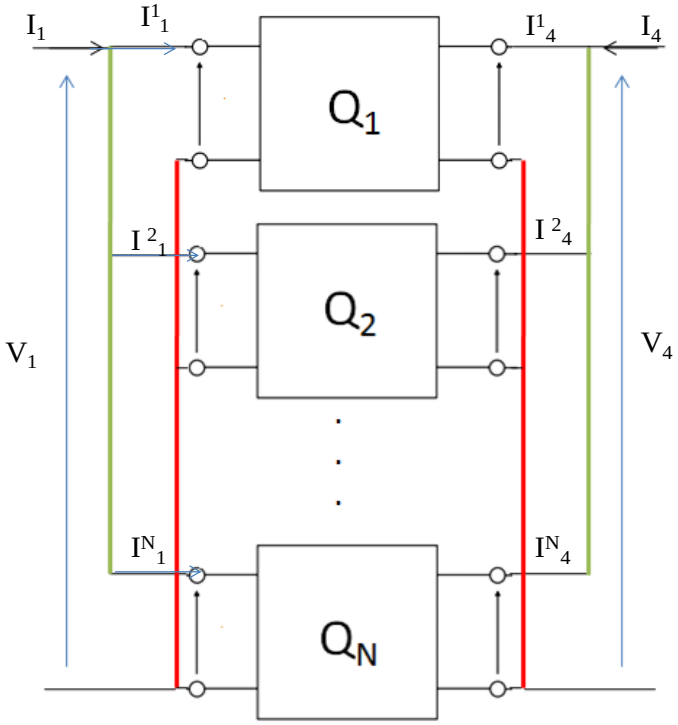

Figure II.12: complete model of excited modes in the cavity

The determination of the transfer function of the complete model involves evaluating the transmission coefficient S_{21}. In order to simplify the calculation of the transmission coefficient expression, the calculation is firstly shown for three modes only

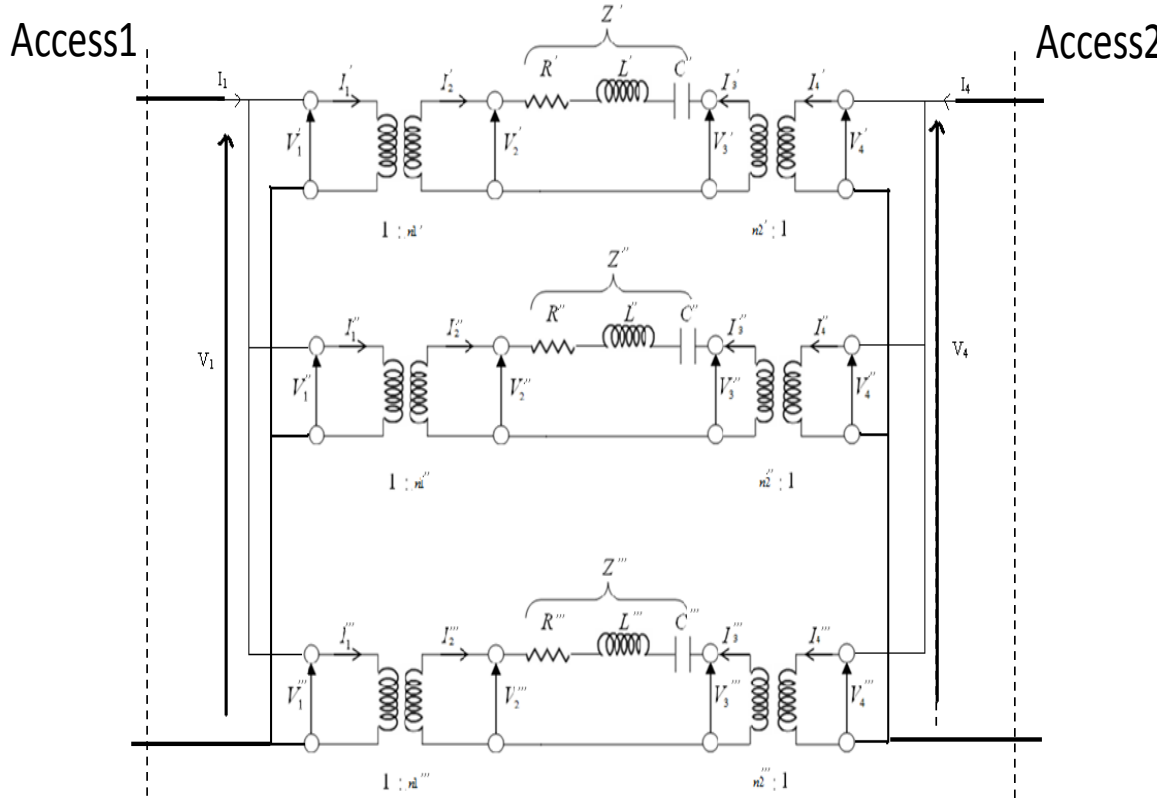

Figure II.13: Equivalent model of three excited modes

Each stage of Figure II.13 is equivalent to one resonant mode. This model implies that:

$$\begin{cases} I_4 = I_4^{'} + I_4^{''} + I_4^{'''} \\ V_4 = V_4^{'} = V_4^{''} = V_4^{'''} \end{cases}; \begin{cases} I_1 = I_1^{'} + I_1^{''} + I_1^{'''} \\ V_1 = V_1^{'} = V_1^{''} = V_1^{'''} \end{cases}; \qquad (II.47)$$

The system defined by equation (II.29) and (II.30) allows writing:

$$I_4 = \frac{n_2^{'}}{n_1^{'}} I_1^{'} + \frac{n_2^{''}}{n_1^{''}} I_1^{''} + \frac{n_2^{'''}}{n_1^{'''}} I_1^{'''} = \frac{n_2^{'}}{n_1^{'}} \left(V_4 - \frac{n_1^{'}}{n_2^{'}} V_1 \right) \frac{n_1^{'} n_2^{'}}{Z^{'}} + \frac{n_2^{''}}{n_1^{''}} \left(V_4 - \frac{n_1^{''}}{n_2^{''}} V_1 \right) \frac{n_1^{''} n_2^{''}}{Z^{''}} + \frac{n_2^{'''}}{n_1^{'''}} \left(V_4 - \frac{n_1^{'''}}{n_2^{'''}} V_1 \right) \frac{n_1^{'''} n_2^{'''}}{Z^{'''}}$$

By simplifying the expression below, we find:

$$I_4 = V_4 \left[\frac{n_2^{'2}}{Z^{'}} + \frac{n_2^{''2}}{Z^{''}} + \frac{n_2^{'''2}}{Z^{'''}} \right] - V_1 \left[\frac{n_1^{'} n_2^{'}}{Z^{'}} + \frac{n_1^{''} n_2^{''}}{Z^{''}} + \frac{n_1^{'''} n_2^{'''}}{Z^{'''}} \right] \qquad (II.48)$$

Using the same reasoning, we find:

$$I_1 = V_4 \left[\frac{n_1^{'} n_2^{'}}{Z^{'}} + \frac{n_1^{''} n_2^{''}}{Z^{''}} + \frac{n_1^{'''} n_2^{'''}}{Z^{'''}} \right] - V_1 \left[\frac{n_1^{'2}}{Z^{'}} + \frac{n_1^{''2}}{Z^{''}} + \frac{n_1^{'''2}}{Z^{'''}} \right] \qquad (II.49)$$

The generalization of equations (II.48) and (II.49) for k modes, gives the following expressions:

$$\begin{cases} I_4 = V_4 \sum_k \frac{n_2^{k2}}{Z^k} - V_1 \sum_k \frac{n_1^k n_2^k}{Z^k} \\ I_1 = V_4 \sum_k \frac{n_1^k n_2^k}{Z^k} - V_1 \sum_k \frac{n_1^{k2}}{Z^k} \end{cases} \quad (II.50)$$

Where *k* is the index of the excited mode.

S_{21} is derived from the incident voltage *Vi* and the reflected voltage *Vr* on each port. Based on the system of equations shown in (II.33), the S_{21} coefficient can be expressed by:

$$S_{21} = \frac{2C}{(1 - A + D + BC - AD)} \quad (II.51)$$

Where:

$$\begin{cases} A = \sum_k \frac{n_2^{k2}}{Z^k}; B = -\sum_k \frac{n_1^k n_2^k}{Z^k} \\ C = \sum_k \frac{n_1^k n_2^k}{Z^k}; D = -\sum_k \frac{n_1^{k2}}{Z^k} \end{cases} \quad (II.52)$$

To conclude this part, an analytical model based on a circuit approach, taking into consideration the empty cavity and the presence of the antennas inside the cavity is set up. Comparisons between CST and analytical method are made in the next section.

Simulation results

As validation example, we set two antenna of 10mm oriented according to **y** inside a small metallic cavity of 20 x 20 x 10 cm^3. The simulation is made over a frequency band between 2GHz and 3GHz.

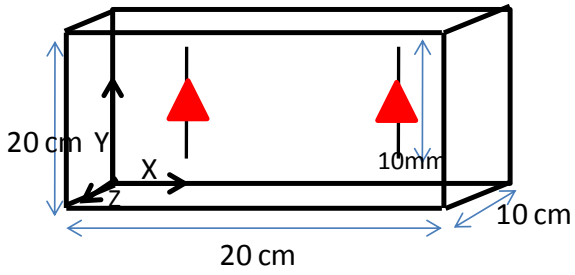

Cavity Dimension		(20x20x10)cm^3
Antennas Position (cm)	Antenna1 (X1,Y1,Z1)	(5,5,5)
	Antenna2 (X2,Y2,Z2)	(15,5,5)

Figure II.14: simulation configuration

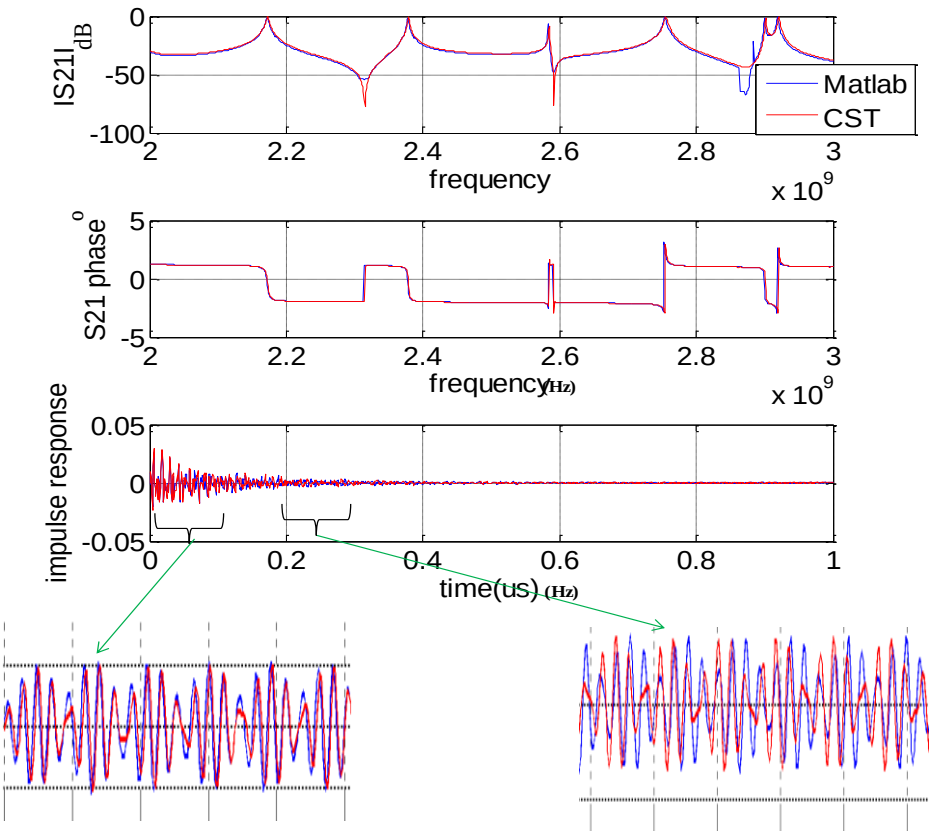

Figure II.15: Simulations results

Figure II.15 shows a very good concordance between the electromagnetic and circuit approach methods.

The channel impulse response (CIR) shows in Figure (II.15), a great similarity that is observed in terms of amplitude, and attenuation, which confirms the correctness of proposed method.

We can note that simulation with different dipole orientation have shown the efficiency of the calculation method to take into account others polarisations and then the excitation of TE and TM modes

Finally simulations with bigger cavities have shown the interest of this method in terms on calculation time while keeping a great accuracy on the obtained results. For example a cavity of 50 x 10 x 20 cm3 needs more than 4 hours of simulation under CST MS, and only 5 minutes using the proposed method under matlab.

At this level of the study, an analytical model that takes into account the cavity and antennas is made. Below, an interest is taken to full analytical modelling of the MSRC, taking into account the cavity, antennas, losses and stirrers.

The losses and stirrers method modelling will be described in the following section. This section will be completed by the presentation of the comparison results between measurements and Matlab simulations.

3.2. Losses and stirrer modelling

A. Losses modelling

The analytical model developed until now takes into account the losses related to the cavity walls and losses related to antennas. Other losses to consider are, the ones that will be introduced inside the MRSC in order to control the channel delay spread. These losses will affect the quality factor of the chamber.

Generally, the absorption cross section $\langle \sigma_a \rangle$ [28][29], of a lossy object depends on the polarization and the incidence angle of the incoming plane wave. In a MSRC, we suppose that the fields in a metallic cavity can be written as a superposition of plane waves of all polarization and incidence angles. If lossy object is located in an isotropic area, the absorbed power (P) by the lossy object can be written as the product of the power density of the cavity S_c, and the averaged absorption cross section $\langle \sigma_a \rangle$.

$$P = S_c \langle \sigma_a \rangle \quad [28] \qquad (II.53)$$

$$Where:\ S_c = cW;\ W\ is\ energy\ density$$

Where $\langle\ \rangle$ indicates an incidence angle average over 4π steradians, and an average over all polarizations.

The quality factor related to the lossy object can be expressed as:

$$Q_{losses} = \omega \frac{Us}{P};\ Where\ Us\ is\ the\ stored\ energy$$

$$Us = W.V;\ Where\ V\ is\ the\ chamber\ volume$$

$$Q_{losses} = \frac{2\pi V}{\lambda \langle \sigma_a \rangle} \qquad (II.54)$$

Where λ is the free space wave length.

From the expression below, it can be seen very well that the unique key parameter to estimate, is the average absorption cross section $\langle \sigma_a \rangle$.

Permittivity and permeability are essential properties of the materials, absorption properties of lossy object depend also on incoming wave polarization, direction of incidence and geometry.
In this part we consider the penetration of the cavity field inside a lossy object in order to characterize its absorbing properties and determine the average absorption cross section.
In the following, two approaches allowing the calculation of the absorption cross section are exposed.

- Numerical approach

The numerical approach is based on the solution given by CST Microwave Studio© that consist in the extraction of the broadband scattering response of the lossy object by using a broadband farfield monitor. The farfield monitor calculation deals with the field behaviour far away from the corresponding source of the electromagnetic waves.
This monitor already automatically writes the absorption cross section (total ACS). The total absorption cross section is defined as the ratio of the absorbed power by lossy object to the intensity of the incident plane wave.

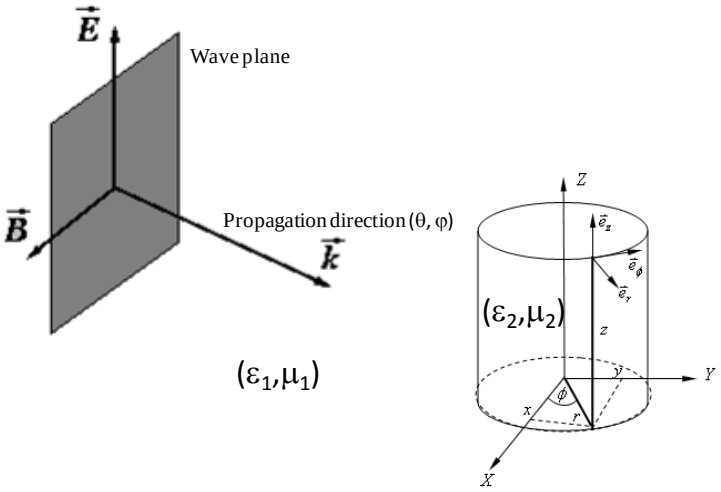

Figure II.16: Illumination of the lossy object illuminated by a plane wave

The implemented simulation consists to vary the angle of incidence (θ, φ) of the plane wave, that illuminates the considered form

This approach is efficient, but needs a huge computation time for isotropic angle of arrival. In order to minimize the simulation time, it is necessary to look for another alternative capable to achieve the calculation of ACS with a tolerable error.

- Analytical approach

In figure II.16, the lossy object is illuminated by a plane wave. Analytical calculation of ACS requires the determination of a transmission coefficient that will be multiplied by the average surface of the object.

$$ACS = \langle T(\theta,\varphi) \rangle S, \qquad (II.55)$$

Where T is transmission coefficient, and S is avreage surface of the lossy object

We assume that the electric component is unchanged, and the magnetic field will change its direction.

Therefore:

The incident wave is explained by: $E_{y,i}(z,t) = A_i e^{j(\omega t - k_1 z)}$

The reflected wave is explained by: $E_{y,r}(z,t) = B_r e^{j(\omega t + k_1 z)}$ $(II.56)$

The transmitted wave is explained by: $E_{y,t}(z,t) = A_t e^{j(\omega t - k_2 z)}$

Here, k_1 and k_2 are the wave numbers for the regions (media) 1 and 2 respectively, constants A and B indicate the terms propagating in the +z and –z directions.

The magnetic field intensities can be found from the Maxwell's equations or by using the characteristic impedances for two regions.

Therefore:

The incident wave is explained by: $H_{x,i}(z,t) = \frac{-A_i}{Z_{c,1}} e^{j(\omega t - k_1 z)}$

The reflected wave is explained by: $H_{x,r}(z,t) = \frac{B_r}{Z_{c,1}} e^{j(\omega t + k_1 z)}$ $(II.57)$

The transmitted wave is explained by: $H_{x,t}(z,t) = \frac{-A_t}{Z_{c,2}} e^{j(\omega t - k_2 z)}$

We chose the interface between two media to be at $z = 0$, the exponent will be

$$e^{j(\omega t \pm kz)}\Big|_{z=0} = e^{j\omega t} \qquad (II.58)$$

Therefore, at the boundary $z = 0$, we can write:

$$\begin{cases} E_{y,i}(z=0,t) + E_{y,r}(z=0,t) = E_{y,t}(z=0,t) \\ H_{x,i}(z=0,t) + H_{x,r}(z=0,t) = H_{x,t}(z=0,t) \end{cases} \qquad (II.59)$$

Substituting the last results to (eq II.56) and (eq II.57), we obtain:

$$\begin{cases} A_i + B_r = A_t \\ \dfrac{A_i}{Z_{c,1}} - \dfrac{B_r}{Z_{c,1}} = \dfrac{A_t}{Z_{c,2}} \end{cases} \qquad (II.60)$$

We specify the reflection and transmission coefficients as:

$$\text{Reflection:} \quad \Gamma = \frac{B_r}{A_i} = \frac{Z_{c,2} - Z_{c,1}}{Z_{c,2} + Z_{c,1}}$$

$$\text{Transmission:} \quad T = \frac{A_t}{A_i} = \frac{2Z_{c,2}}{Z_{c,2} + Z_{c,1}} \qquad (II.61)$$

Since the characteristic impedance is: $Z_c = \sqrt{\dfrac{\mu}{\varepsilon}}$

For two dielectric materials:

$$\text{The reflection coefficient can be explained by:} \quad \Gamma = \frac{\sqrt{\varepsilon_1} - \sqrt{\varepsilon_2}}{\sqrt{\varepsilon_1} + \sqrt{\varepsilon_2}}$$

$$\text{The Transmission coefficient can be explained by:} \quad T = 1 + \Gamma = \frac{2\sqrt{\varepsilon_1}}{\sqrt{\varepsilon_1} + \sqrt{\varepsilon_2}} \qquad (II.62)$$

This section aims to calculate the total transmission coefficient of a cylindrical object filled with water placed inside the MSRC. The cylindrical object with known thickness *d* and dielectric constants are $\varepsilon_2 = \varepsilon_r \varepsilon_0$; with $\varepsilon_1 = \varepsilon_3 = \varepsilon_0$.

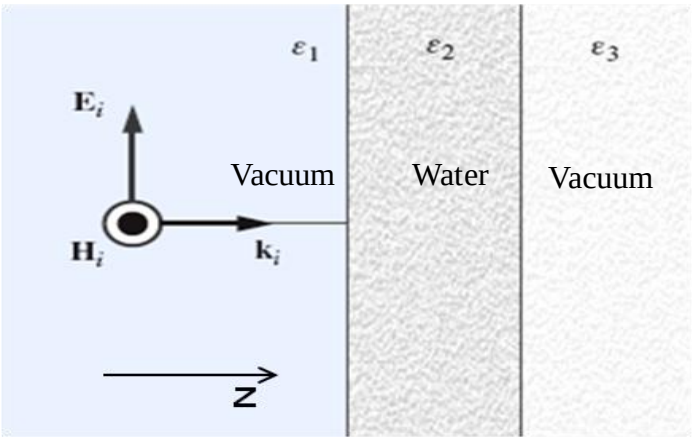

Figure II.17: Plane wave propagation through the cylindrical object filled with water

The amplitudes of the total transmitted and reflected fields are

$$\begin{cases} E_t(z) = \sum_{n=1}^{\infty} E(z)_{+3}^{n} \\ E_r(z) = \sum_{n=1}^{\infty} E(z)_{-1}^{n} \end{cases} \qquad (II.63)$$

Taking into account the huge number of reflections that exists inside the MSRC. The wave incident to the boundary with the second region is partially reflected back and partially transmitted to region 2. At the interface between materials 2 and 3, the transmitted to material 2 field is partially reflected back and partially transmitted to the material 3, etc.

We assume next that the reflection coefficient from the first interface is Γ_1 in the $+z$ direction and $-\Gamma_1$ in the $-z$ direction. Since the region 3 is identical to region 1, $\Gamma_2 = -\Gamma_1$, and $-\Gamma_2 = \Gamma_1$. Similarly, the transmission coefficient through the first interface will be $T_1^+ = 1 + \Gamma_1$ in the $+z$ direction and $T_1^- = 1 - \Gamma_1$ in the $-z$ direction.

The total reflected electric field is:

$$\begin{aligned} E_r(z) &= E_i\left[\Gamma_1 + T_1^+\Gamma_2 T_1^- e^{j2k_2d} + T_1^+\left(-\Gamma_2\Gamma_1\right)\Gamma_2 T_1^- e^{j4k_2d} + T_1^+\left(-\Gamma_2\Gamma_1\right)^2\Gamma_2 T_1^- e^{j6k_2d} + \ldots\right] \\ &= E_i\left[\Gamma_1 - \left(1-\Gamma_1^2\right)\Gamma_1 e^{j2k_2d}\left\{1+\left(\Gamma_1^2 e^{j2k_2d}\right)+\left(\Gamma_1^2 e^{j2k_2d}\right)^2+\ldots\right\}\right] \end{aligned} \qquad (II.64)$$

The total reflection coefficient is:

$$\Gamma \equiv \frac{E_r(z)}{E_i} = \Gamma_1\left[1 - \frac{\left(1-\Gamma_1^2\right)e^{j2k_2d}}{1-\Gamma_1^2 e^{j2k_2d}}\right] = \frac{\Gamma_1\left(1-e^{j2k_2d}\right)}{1-\Gamma_1^2 e^{j2k_2d}} \qquad (II.65)$$

Similarly, the total transmitted electric field is:

$$\begin{aligned} E_t(z) &= E_i\left[T_1^+ T_1^- e^{jk_2d} + T_1^+\left(-\Gamma_2\Gamma_1\right)T_2^- e^{j3k_2d} + T_1^+\left(-\Gamma_2\Gamma_1\right)^2 T_2^- e^{j5k_2d} + \ldots\right] \\ &= E_i\left[\left(1-\Gamma_1^2\right)e^{jk_2d}\left\{1+\left(\Gamma_1^2 e^{j2k_2d}\right)+\left(\Gamma_1^2 e^{j2k_2d}\right)^2+\ldots\right\}\right] \end{aligned} \qquad (II.66)$$

The total transmission coefficient is:

$$T \equiv \frac{E_t(z)}{E_i} = \frac{\left(1-\Gamma_1^2\right)e^{jk_2d}}{1-\Gamma_1^2 e^{j2k_2d}} \qquad (II.67)$$

Where ε_r is the relative permetivity of the lossy object
λ is the wavelength

Figure below shows the results of comparisons between the numerical approach and the analytical approach. Simulations are performed for two different volumes of water (Voume1 & volume2). Simulations are performed over a frequency band of 10GHz.

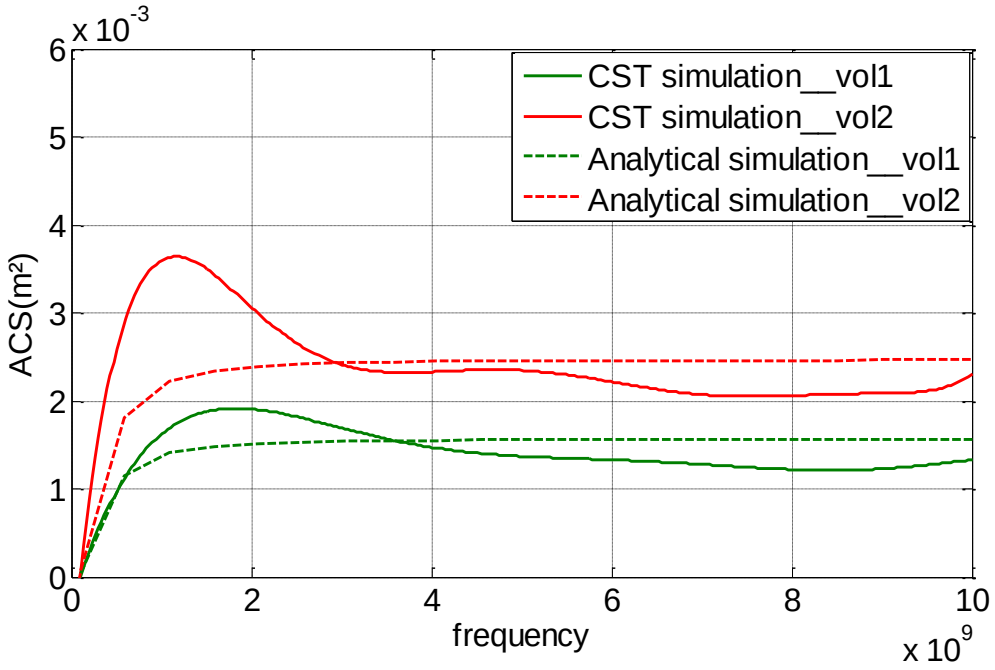

Figure II.18: Comparison of ACS's simulated with CST Microwave Studio and calculated analytically

The simulations results show that the error remains tolerable. The analytical approach is adopted during this work.

B. Stirrer modelling

The stirrer consists of metal paddles attached on a pivoting axis. The stirrers' rotation allows the modification of the chamber boundary conditions. This modification implies a shift of resonance frequencies. A second property of stirring method is that it makes the field statistically isotropic and homogeneous over a stirring revolution. This means that over a stirring revolution, the maximum value of the electromagnetic field is almost identical in every points of the chamber and in all directions.

Let us assume that the X dimension of the cavity observe an amplitude excursion of ΔX that is small compared to X. Using the equation (II.1) and under condition that the wavelength is

small compared to X, the use of Taylor development [7] shows that the deviation of the Eigen mode frequency f_{mnp} correspond to a variation ΔX close to an amount of Δf_{mnp} (II.68).

$$\Delta f_{mnp} = \frac{c^2}{4 f_{mnp}} \left(\frac{m}{X} \right)^2 \frac{\Delta X}{X} \qquad (II.68)$$

The variation in one direction remains a simple case. The expression of equation (II.68) can be generalized to have a variation in the three directions X, Y, and Z. The equations (II.68) becomes:

$$\Delta f_{mnp} = \frac{c^2}{4 f_{mnp}} \left(\left(\frac{m}{X} \right)^2 \frac{\Delta X}{X} + \left(\frac{n}{Y} \right)^2 \frac{\Delta Y}{Y} + \left(\frac{p}{Z} \right)^2 \frac{\Delta Z}{Z} \right) \qquad (II.69)$$

The choice of a statistical modelling of stirrers is adopted. Since, the stirrers' rotation provides a virtual variation of the dimensions of the chamber. The stirrers' effect is introduced in the analytical simulator through the use of the equation (II.69)

The full analytical modelling of the MSRC is completed. The next step aims to validate the full model by performing simulations/measurements comparisons.

C. Model simulations/ Measurements comparisons

The simulation results obtained with the method developed in Matlab©, is compared with the measurements results performed for several stirrers' positions inside the MSRC with the use of a vector network analyzer.

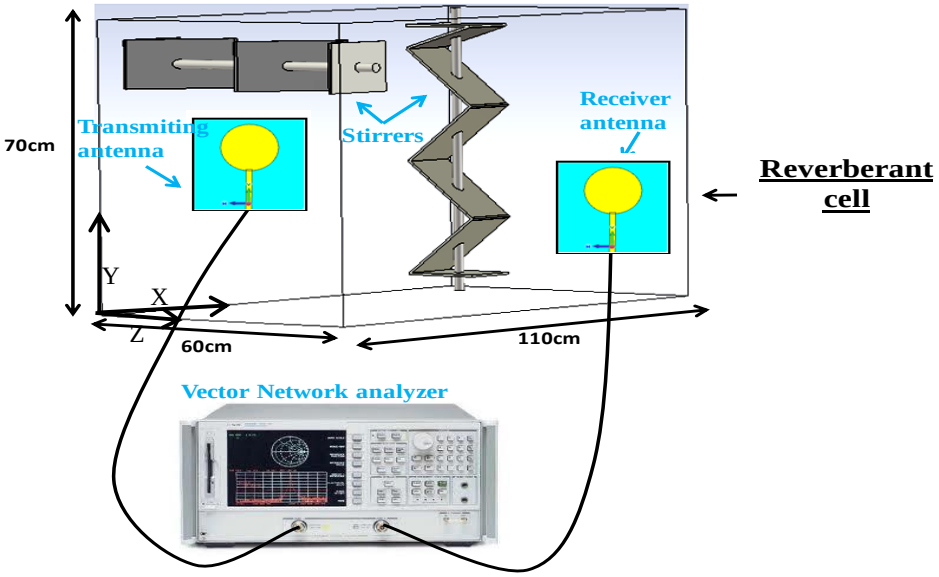

Figure II.19: View of simulated reverberation chamber

For the validation of Matlab Simulator, the measurements are performed for a bandwidth of 50 MHz around a central frequency of 2.5 GHz. The absorbing material used during the measurements campaign is a water cylinder. The amount of water will be varied from 0 litter (the case when the chamber is empty) to 4 litter.

During this validation, the antennas are placed the following coordinates (Transmitting antenna (X=0.1m, Y=0.2m, Z=0.1m), Receiving antenna (X=0.6m, Y=0.2m, Z=0.2m)). Stirring type chosen during measurements is a step by step stirring, allowing achieving 1600 different position. Regarding the location of losses, they will be placed in the corner of the chamber.

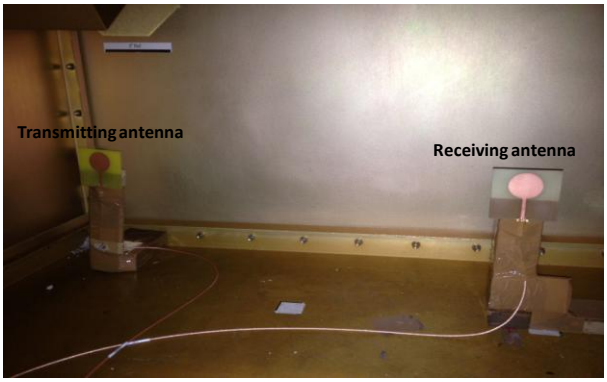

Figure II.20: the positioning of the antennas within the MSRC

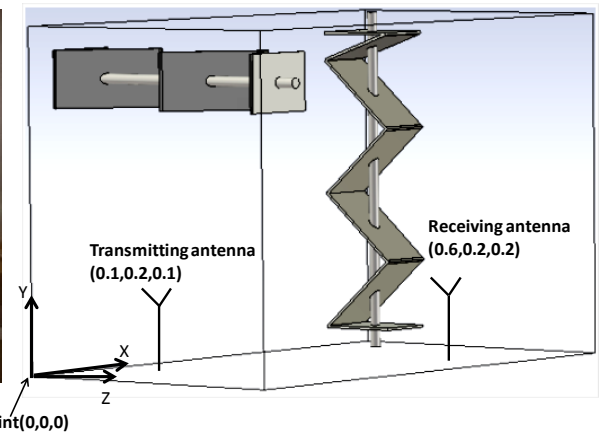

Figure II.21: Overview of antennas location inside the MSRC

The key parameter of this study remains the Power Delay Profile (PDP). This parameter allows describing the behaviour of the propagation channel. Below four figures show the evolution of the simulated and measured averaged PDP for different water quantities.

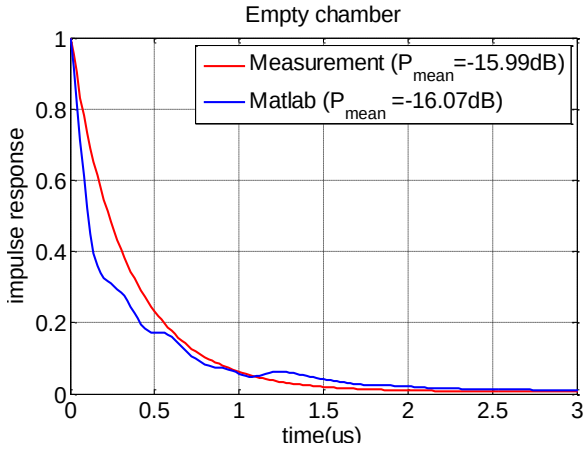

Figure II.22: Simulated and measured impulse response for empty chamber

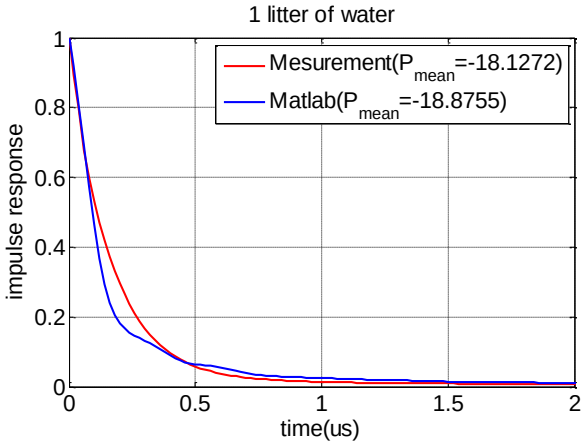

Figure II.23: Simulated and measured impulse response for chamber with one litter of water

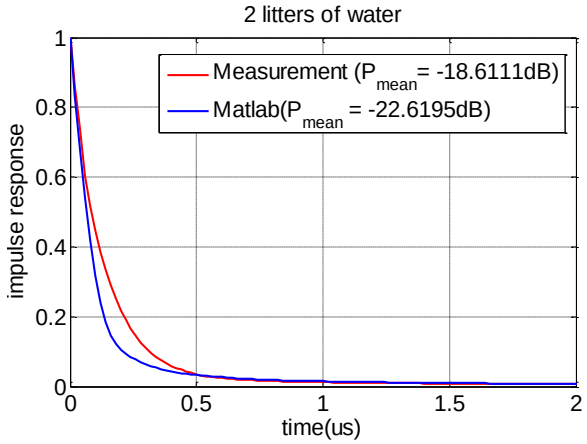

Figure II.24: Simulated and measured impulse response for chamber with two litter of water

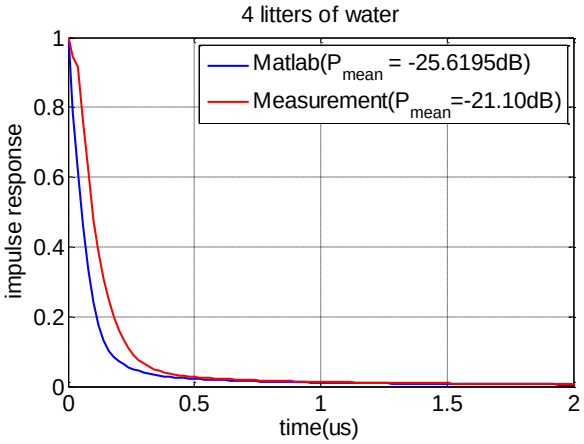

Figure II.25: Simulated and measured impulse response for chamber with four litter of water

In figures II.22-25, the exponential decay of the PDP is observed. Moreover, It is also noted the influence of losses on the channel that is manifested in the fast decay. This influence appears concretely in figures II.26-27, which represents the evolution of the transmission coefficient as a function of stirrers' positions, for different amounts of water. As we can see, the difference between the mean simulated and the mean measured transmission coefficient is less than 3 dB.

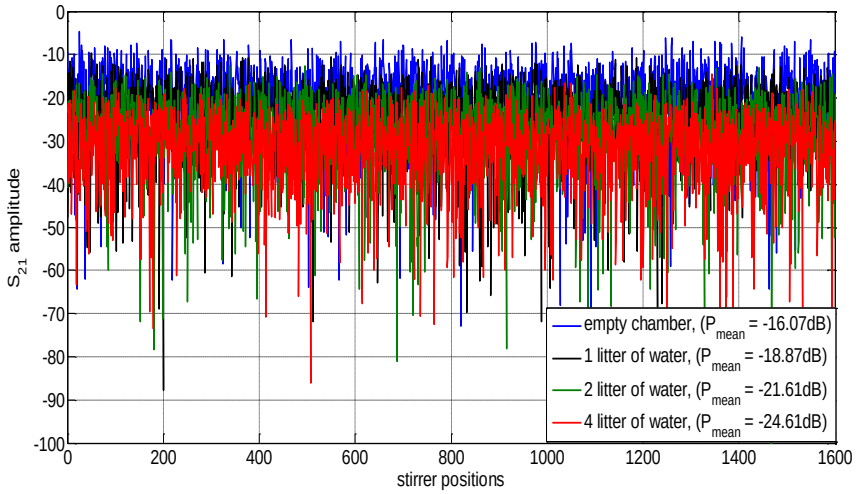

Figure II.26: Simulated transmission coefficients for different losses quantities.

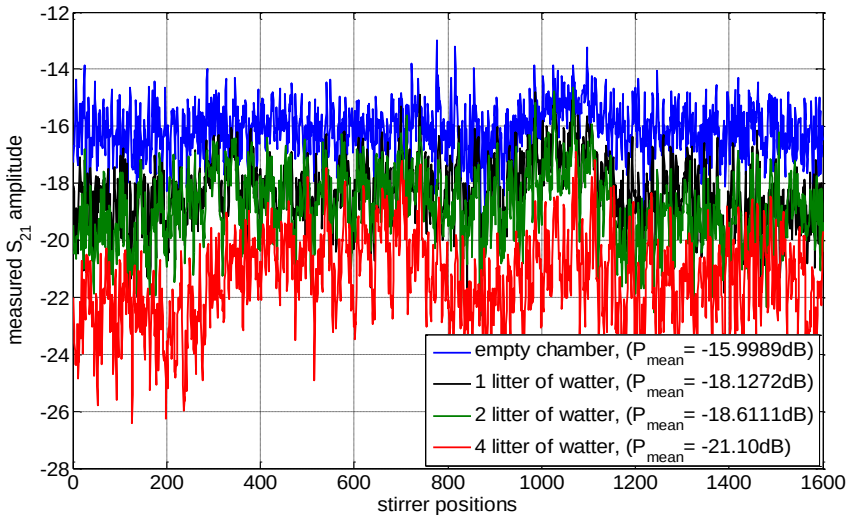

Figure II.27: Measured transmission coefficients for different losses quantities.

	0 litter of water	**1 litter of water**	**2 litters of water**	**4 litters of water**
Simulated RMS delay spread (ns)	284.5548	183.9345	151.6424	135.1126
Measured RMS delay spread (ns)	296.2542	193.3663	168.4541	145.7142
Mean measured transmission coefficient $S_{21(dB)}$	-15.99	-18.13	-18.61	-21.10
Mean simulated transmission coefficient $S_{21(dB)}$	-16.07	-18.87	-21.61	-24.6

Table II.2: Comparison between measured and simulated RMS delay spread for different quantities of water

The comparison of simulated and measured values of the RMS delay spread shows a maximum difference of 9.5%. This difference remains tolerable, since we reach a rough estimation versus losses. For the case of empty chamber (no bottle filled with water inside the chamber), the delay spread represents a high value (about 296ns). The introduction of losses in the chamber (a bottle filled with four litters of water) showed a significant decrease in the RMS delay spread, since we go from 300ns to 145ns.
This estimation has the effect of limiting channel sounding campaigns.

4. Conclusion

This chapter was aim to study the possibility of setting up an analytical Matlab© simulator able to estimate the value of the channel RMS delay spread in a reverberant room. The novelty brought by this simulator is that it was based on a circuit approach and takes in account the antenna, the stirrer, and losses effects.

The description of the circuit approach that has allowed the development of this simulator has been made. The challenge of this method was to calculate the coupling between the antenna and the mode excited in the metal cavity. For this reason a calculation method using the theorem of reciprocity and equivalence theorem has been developed.

The validation of the results obtained from Matlab simulator with CST simulations and measurements, has shown the performance of the developed simulator. The obtained results remain satisfactory.

The analytical simulator developed with Matlab allows having an idea about the average value of the RMS delay spread versus losses. The knowledge of this value will optimize the measurements campaigns time. And subsequently estimate the amount of losses to be introduced inside MSRC in order to obtain the desired channel RMS delay spread value.

References

[1] B.H. Liu, D.C. Chang & M.T. Ma "Eigenmodes and the Composite Quality Factor in a Reverberating Chamber" NBS Technical Note 1066, Août 1983.

[2] M.W. Zemansky "Heat and Themodynamics 5Th Edition" Mc Graw-Hill, 1968.

[3] N. Lamblain "Etude du Brassage Electronique de Modes en Chambre Réverbérante Appliqué aux Mesures d'Immunité Electromagnétique" Thèse de Doctorat en Electronique, Université de Lille, Novembre 1996.

[4] R.H. Price, H.T. Davis & E.P. Wenaas "Determination of the Statistical Distribution of Electromagnetic-field Amplitudes in Complex Cavities" Physical Review, Vol. 48, n°6, Décembre 1993.

[5] B. Démoulin, L. Kone, C. Gouyer, C. Si Ahmed "Résumé d'un Etat de l'Art Relatif aux Chambres Réverbérantes à Brassage de Modes" Rapport interne d'avancement du projet MADERE, Juillet 1999.

[6] J.G. Kostas & B. Boverie "Statistical Model for a Mode-Stirred Chamber" IEEE Trans. on EMC, Vol. 33, n°4, Novembre 1991.

[7] C. Si-Ahmed "Contribution à l'Etude du Coefficient de Qualité dans une Chambre Réverbérante à Brassage de Modes" Thèse de Doctorat en Electronique, Université de Lille, Mars 2001.

[8] B. Démoulin "Les Chambres Réverbérantes à Brassage de Modes - Principes et Applications" 9ème Colloque International sur la Compatibilité Electromagnétique, Brest, France, 1998.

[9] M.L. Crawford, G.H. Koepke "Design, Evaluation and Use of a Reverberation Chamber for Performing Electromagnetic Susceptibility/Vulnerability Measurements" National Bureau of Standards, Technical Note 1092, April 1986.

[10] D.A.Hill "Plane Wave Integral Representation for Fields in Reverberation Chambers" IEEE Trans. on EMC, Vol. 40, n°3, Août 1998.

[11] A. Hald "Statistical Theory with Engineering Applications" John Wiley & Sons, Inc, 1952.

[12] M. Höijer; A.M. Andersson, O. Lundén, M. Bäckström "Numerical Simulations as a Tool for Optimizing the Geometrical Design of Reverberation Chambers" IEEE Int. Symp. on Electromagnetic Compatibility, Washington, USA, Août 2000.

[13] L. Bai, L. Wang, B. Wang, J. Song "Reverberation Chamber Modeling Using FDTD" IEEE International Symp. on Electromagnetic Compatibility, Seattle, USA, Août 1999.

[14] D.I. Wu, D.C. Chang "The Effect of an Electrically Large Stirrer in a Mode-Stirred Chamber" IEEE Trans. on EMC, Vol. 31, n°2, Mai 1989.

[15] P. Besnier "Analyse modale d'une chambre réverbérante à brasseur de modes à l'aide d'une simulation numérique de la propagation du champ électromagnétique basée sur la méthode TLM" 8ème Colloque International sur la Compatibilité Electromagnétique, pp. 159-164, Lille, France, Septembre 1996.

[16] C.F. Bunting, K.J. Moeller, C.J. Reddy, S.A. Scearce "Finite Element Analysis of Reverberation Chambers : A Two-Dimensional Study at Cutoff" IEEE Int. Symp. on Electromagnetic Compatibility, Denver, USA, Août 1998.

[17] D.H. Kwon, R.J. Burkholder, P.H. Pathak "Ray Analysis of Electromagnetic Field Buikd-Up and Quality Factor of Electrically Large Shielded Enclosures" IEEE Trans. on EMC, Vol. 40, n°1, Février 1998.

[18] F. Hoëppe, S. Baranowski, P.N. Gineste, B. Demoulin "Use of a Statistical Gauge to Test Theoretical Simulations of the Field Distribution in Over Sized Electromagnetic Cavities" 4th European Symposium on Electromagnetic Compatibility, vol. 1, pp. 557-561, Bruges, Belgique, Septembre 2000.

[19] D. A. Hill "A Reflection Coefficient Derivation for the Q of a Reverberation Chamber" IEEE Trans. on EMC, Vol. 38, n°4, Novembre 1996.

[20] C. Fiachetti, B. Michielsen, F. Issac, A. Reineix "Etude d'un modèle de champ aléatoire pour la modélisation du couplage sur un équipement électronique dans une chambre réverbérante à brassage de modes" 10ème Colloque International sur la Compatibilité Electromagnétique, pp. 324-329, Clermont-Ferrand, France, Mars 2000.

[21] L. Musso, B. Démoulin, F.G. Canavero, V. Bérat "Susceptibility of a Transmission Line in Two Reverberation Chambers" COST 261, Workshop on EMC Measurement Techniques for Complex and Distributed Systems, Lille, France, Juin 2001.

[22] E. Amador, C. Lemoine, P: Besnier, A. Lainé, "Reverberation Chamber Modeling Based on Image Theory: investigation in pulse Regime", IEEE transactions on Electromagnetic compatibility 52, 4 (2010), pp 778-789.

[23] R. Harrington, "Time Harmonic Electromagnetic fields", New York: McGraw-Hill Book Company, 1981, pp 103-105.

[24] Y.Huang and D. Edwards, " A Novel reverberating chamber: the source stirred chamber", Sep 1992, pp 120-124.

[25] J. Kuthong and C. Burting, "Statistical characterization of the 900MHz and 1800 MHz indoor propagation using reverberation source stirring technique", in Antennas and Propagation society International symposium, 2009. APSURSI'09, IEEE. June 2009, pp. 1-4.

[26] H. Moussa, S. Baranowski, M. Cauterman, B. Demoulin, "Simulation of a 2D cavity under Qucs", 2emc IEEE symposium on embedded EMC, Rouen, France, October 2007

[27] P.F.Combes, " Micro-ondes, Tome 1, lignes, guides et cavités", Dunod 1996, ISBN :2.10.002840.5.

[28] G. Gradoni, D. Micheli, F. Moglie, V. Mariani Primiani, " ABSORBING CROSS SECTION IN REVERBERATION CHAMBER: EXPERIMENTAL AND NUMERICAL RE-SULTS ", Progress In Electromagnetics Research B, Vol. 45, 187-202, 2012

[29] D. A. Hill, M. Ma, B.F. Riddle, M. L. Crawford, R.A.R.Ondrejka, T. Johnk, "Aperture Excitation of Electrically Large, Lossy Cavities",IEEE TRANSACTIONS ON ELECTROMAGNETIC COMPATIBILITY, VOL. 36, NO. 3, AUGUST 1994

Chapter III: Emulation of realistic multi path channel for wireless communication system testing

1. Introduction

In recent years, the characterization of the MIMO (Multiple Input Multiple Output) terminals has been the subject of many works, through research actions, such as COST 2100 or COST1004 [1]. Such "Over the Air" measurements, currently undergoing standardization (3GPP, CTIA), require the ability to emulate multipath propagation channels, which represent typical environments for testing mobile terminals.

Three approaches are currently being considered by the standardization committees [2], for the implementation of test scenarios in controlled environment. These approaches are: Mode Stirred Reverberation Chamber (MSRC), Anechoic Chamber (AC) and two stage method.

In real environment, the mobile terminals are submitted to strong constraints related to the multipath character of the propagation channel. Since the multi paths have different magnitudes and delays, their recombination at the terminal cause interferences, resulting in more or less deep fading on one hand and frequency selectivity on the other hand. This leads to a significant decrease of signal to noise ratio and therefore an increase of the link error rate.

The emulation and characterization of a reference propagation channel are necessary before starting performances measurement of MIMO terminals.

In this work, the proposed MIMO measurement scenarios test is based on MSRC. From a practical point of view, this solution is faster to implement, since it allows submitting the terminal at an instantaneous 3D multipath environment. Reverberation chamber (RC) is considered as a useful tool to emulate a rich multipath environment; this emulation is characterized by a given fading [3; 4] whose distribution can be Rayleigh, Rice, or Nakagami…

The MSRC can be used to measure the diversity gain, the bit error rate, the total isotropic sensitivity [5], the total radiated power [6], or MIMO transmission quality in frequency selective channels [7; 8] of wireless devices. For the measurement of the diversity gain and the sensitivity the channel delay spread in MSRC may influence the results. Several research studies [9; 10; 11; 12] have shown the ability to manage the delay spread. This control of delay spread can be achieved through modifying the MSRC quality factor by loading it with absorbing materials.

Hence, in this contribution we suggest an experimental study using a small size reverberation chamber [13] in order to qualify performances of MIMO terminals for different scenarios and algorithms in terms of Error Vector Magnitude (EVM) [14, 15, 16], Block Error Rate (BLER) [17, 18, 19], throughput and total isotropic sensitivity (TIS) while maintaining a Rayleigh fading. In this experimental study, a multi cluster channel emulation which is conforming to channels models defined in literature is implemented. This emulation must be accompanied by a strict control of delay spread.

The work outlined in this chapter is divided into three phases:

- **Phase1** is devoted to the analysis of the antenna diversity performance dependence on channel delay spread for a WiMAX application.
- **Phase2** is dedicated to no-real time performances evaluation of the MIMO-LTE systems for different emulated realistic channel models inside reverberation chamber.
- **Phase3** is devoted to real time measurements of MIMO LTE terminals. During this phase, measurements of EVM (Error Vector Magnitude), and BLER (block error rate) and TIS (total isotropic sensitivity) will be conducted in SISO and MIMO mode.

2. Analysis of antenna diversity performance dependence on multi-antenna channel delay spread in MSRC

One of the major problems in a mobile communication system is the deep fading caused by the multipath propagating environment. To overcome this problem, one solution consists in using some diversity technique at the terminal side of the wireless link by means of gathering several antennas [20]. In order to assess the consequent diversity performance improvement, effective antenna diversity gain is the figure-of-merit (FOM) typically used to present the effectiveness of the diversity antenna system. Effective diversity gain (EDG) can be defined as the improvement in time-averaged signal-to-noise ratio (SNR) from combined signals of all the radiators of a multi-antenna system, relative to the SNR from a single reference antenna in the system. This definition is conditioned by the probability that the SNR is above a reference level. The probability value is arbitrary but usually set to 1% or 10% reliability level [21, 22]. Despite the importance of diversity gain as figure-of-merit in multi-antenna OTA communication systems, scarce publications can be found in the literature related to how it is affected by the root mean square (RMS) delay spread of the communication channel. Thus, diversity gain dependence on this characteristic must be

analyzed for a better understanding of MIMO OTA active measurements for device characterization. Even though MIMO OTA channels are usually characterized by their coherence distance, time and bandwidth, or equivalently by their reciprocal counterparts: angular, Doppler and RMS delay spread, respectively [23, 24, 25, 26], in order to simplify the analysis, this contribution is focused on the study of the antenna effective diversity gain dependence on the RMS delay spread of a frequency selective channel, with a fixed bandwidth modulated signal, by means of measurements using an RC. Diversity gain has been found to be in inverse variation to the RMS delay spread of the channel when it is varied through the introduction of absorbing material within the inner cavity of the RC.

Nevertheless, scarce publications related to the effect of root mean square (RMS) delay spread on these figures-of-merits can be found in the literature. In this work, we present an analysis of the dependence of the effective antenna diversity gain on the RMS delay spread of a wireless channel by means of a multi-antenna OTA communication system using a QPSK modulation inside an RC. For that purpose, several channel RMS delay spread profiles have been achieved inside the RC by varying the amount of absorbing material placed in the cavity.

2.1.Channel characterization

A. Measurement platform

The MSRC used in this study has dimensions of (110x 70x 60) cm^3, as depicted in Figure. (III.1) Rotating its two mechanical stirrers step wisely, the electromagnetic field inside (at a reasonable distance from the walls of the order of the wavelength) has a statistical uniformity at all points of measurement in all directions and for all positions of the radiation source, and the Doppler spread of the channel is negligible.

Figure III.1: Mode stirred reverberation chamber (RC)

At the beginning we are interested to characterize the propagation channel emulated inside the reverberation chamber for different amount of absorbing materials. In this section, we are looking for measuring the channel impulse response. This channel characterization is based

on sliding correlation technique that uses the autocorrelation properties of PN (Pseudo Noise) sequences. This technique comprises to correlate the PN sequence to be transmitted with the PN sequence generated at reception side. At the transmission side the generation of the PN sequence and reshape of data are performed with Matlab. The transmitted PN sequence is resulting from the concatenation of two sequences PN1 and PN2 having the same length.

The obtained PN sequence by concatenation has a length of 1022 symbols. A reshape of this sequence involve realizing BPSK modulation followed by a filtering in order to limit the band of the transmitted PN signal. An over sampling coefficient (OSR) of 4 has been fixed which leads to a sequence transmitted to generator composed of 4088 samples.

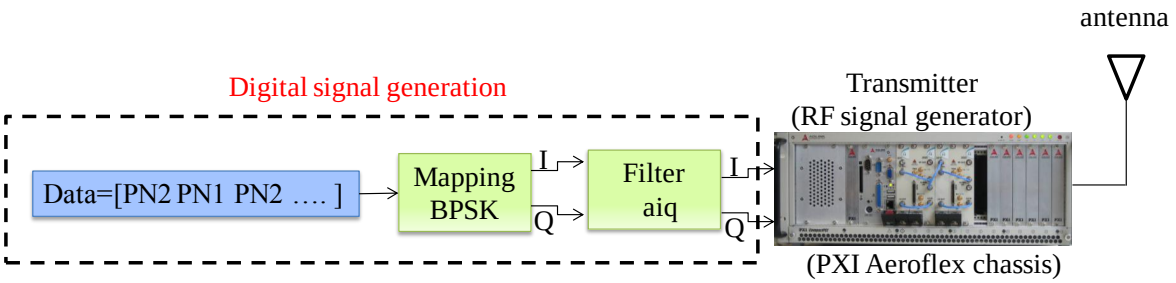

Figure III.2: transmitting module of the measurement platform

The sequences are transmitted to the RF generator, after created under Matlab. The sequences are transmitted in baseband. Then, the generator sends PN sequence at a carrier frequency of 5.5 GHz. More details concerning the realization of the PN sequence and the software used in this generation are presented in [30].

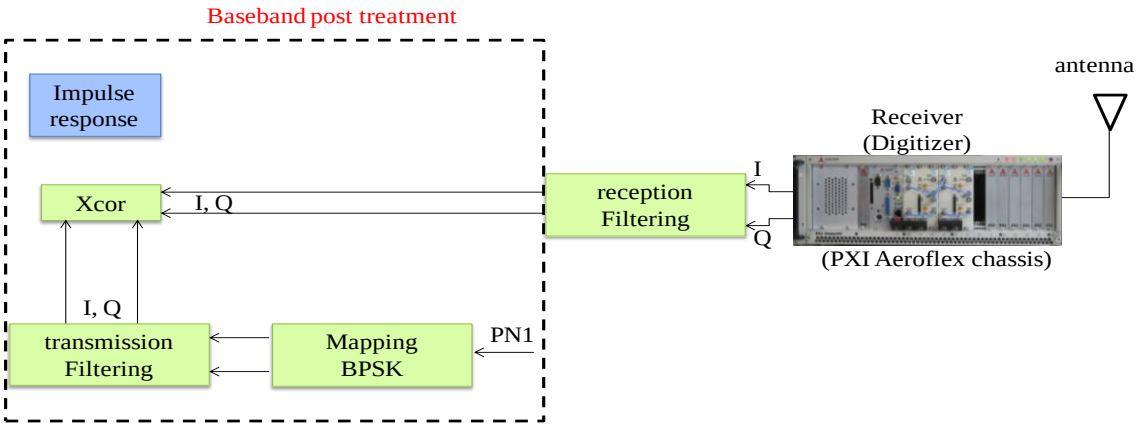

Figure III.2: receiving module of the measurement platform

At the reception (figure III.3), the digitizer transposes the RF signals to intermediate frequency of 77 MHz in order to be digitized. The IQ data resulting from the digitization is computed in Matlab.

B. Test plan

The use of a single antenna in transmission to illuminate one of the stirrers did not allow obtaining an isotropic Rayleigh channel.

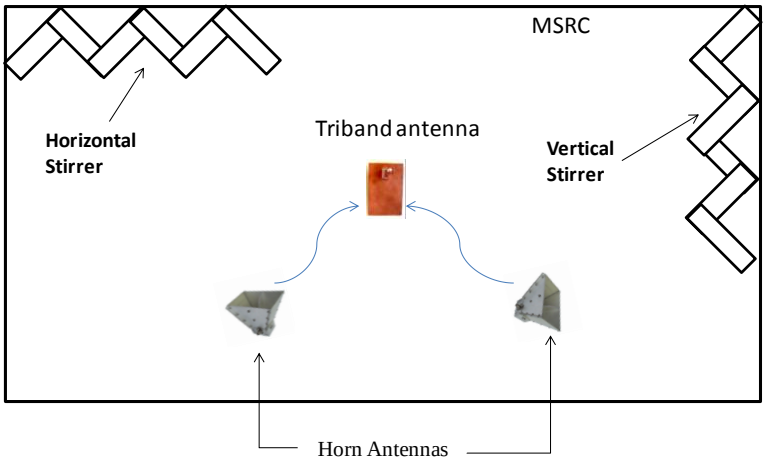

Figure III.4: configuration used during measurements

The configuration presented in this part aim to show that the use of two transmitting antennas (a horn antenna illuminating the horizontal stirrer, and a horn antenna illuminating vertical stirrer) are necessary to generate a propagation environment statistically isotropic and obtain a Rayleigh fading distribution. This therefore requires two illumination antennas for SISO and SIMO mode.

After the introduction of the measurement platform used for the channel sounding and the configuration showing the location of the antennas inside the MSRC, an interest will be brought to the presentation of the channel sounding results.

C. Emulation measurement results

In order to study the dependence of the antenna diversity system performance on the RMS delay spread of the multi-path channel in the RC, different amounts of absorbing material have been introduced inside its inner cavity, thus modifying the power-delay profile (PDP) of the channel, and achieving scenarios with different RMS delay spread values, as depicted in Figure (III. 5).

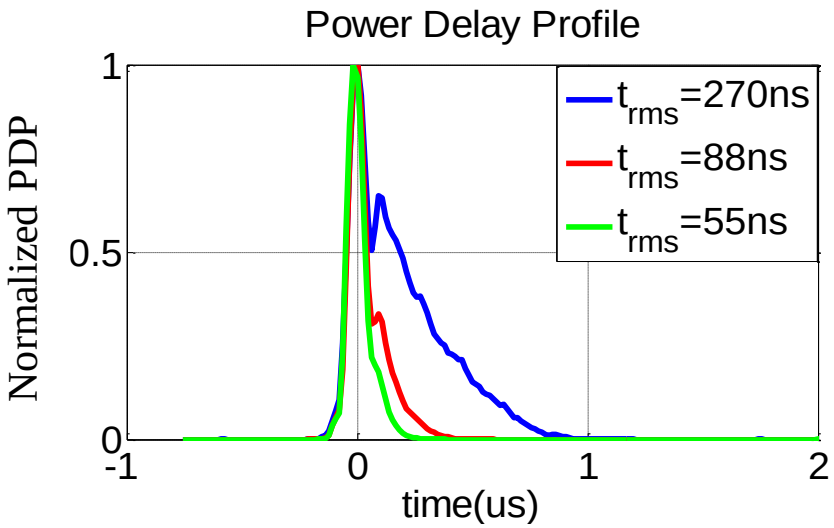

Figure III.5: Measured PDPs for different RMS delay spread values

The results in figure III.5 highlight the dependence of the RMS delay spread measured value on the amount of absorbing material located inside the RC. The use of absorbing material decreases considerably the RMS delay spread value [31, 32]. Of course, the introduction of absorbing materials also increases the power losses (see figure III.6).

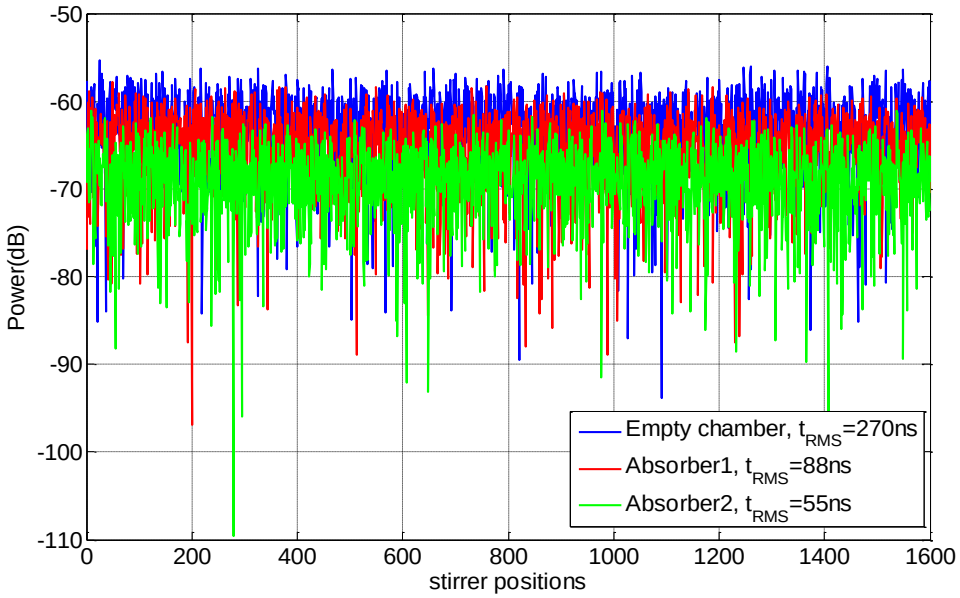

Figure III.6: Measured received power for different absorbing material quantities

In order to check the fading distribution, a power measurement was also made at the central frequency in order to plot the normalized CDF (see the CDF definition in chapter I). Figure III.7 below shows that the fading is still Rayleigh even after the addition of losses. The CDFs presented in Figure III.7 show respectively the analytical Rayleigh CDF, CDF calculated from measured data for empty chamber case and for the chamber with RMS delay spread of 88ns.

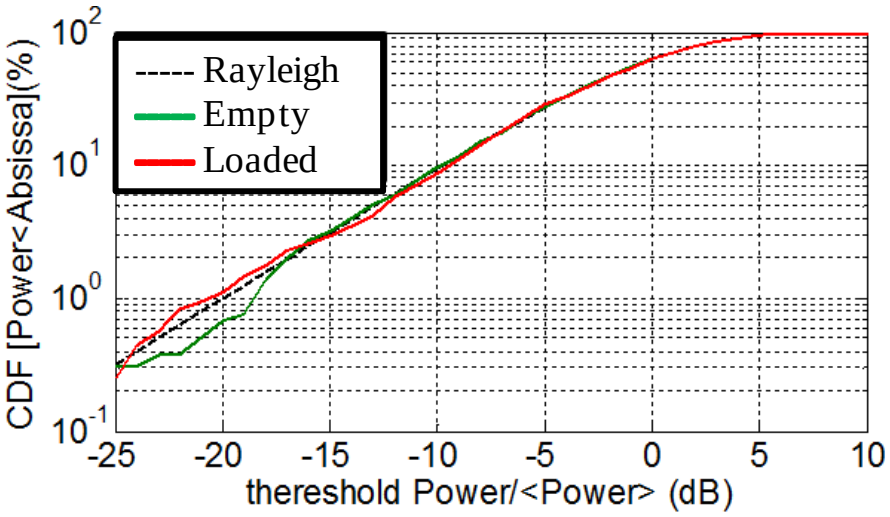

Figure III.7: CDF measured in the loaded and unloaded RC.

Channel sounding has allowed the characterization of the propagation channel, in which a diversity system is supposed to be tested. Performances Evaluation of this system will be the goal of the next section.

2.2.Measurements of diversity performance of multi-antenna system depending on channel delay spread

2.2.1. Presentation of the diversity measurement test bed

The measurement platform consists in a PXI chassis, as depicted in Figure III.8. The chamber is excited by two horn antennas connected to the transmitter, which integrates the controller and Aeroflex modular RF signal generator with an integrated dual-channel arbitrary waveform generator, and with a modulation bandwidth up to 66 MHz. The antennas under test are compact wideband tri-band antennas for mobile terminals [27], based on planar inverted-F antenna (PIFA) elements, as depicted in figure III.10. They are connected to the receiver, which integrates two Aeroflex digitizers with conversion of the RF signal to digital IQ data. At the transmitter and receiver, IQ data processing is done under MATLAB, and via the PXI controller. Diversity combining techniques such as maximal-ratio combining (MRC) and equal gain combining (EGC) have been implemented and are based on a channel estimation algorithm, using a pilot sequence inserted in the transmitted frames. For the measurements presented here, a bandwidth of 1 MHz has been chosen, with a QPSK modulation scheme, over a carrier frequency of 5.5 GHz. For each measurement point, $2 \cdot 10^5$ symbols are captured to estimate the Frame Error Rate and the Signal to Noise Ratio (based

on the Error Vector Magnitude calculation [28]). Equalization or error correcting code has not been used along this study in order to present the raw performance of the system under test.

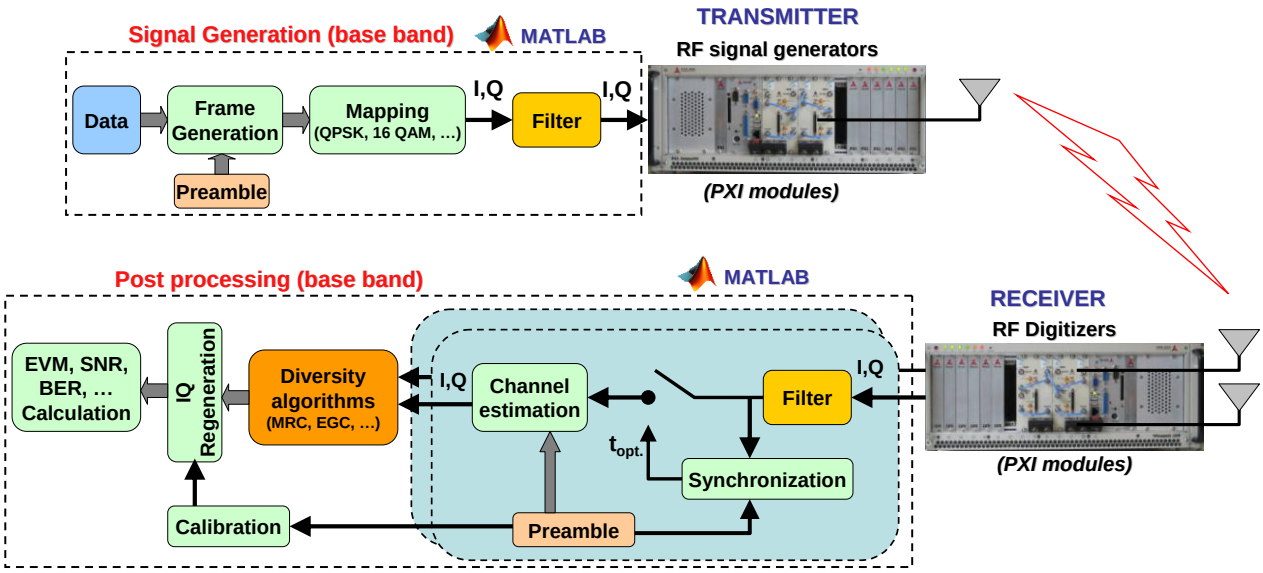

Figure III.8.a: SIMO diversity measurement platform

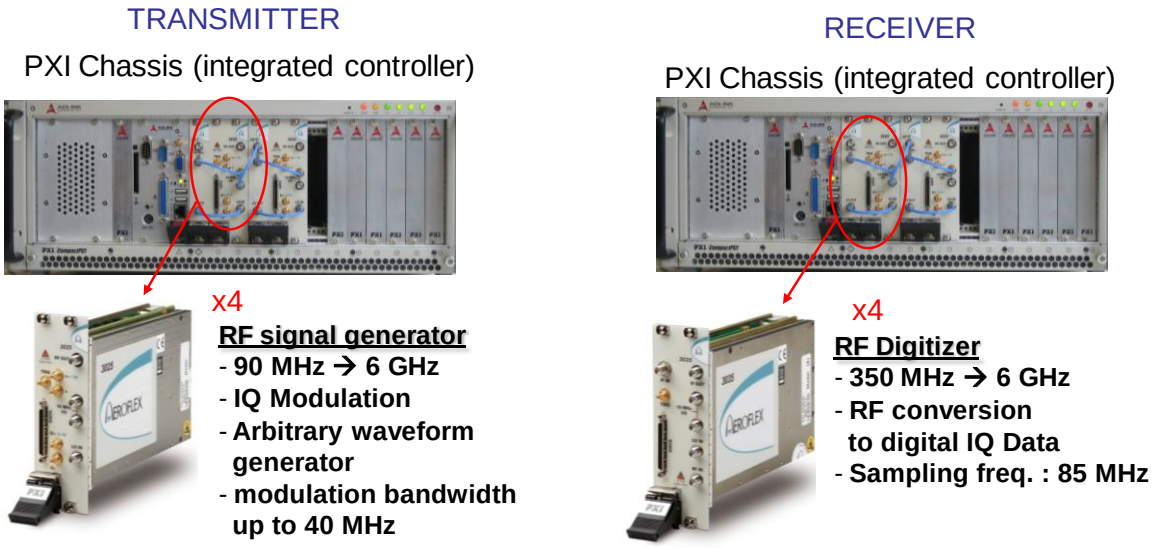

Figure III.8.b: transmitter and receiver module

A. Frame used for diversity measurements

The signals are generated in the form of data frames. The downlink frames are composed by a preamble with a portion size of N_{TS}=32 representing the number of symbols and a part of useful data with size of N_d=100.

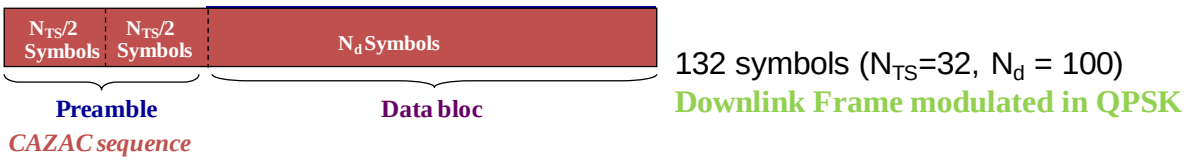

Figure III.9: Data frame form

The size of the data frame is equal to 132 symbols. The frame preamble that is modulated in QPSK consists of 16 symbols of a CAZAC sequence (Constant Amplitude Zero Auto-Correlation sequence) repeated once, the CAZAC sequence is also used in the WiMax standard. The QPSK modulation is chosen for all subsequent measurements. The 16 symbols of CAZAC sequence are [29]:

1+j, -1+j, -1-j, 1-j, 1+j, -1-j, 1+j, -1-j, 1+j, 1-j, -1-j, -1+j, 1+j, 1+j, 1+j & 1+j.

The symbols are processed by a square root digital filter with a raised cosine. The first step allowing generating digital signals in the baseband is performed with a Matlab program. The symbols (I, Q) are filtered and transmitted to the transmitter integrated in Aeroflex PXI chassis (Figure.III.8.a).

B. Antennas

For all measurements we are going to use reference and diversity system. These two systems use a compact tri-band antenna based on PIFA elements. The antennas operate at following frequencies: 2.35 GHz, 3.5 GHz, and 5.5 GHz.

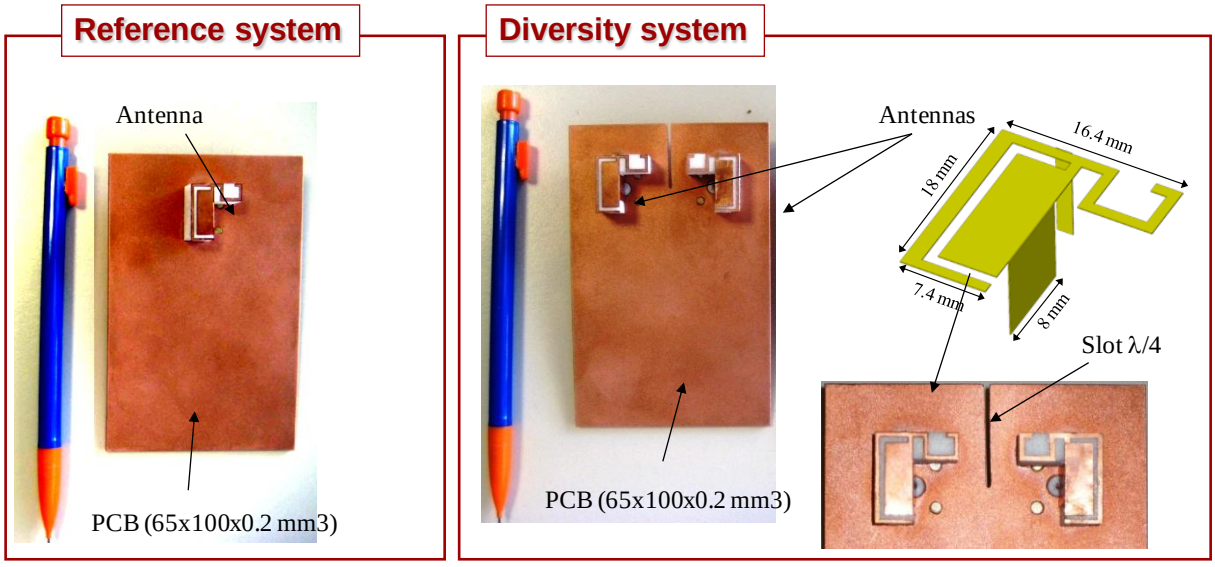

Figure III.10: Compact wideband triband antennas for mobile terminals based on planar inverted-F antenna (PIFA) [27]

	Frequency (GHz)		
	2.4	3.5	5.5
Correlation coefficient in isotropic channel	$5.3\ 10^{-3}$	$6.2\ 10^{-3}$	$1.5\ 10^{-3}$

The correlation coefficient is calculated according to the equation (I.9) shown in chapter I.

The diversity measurement test bed is implemented, in order to evaluate the performance of wireless diversity system for different emulated propagation channels. The obtained results are exposed in the following.

2.2.2. Performance evaluation of multi-antenna system versus channel delay spread

A. Correction of averaged received power

Adding absorbing materials and using the same level of transmitted power, applies that the averaged received power is not the same (see figure III.11). A different transmitted power has been chosen for each scenario, in order to compensate these losses, and thus obtaining the same average power at the diversity antennas as shown in (figure III.13) for each scenario, in order to make the all results directly comparable.

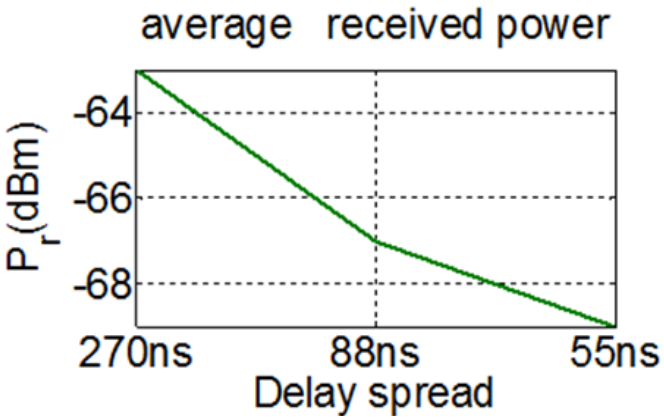

Figure III.11: measured average received power before compensation

To solve this problem, we thought to realize losses compensation at the transmitted signal and for each emulated channel with different transmitted power. Figure III.12 present the transmitted power versus delay spread, as it can see on this figure the values go from -38 dBm for channel emulated with RMS delay spread of 270 ns to -32 dBm for channel emulated with RMS delay spread of -55 ns.

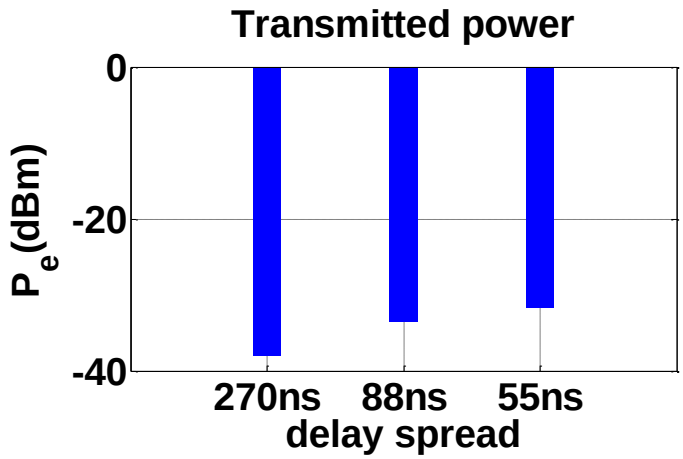

Figure III.12: Different transmitted power versus channel delay spread

The results of measured averaged received power after compensation versus delay spread can be observed on figure III.13. It can be seen that the same level of the mean received power is obtained.

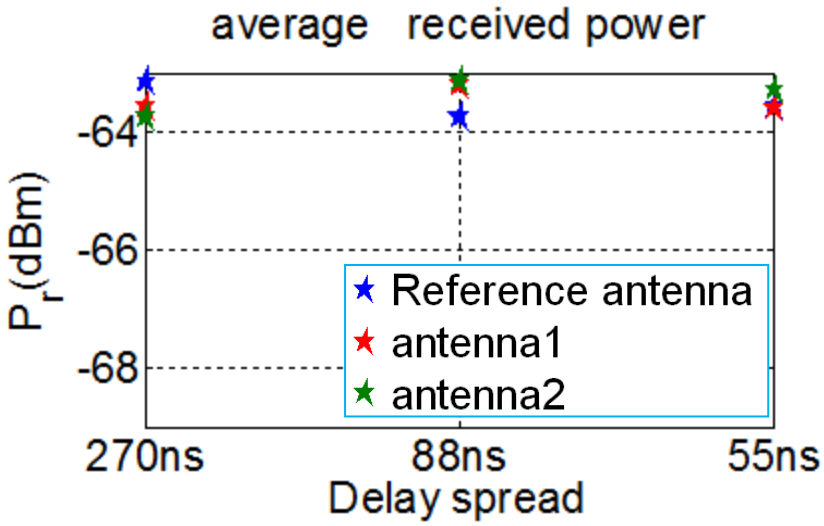

Figure III.13: measured average received power after compensation

B. Measurement results

The cumulative distribution function (CDF) of the signal to noise ratio (SNR) from the reference antenna and from the diversity antennas has been studied for the previously presented 1x2 SIMO antenna system in three different scenarios, which are characterized by their RMS delay spread values, as shown in (Figure III.5). The CDF of the SNR from the reference antenna along with the ones obtained from the diversity antennas using EGC and

MRC diversity combining techniques are presented in Figure III. 14-16, after normalize them to the mean SNR from the reference antenna.

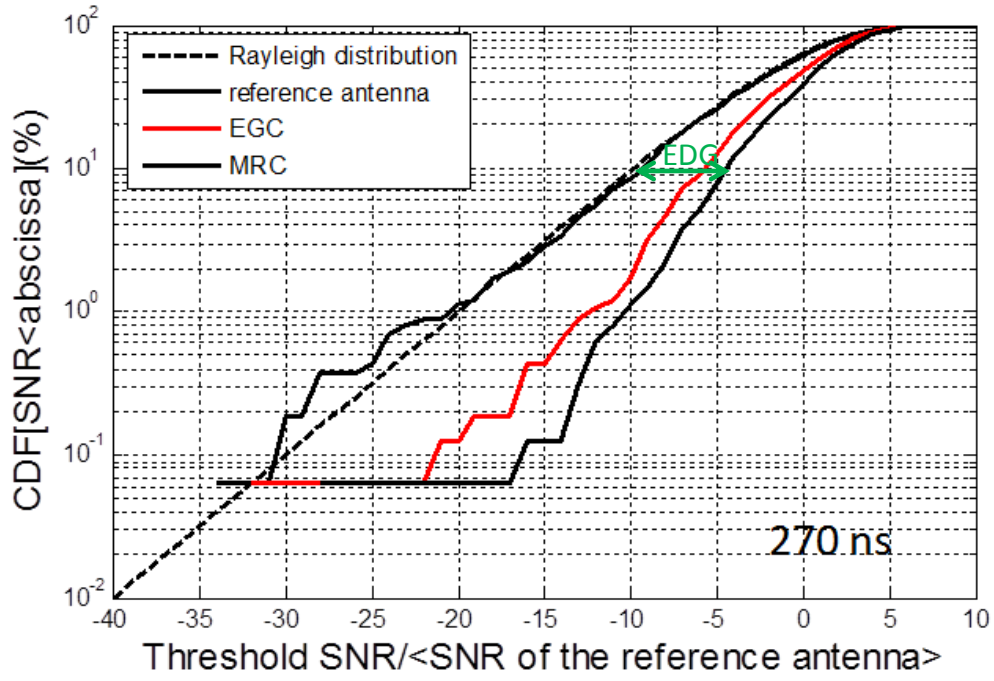

Figure III.14: Cumulative Distribution function: EDG using MRC & EGC combining for τ_{RMS}=270ns

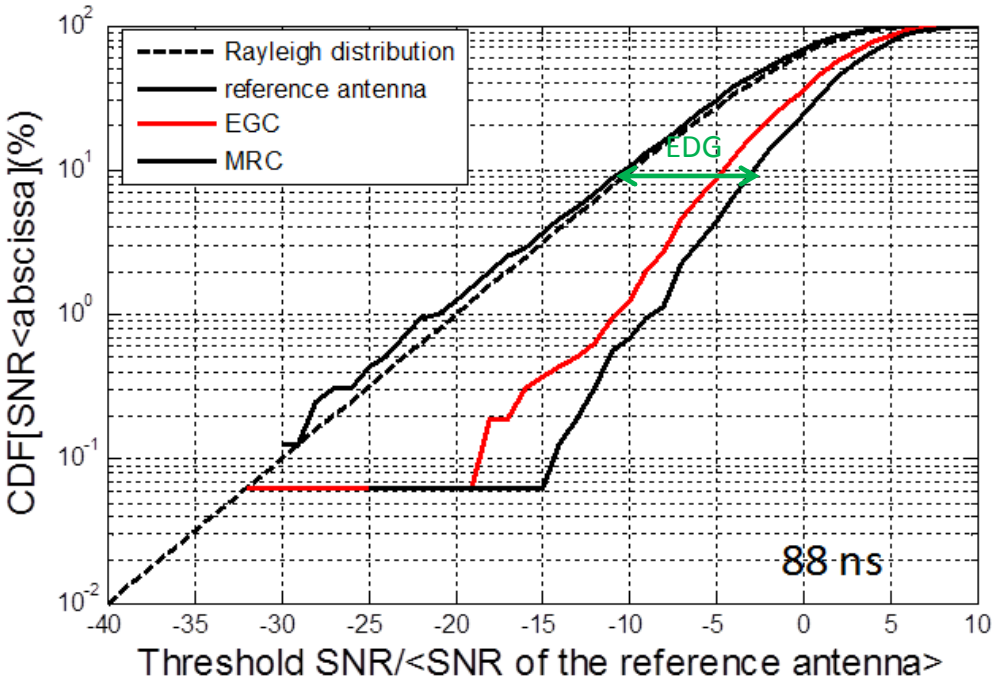

Figure III.15: Cumulative Distribution function: EDG using MRC & EGC combining for τ_{RMS}=88ns

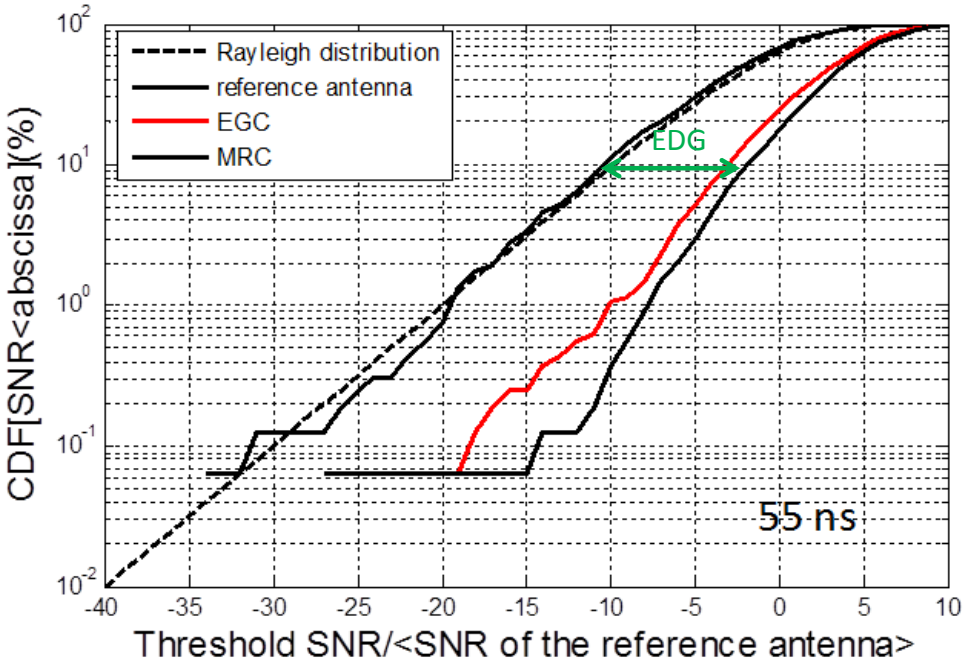

Figure III.16: Cumulative Distribution function: EDG using MRC & EGC combining for τ_{RMS}=55ns

As we can observe in these figures, the CDF calculated from the SNR of the reference antenna is Rayleigh distributed, and this is maintained along the different scenarios, even with the addition of absorbing materials, which will permit to compare their effective diversity gain results, since the environment remains a Rayleigh channel. The scenarios transmission performance is synthetized in Table I.

Scenario RMS delay spread (ns)	Antenna system	Mean SNR (dB)	BER	FER	EDG(10%)	
					EGC	MRC
270	Reference antenna	13.8	$2.8\,10^{-2}$	$2.2\,10^{-1}$	3.8 dB	4.8 dB
	Antenna1	13.54	$3.1\,10^{-2}$	$2.3\,10^{-1}$		
	Antenna2	14.8	$2.2\,10^{-2}$	$1.8\,10^{-1}$		
	EGC	14.34	$5.5\,10^{-3}$	$5.7\,10^{-2}$		
	MRC	15.2	$1.6\,10^{-3}$	$2.7\,10^{-2}$		
88	Reference antenna	14.95	$1.1\,10^{-2}$	$1.1\,10^{-1}$	4.8 dB	6.7 dB
	Antenna1	14.32	$1.9\,10^{-2}$	$1.3\,10^{-1}$		
	Antenna2	15.12	$9.7\,10^{-3}$	$9\,10^{-2}$		
	EGC	17.5	$1.2\,10^{-3}$	$1.7\,10^{-2}$		
	MRC	18.55	2.810^{-4}	$8.6\,10^{-3}$		
55	Reference antenna	15.73	$6.6\,10^{-3}$	$7\,10^{-2}$	6.2 5dB	7.28 dB
	Antenna1	15.76	$1.8\,10^{-2}$	$1.2\,10^{-1}$		
	Antenna2	15.49	$7.2\,10^{-3}$	$6.4\,10^{-1}$		
	EGC	19.05	$8.4\,10^{-4}$	$1.2\,10^{-2}$		
	MRC	19.82	$2.7\,10^{-4}$	$6\,10^{-3}$		

Table 1 : Scenarios transmission performances

As we can deduct from the results in Table I, the more absorbing material is introduced in the RC, the less multi-path components arrive at the receiving antennas, and therefore not only RMS delay spread value is reduced, but also mean SNR value is increased.

As presented in the table I the SNR is better for EGC and MRC than reference antenna. Concerning the BER and FER are less for EGC and MRC than reference antenna.

Finally, the EDG of the 1x2 SIMO antenna systems is evaluated using EGC and MRC diversity combining techniques for 10% reliability levels. The results are presented in Table I and depicted in figures III.17-18.

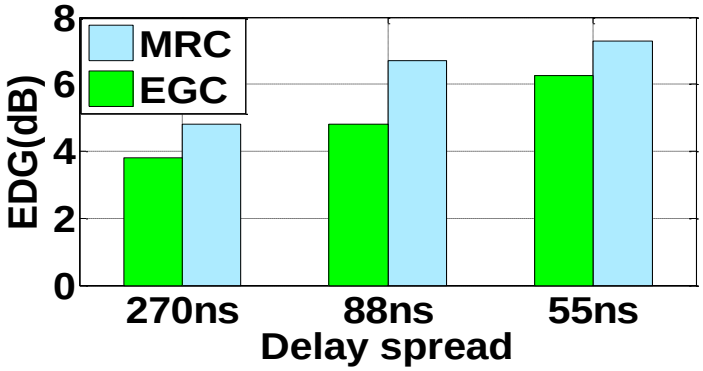

Figure III.17: EDG for MRC & EGC techniques at (10%)

From these results it can be seen that an increase of the RMS delay spread of the channel inside the RC, not only reduces the mean SNR for both the reference and diversity antennas, but also the gap between them, and thus the EDG value decreases . The figure III.17 present the evolution of EDG versus delay spread, and it can be observed that when the delay spread decrease the DG increases, this phenomenon can be explained since the employment of diversity techniques can correct the channel fading effects in the system performance, but not the ones related to the frequency selectivity of the channel, which is increased when the RMS delay spread value increases, and thus EDG value becomes lower.

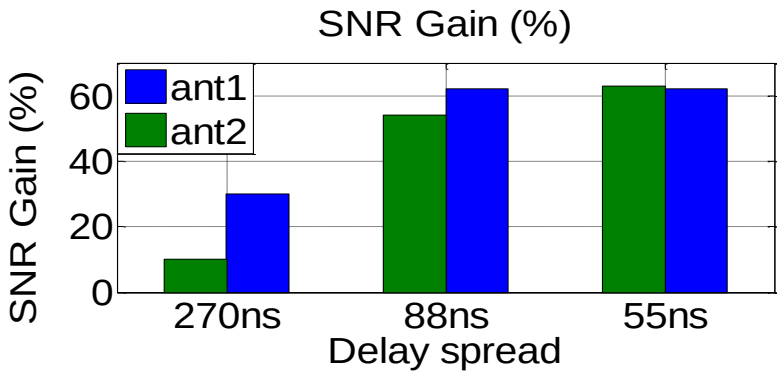

Figure III.18: SNR improvement between MRC combining and antenna1 & antenna2

In the legend of figure III.18, ant 1 and ant 2 present the two antennas of the diversity system depicted in Figure III.10.
These results can be confirmed by the figure III.18 that presents the SNR gain versus delay spread that allows observing the evolution of the wireless system performances versus the channel delay spread.

This part present a major interest in analysis of wireless systems depending on the channel delay spread. An experimental control of the delay spread is shown possible. In following section a performance analysis of wireless terminals for the LTE technology will be target.
During this analysis two kinds of measurements will be performed: no-real time measurements and real time measurements.
Real-time measurements are performed in the context of a project that aims to characterize the real 4G mobile devices. This project brings together XLIM institute, the Bouygues telecom operator and ANOVO society.

3. Analysis of MIMO-LTE terminals performances in reverberation chamber

In this section, two points dedicated to non real time and Real time Over The Air (OTA) measurement for evaluating wireless communication terminals performance are investigated.
Firstly, an emulation methodology of multiple clusters channels for evaluating wireless communication devices over-the-air (OTA) performance is investigated. This methodology has been used along with the implementation of the SIMO LTE standard. This method consists of evaluating effective diversity gain (EDG) level of SIMO LTE-OFDM system for different channel models according to the received power by establishing an active link between the transmitter and the receiver. The measurement process is set up in a Reverberation Chamber (RC). The obtained results are compared to the reference case of single input-single output (SISO) in order to evaluate the real improvement attained by the implemented system. The measurement process is performed in non real time.
Second part of this section aims to introduce a measurement test bed that has been associated along with a channel emulation platform in order to evaluate the terminals performances in real time. It consists of assessing the throughput and the total isotropic sensitivity (TIS) level of the 4G MIMO-LTE terminals by establishing a real communication between the base station (R&S CMW500) and the user equipment (mobile terminals). The performances evaluation is performed for different emulated channel models in reverberation chamber. This

emulation must be accompanied by a strict control of delay spread**.** The obtained TIS results are compared to the results obtained in anechoic chamber.

Before taking an interest to measurements of LTE terminals a short presentation of LTE standard in downlink will be crucial.

3.1. Long Term Evolution (LTE) Downlink transmission.

A long term evolution (LTE) of the 3rd Generation Partnership Project (3GPP) access technology is being specified in Release 8 of the 3GPP standard. The LTE specification provides a framework for increasing capacity, improving spectrum efficiency, improving coverage, and reducing latency compared with current HSPA implementations. In addition, transmission with multiple input and multiple output (MIMO) antennas is supported for greater throughput, as well as enhanced capacity or range. To support transmission in both the paired and unpaired spectrum, the LTE air interface supports both frequency division duplex (FDD) and time division duplex (TDD) modes. The LTE downlink (DL) transmission system is based on orthogonal frequency division multiplexing access (OFDMA) and the DL OFDM supports high data rates. The following section provides a high-level description of the LTE physical layer (PHY).

LTE also uses adaptive modulation and coding to get better data throughput. This technique varies the downlink modulation coding scheme based on the channel conditions for each user. When the link quality is good, the LTE system can use a higher order modulation system (more bits per symbol). On the other hand, when link conditions are poor due to troubles such as signal fading, the LTE system can modify to a lower modulation system to keep a satisfactory radio link. The modulation system supported for payload in the uplink and downlink are QPSK, 16QAM and 64QAM.

The LTE PHY is considered to congregate the following goals:

- Carry scalable bandwidths of 1.4, 3.0, 5.0, 10.0, 15.0, and 20.0 MHZ.
- High performances at speeds up to 120km/hr.
- Supported antenna configurations
    - Downlink: 4x2, 2x2, 1x2, 1x1.
    - Uplink: 1x2, 1x1.

In OFDMA, users are allocated a specific number of subcarriers for a determined amount of time. These are referred to as physical resource blocks (PRBs) in the LTE characteristics. PRBs thus have both a time and frequency dimension. Allocation of PRBs is handled by a development function at the 3GPP base station.

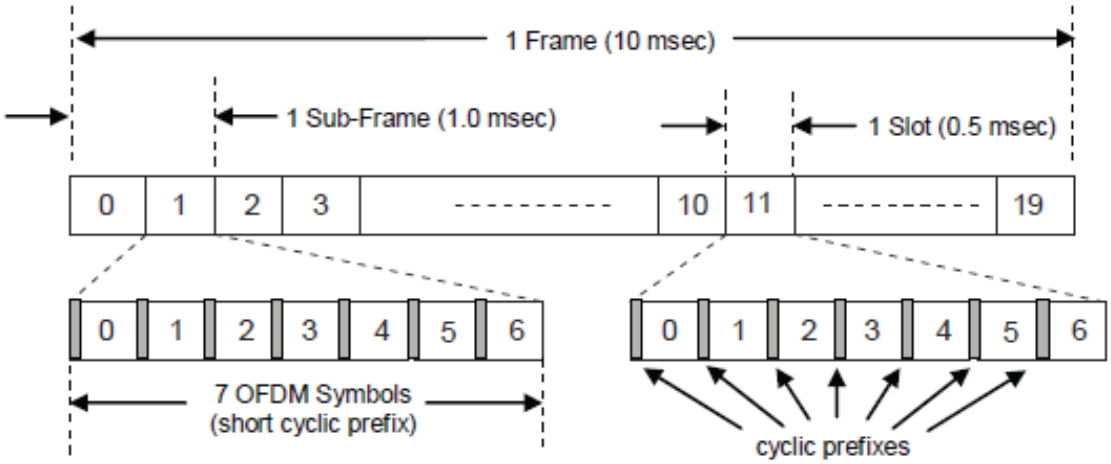

Figure III.19: LTE Frame Structure (Ref: TS 36.101 V9.3.0)

To explain sufficiently the OFDMA inside the environment of the LTE, we must study the PHY layer generic frame structure. The generic frame structure is used with FDD. Alternative frame structures are defined for use with TDD. However, TDD is beyond the scope of this paper. Alternative frame structures are therefore not considered.

As shown in (figure III.19), LTE frames are 10 msec in duration. They are divided into 10 sub frames, each sub frame being 1.0 msec long. Each sub frame is composed by two slots, each of 0.5 msec duration. Slots consist of either 6 or 7 ODFM symbols, depending on whether the normal or extended cyclic prefix is employed.

The transmission bandwidth of system gives us an idea concerning the total number of available subcarriers. The LTE specifications define parameters for system bandwidths from 1.4 MHz to 20 MHz as shown in Table 2. A PRB is defined as consisting of 12 consecutive subcarriers for one slot (0.5 msec) in duration. A PRB is the smallest element of resource allocation assigned by the base station scheduler.

Bandwidth (MHz)	1.25	2.5	5.0	10.0	15.0	20.0
Subcarrier bandwidth (kHz)	15					
Physical resource block (PRB) bandwidth (kHz)	180					
Number of available PRBs	6	12	25	50	75	100

Table 2: Available downlink bandwidth is divided into Physical Resources Blocks

The LTE DL is composed of two sets of physical layer channels: physical channels and physical signals. Physical channels take information from higher layers and are used to carry user data, as well as user control information. Physical signals are used for system synchronization, cell identification and radio channel estimation, but do not carry information originating from higher layers.

3.2. Not-real time OTA measurements of MIMO-LTE system: Performances analysis for different 3GPP channel models emulated inside Reverberation Chamber

Active measurement methods are often based on the use of a channel emulator associated with a real-time transmission system, to test the operational terminals. In this part of work, the aim is to suggest an experimental platform using a small size reverberation chamber (described before) in order to study the feasibility of emulating multipath channel while maintaining a Rayleigh fading (in order to be able to compare deferent receivers in reference environments with the same distribution). On this platform, a multi cluster emulation method which complies with standardized 3GPP channel models is implemented, using only one vector signal generator (figure III.8.b). This emulation must be accompanied by a strict control of delay spread, to generate realistic channels [33–34].

This methodology, along with the presented model, emulates a Spatial-Channel-Model-Extended (SCME) for MIMO OTA active measurements.

The presented approach aims to develop a soft OTA methodology for characterization and implementation of digital multi antenna transmission systems inside a small size reverberant cell. On this test bed, the measurements are not carried out in real time and are not dedicated to performance evaluation in terms of throughput. However, it allows (through the use of an RF digitizer and baseband processing in MATLAB) to study in detail the impact of several transmission chain parameters, as antenna aspects (in MIMO context: coupling, correlation coefficient ρ), and test of signal shaping and reception algorithms (synchronization, equalization, MIMO coding). This method is applied to test the 3GPP LTE standard, by implementing an LTE-OFDM frame and using diversity at the receiver side. The frame is generated based on the 3GPP standard [35, 36], which specify a downlink (DL) transmission system using an orthogonal frequency division multiplexing access (OFDMA) [37, 38] as shown in the paragraph before.

After having introduced the LTE requirements, it is necessary to focus on parameters for evaluating the performance of a system under test [39, 40, and 41]. Generally, these parameters are aimed to SIMO passive measurements at one frequency, which will be applied to the case of LTE active measurements [42, 43, and 44].

3.2.1. Measurement test bed

The LTE signal described previously is implemented on the measurement test bed (Figure III.20). The measurement test bed is based on the Aeroflex PXI 3000 series architecture described in (III.8.b), with two PXI chassis integrating a control PC for generating frames on transmission and for processing received data. The transmitter part includes one RF signal generator (76 MHz–6 GHz), which can provide a level of RF power from −120 dBm to +5 dBm over a modulation bandwidth of 33 MHz. The receiver integrates two digitizers, which provide conversion of RF signal to baseband digital IQ symbols [45]. Data processing is done with MATLAB.

At the transmitter side, a frame based on LTE specifications is generated. The duplex mode used is TDD, and a bandwidth of 5 MHz has been chosen, with 64QAM modulation scheme, over a carrier frequency of 2.35 GHz.

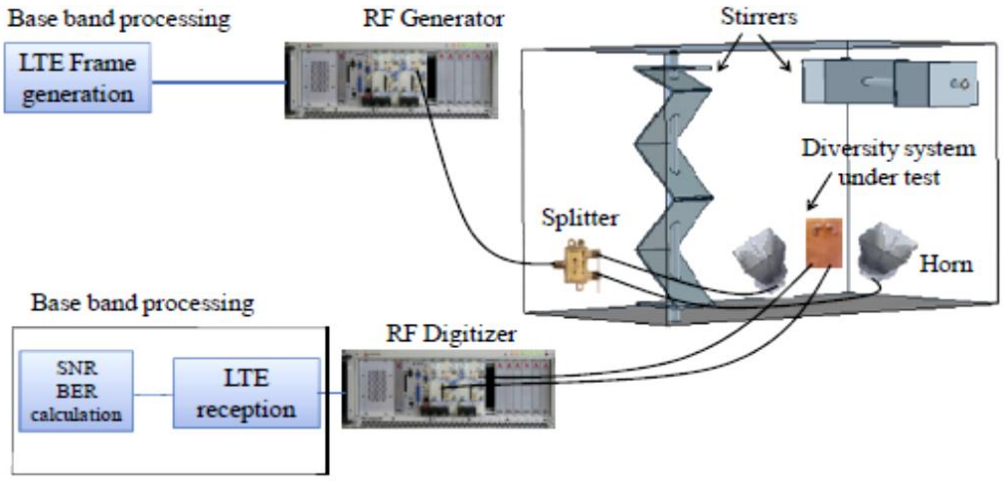

Figure III.20: Measurement test bed

Before taking an interest for measurements, it is necessary to introduce the method with which it is wanted to emulate different channels inside the MSRC. This emulation is based on the idea of convolving the desired model to emulate with the signal to be transmitted. Further explanation will be presented in the following.

3.2.2. Channel Emulation

The characteristics of the LTE-OFDM frame and measurement system to be used has been explained previously. This section will focus on establishing a method for the emulation of 3GPP channel models with a particular delay spread, which requires a control of the delay spread inside the RC.

A. 3GPP channel model

The 3GPP urban microcell and urban macro cell channel models in [35, 36] are defined to be used for multi antenna OTA comparison measurements. The taps delay in urban micro-cell and urban macro-cell channel models are depicted in (Figure III.21). It can be seen that the urban macro cell channel presents a high delay spread compared to the urban microcell. The taps delay and the power magnitude are listed in details in Table 3.

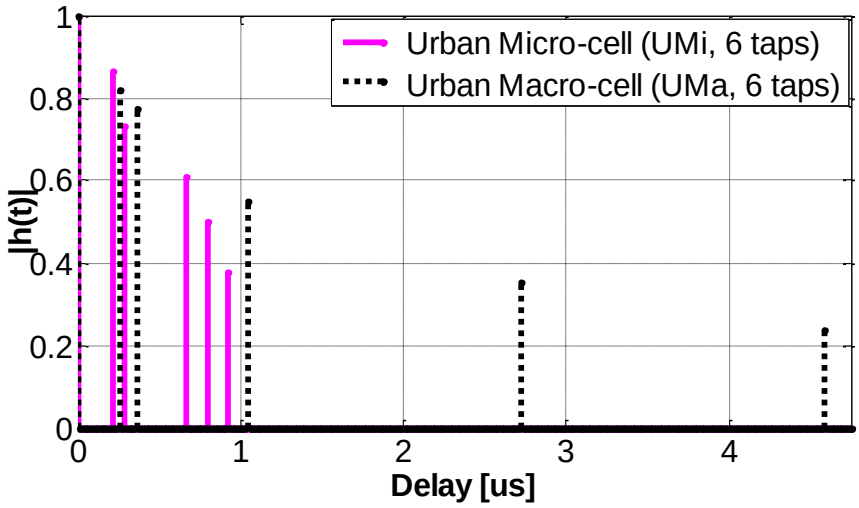

Figure III.21: Urban micro- and macro cell channel model taps.

Some special consideration should be taken into account when implementing channel models in an RC. Indeed these models introduce intra cluster delay spread. Then, for each tap an RMS delay spread (τ_{rms}) of 90 ± 5 ns has to be considered.

Scenario		Urban Macro		Urban Micro	
Power/delay parameters: Relative path power (dB) Delay(µs)	1	0	0	0	0
	2	-1.7184	0.2527	-1.2651	0.284
	3	-2.2204	0.36	-2.7201	0.2047
	4	-5.1896	1.0387	-4.2973	0.6623
	5	-9.0516	2.73	-6.014	0.8066
	6	-12.5013	4.5927	-8.4306	0.9227
Resulting total DS(µs)		0.841		0.294	

Table 3: Parameters of the urban microcell and urban macro cell scenarios.

B. Control of the RMS Delay Spread.

The same antenna configuration presented in (figure III.4) is adopted in this section. The delay spread τ_{rms} can be changed by loading the chamber with an appropriate amount of absorbing material [34, 46].

In order to check the fading distribution, a power measurement is made at the central frequency to plot the normalized CDF. Figure III.22 shows that the fading measured at 2.35GHz is still Rayleigh even after the addition of losses. The difference concerning the measured mean powers before and after adding absorbing materials is around 3 dB. In this part, the control of the τ_{rms} has been achieved by the use of absorbing material, and maintaining a Rayleigh fading distribution. The goal now is to emulate a multi-cluster channel with the same delay spread for each cluster.

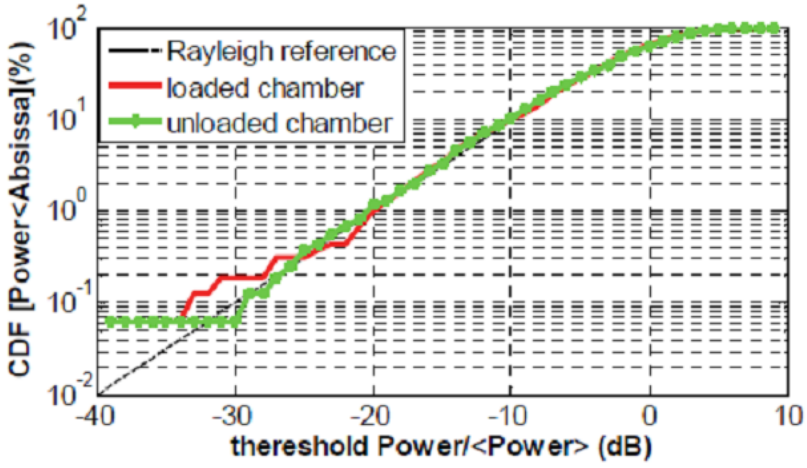

Figure III.22: CDF measured in the loaded and unloaded RC at 2.35GHz.

When the chamber is loaded with a piece of absorbing material, which is solid, pyramidal shaped, and carbon loaded (urethane foam absorber [47]) with dimensions of 16 cm × 9 cm × 4 cm, placed in a corner of the RC, the RMS delay spread is around 93 ns. This value stay depending on the MSRC dimensions. The use of absorbing materials decreases considerably the value of the delay spread and allows achieving the desired result which should be within 90 ± 5 ns.

C. Clusters Emulation

The method to emulate the channel model consists of convolving the base band signal to be transmitted with the urban macro-cell or urban micro-cell channel model tap delay line generated using a MATLAB program (see Figure III.23).

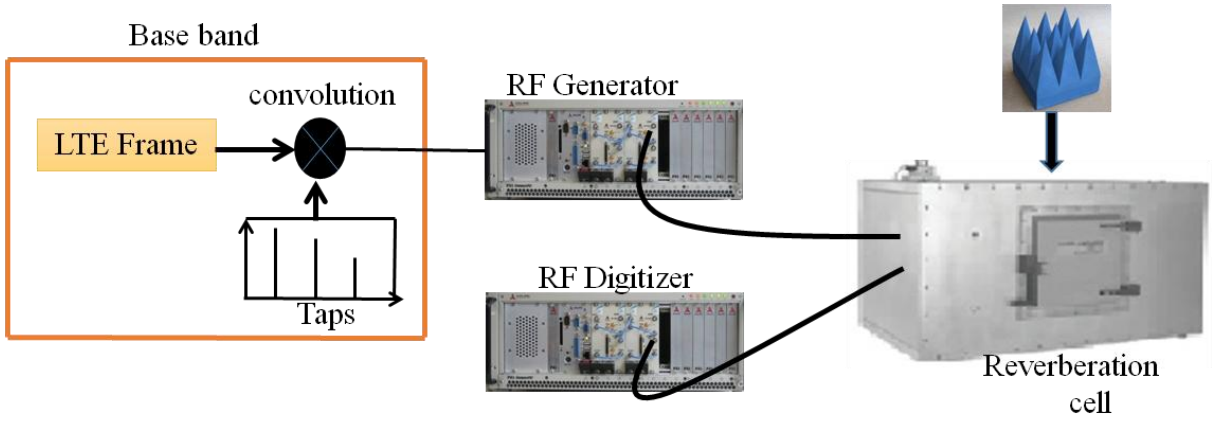

Figure III.23: Channel emulation overview

In order to verify the proper functioning of this method, a channel sounding based on a sliding correlation [48] is performed, with a sampling frequency Fe of 64 MHz at carrier frequency f_0 of 2.35 GHz. The sampling frequency is chosen initially higher, to obtain a good time resolution and verify that the channel is well emulated.

The emulated channel is presented on Figures III.24-25.

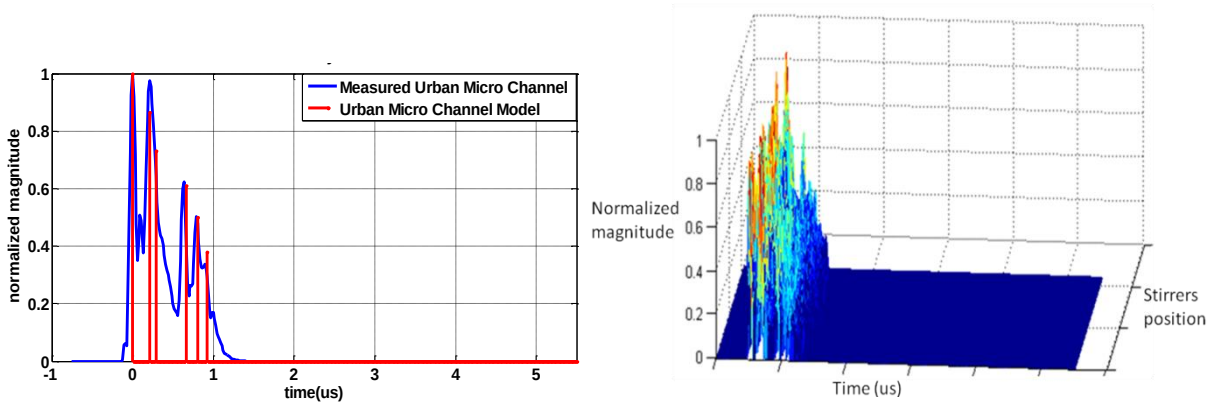

Figure III.24: PDP measured in RC for the urban micro-cell (UMI) channel model emulation.

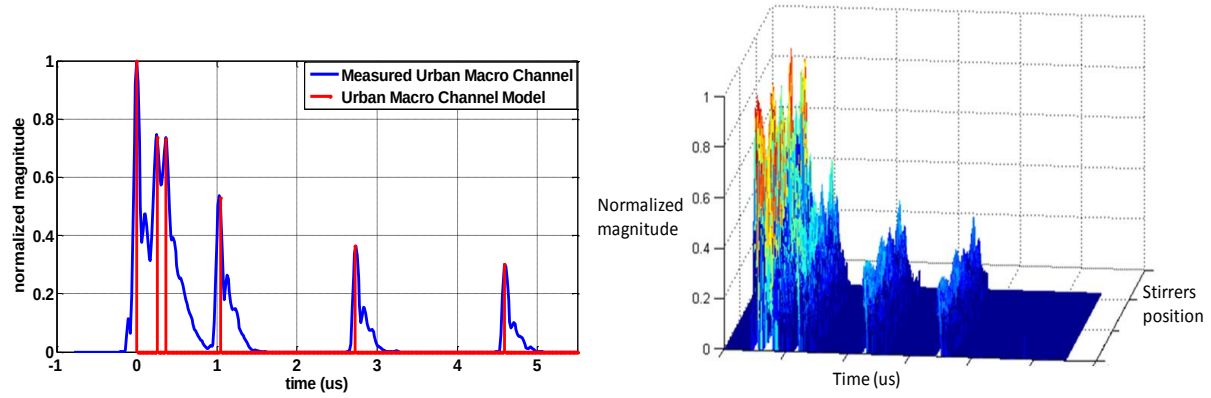

Figure III.25: PDP measured in RC for urban macro-cell (UMA) channel model emulation.

Figures III.24 and III.25 present the power delay profile curves measured in RC urban micro and urban macro-cell channel models, respectively.

The different results presented in this section highlight the possibility of controlling the intra cluster delay spread, and emulating 3GPP urban micro- and macro-cell channel models. This is obtained by combining a digital pre-processing and a RC to manage the τ_{rms} value.

The implemented emulation method has shown great flexibility to reproduce the standardized 3GPP channel models inside the MSRC. This method plays the role of a channel emulator, but the measurements cannot be performed in real time, because the channel model is created in post-processing. This method is important for performance evaluation of the diversity system for different channels.

3.2.3. Measurements of LTE performance of multi-antenna system for different emulated channel models inside RC

In order to realize these measurements, two boards representing a compact terminal are used: one reference board with one tri-band antenna, and diversity board with two tri-band antennas (see Figure III.10). These antennas have been studied previously in [49, 50].

A. SISO measurements

By using the LTE system implemented in Section 2, the SISO configuring measurement will be performed. In order to simplify the analysis, the stirrers of the RC used for this study were rotated step wisely for 1600 positions, so the Doppler spread of the channel is negligible.

The CDF curves plotted in Figure III.26 present two types of results:

(i) Cumulative distribution calculated from the measured power of a sub carrier.

(ii) The CDFs from the averaged power of received signal, demodulated after equalization.

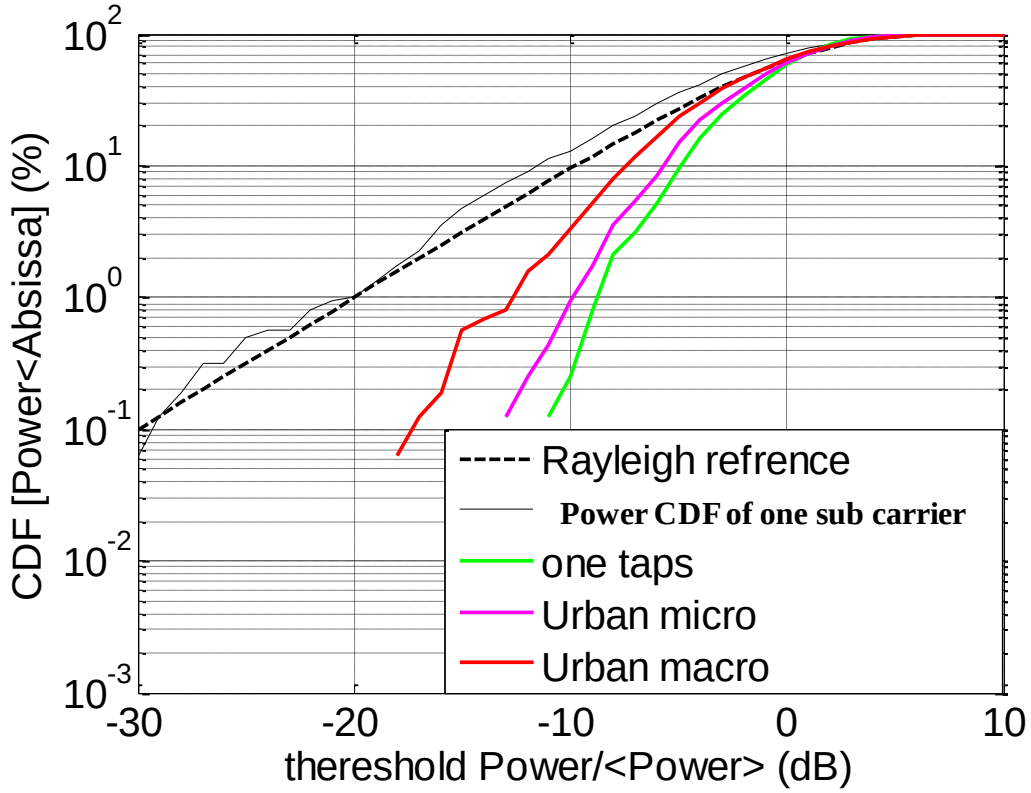

Figure III.26: SISO cumulative distribution function measured in RC for one cluster, urban micro, and urban macro cell channel model cases

For this comparison, each measured power of these results is normalized to its own average power.

As it is known OFDM signal gives better performance than using mono-carrier signal. It is an efficient way to deal against inter-symbol interference, because such interference affects only a small percentage of the subcarriers. These interferences cause a frequency selectivity that can be well observed in Figure III.26. Indeed it can be clearly seen that the cumulative power distributions are influenced by the delay spread of the channel model. The performance in urban micro and urban macro cell channel models is worse compared to the mono cluster case. Nevertheless, the received powers of the LTE signals are higher than those in the mono carrier case (which fit with the Rayleigh reference distribution).

These results can be confirmed by the signal-to-Noise ratio measurement, presented below. The estimation of the measured mean SNR presented in Table 4 is done through the Error Vector Magnitude (EVM) [51]:

	SISO mono cluster	**SISO Urban Microcell**	**SISO Urban Macrocell**
Mean SNR (dB)	**25**	**7.9**	**6.4**

Table 4: Measured mean SNR value for SISO configuring for a 64-QAM modulation scheme.

The SISO measurement method allows assessing the capacity of a complete LTE transmission chain. This method makes it possible to know the performance as function of the receiver antenna, or base band processing (equalization, synchronization, etc.).

B. SIMO measurements

In this section, the tests of the diversity systems performance are under interest. Diversity combining techniques such as Maximum Ratio Combining (MRC) have been implemented.

Multiple antennas are expressed as a T × R combination, where T is the number of transmitting antennas, and R is the number of the receiving antennas.

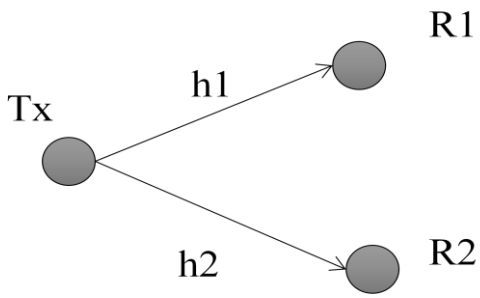

Figure III.27: 1 × 2 Multiple antenna configuring.

The example shown in Figure III.27 presents a total of 2 links between transmit and receive antenna elements. These links are indicated by h 1 and h 2. These expressions are associated jointly to form an H matrix (obtained by channel sounding measurements):

$$H_{meas} = \begin{bmatrix} h1 \\ h2 \end{bmatrix} \quad \text{(III.1)}$$

The channel impulse responses taking in consideration multipath propagation phenomenon are presented by h 1 and h 2. The envelope correlation coefficient is as follows:

$$\rho = \frac{R(1,2)}{\sqrt{R(1,1)R(2,2)}} \quad \text{(III.2)}$$

$$R = E\left\{\left(H_{meas} - E\left[H_{meas}\right]\right)\left(H_{meas} - E\left[H_{meas}\right]\right)^{H}\right\} \quad \text{(III.3)}$$

Where R is the covariance matrix.

The calculation of the fading correlation coefficient for the different channel models generated in the RC is presented in Table 5.

	SISO mono cluster	**SISO Urban Microcell**	**SISO Urban Macro cell**
Fading correlation coefficient	0.15	0.21	0.32

Table 5: correlation coefficient

It can be observed that for each channel model, the fading correlation remains low, which will lead to optimal diversity results.

Regarding the effective diversity gain (EDG), it is typically calculated for a particular frequency (passive measurements). EDG is the figure-of-merit (FOM) typically used to evaluate the efficiency of the diversity antenna system [43]. In our case, the evaluation of the EDG is made through the mean power of the received LTE signal in baseband.

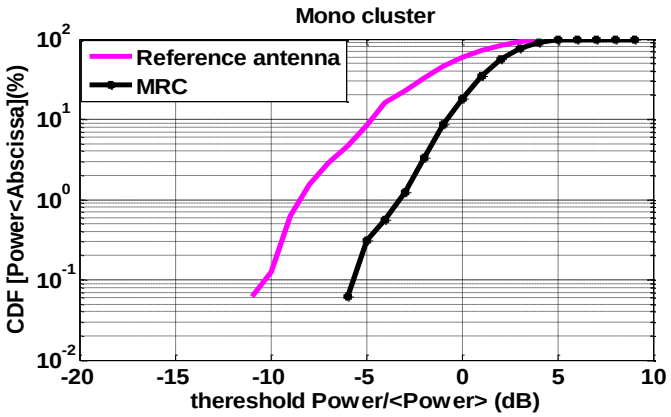

a

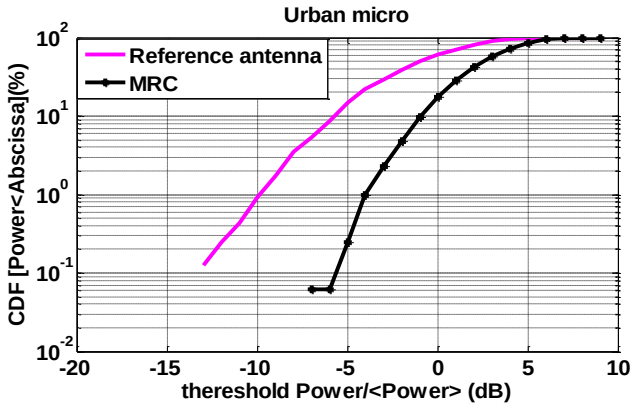

b

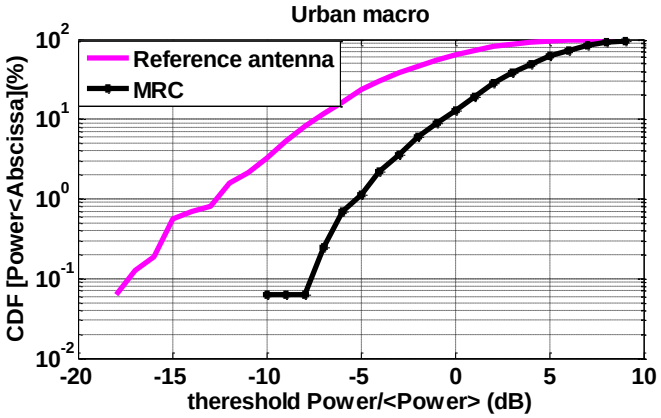

c

Figure III.28: SIMO cumulative distribution function measured in an RC for one cluster (a), urban microcell (b), and urban macro cell (c) channel model cases.

The CDFs of the received power (for the diversity and reference systems) are depicted in Figure III.28. These results are normalized by the mean power received by the reference system in order to calculate the EDG at 1% probability (Figure III.33).

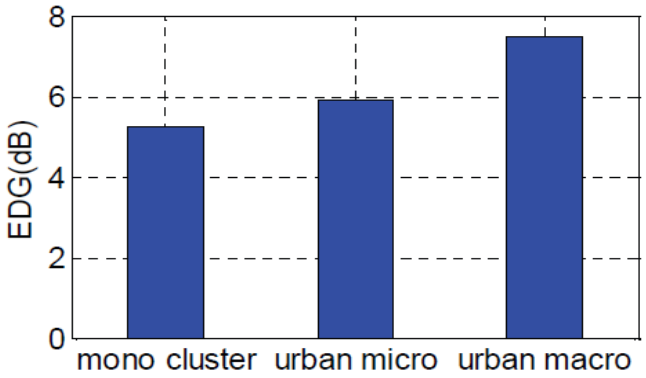

Figure III.29: EDG for MRC technique at (1%) for one cluster and urban micro- and macro cell channel model cases.

In conclusion, as we can observe in Figure III.29 that the more significant improvement in terms of diversity gain is achieved for the macro urban channel case (7.5 dB). The Diversity Gain obtained for the mono cluster case is less important, and it reaches 5.2 dB. This limitation is due to the fact that the SNR of the SISO system in this case was already high when compared to the SNR in multiple clusters channels.

In this part, we achieve to emulate the 3GPP channel models in a small reverberation cell. The performance of an LTE SISO/SIMO-OFDM system has been studied through no-real time active measurements for different channel models with Rayleigh fading distribution. The work developed in this part allowed to evaluate capacity of a wireless system in controlled environments and gives the opportunity to test different transmission chain parameters (base band processing, modulation scheme, antennas, etc.) in the same environment and compare their performance. This approach could be of particular interest for OTA characterization of multi antenna terminals in reverberation chambers, because it helps to understand the impact of the channel characteristics under which measurements have been performed.

The implemented measurement test bed showed large Capacities to evaluate the performance of an LTE system. But this test bed has a disability for the performance evaluation of a terminal in terms of throughput and sensitivity, as these measurements should be carried out in real time. Hence the usefulness to set up a real time tests bed.

3.3. Real time measurements of Total isotropic sensitivity (TIS) and throughput for MIMO-LTE terminals in reverberant cell

Real time Over The Air (OTA) measurement test bed for evaluating wireless communication terminals performance is investigated. In this section, the proposed MIMO-LTE measurement scenarios test is based on MSRC.

From a practical point of view, this solution is faster to implement, since it allows submitting the terminal at an instantaneous 3D multipath environment. The MSRC can be used to measure the total isotropic sensitivity [5], the total radiated power [6], or MIMO transmission quality in frequency selective channels [7; 8] of 4G MIMO-LTE terminals. For the measurement of the sensitivity the channel delay spread in MSRC may influence the result.

Hence, in this contribution we suggest an experimental platform using a small size reverberation chamber ([13]) to qualify performances of LTE-MIMO terminals in terms of Error Vector Magnitude (EVM), Block Error Rate (BLER), throughput and total isotropic sensitivity (TIS) while maintaining a Rayleigh fading in both SISO and MIMO configuration. On this platform, a multi cluster channel emulation which compiles with channels models defined by 3GPP is implemented, using a channel emulator. This emulation must be accompanied by a strict control of delay spread.

As announced before this section of the thesis is conducted as part of a project between the XLIM institute, Bouygues Telecom operator and ANOVO society.

3.3.1. Channel characterization inside MSRC: impulse responses and fading measurements

This section aims to validate the illumination stirrer's method (in SISO and MIMO mode) by measuring the channel transfer function in order to determine the different parameters such as fading distribution (Rayleigh, Rice, …), the correlation coefficient in MSRC versus the chosen configuration (SIMO, MIMO). The correlation coefficient is an important parameter. In fact for a MIMO configuration, the correlation between two receiving antennas has to be the lowest as possible in order to obtain a good separation of received signals. After the channel delay spread of the chamber is measured to control it. Finally the influence of mobile terminals on these parameters is studied. This channel characterization and measurements were performed with a Vector Network Analyzer (VNA).

3.3.1.1. Channel sounding platform

The channel sounding aims to measure the impulse response or the transfer function between the transmitting antenna and the receiving antenna. To perform these measurements, a vector network analyzer (VNA) is used. The VNA allows characterizing the propagation channel by the use of frequency sweeping. The port 1 of the VNA is connected to the transmitting antenna, and the port 2 is connected to the receiving antennas (UWB dipoles). The channel transfer function is determined by measuring the transmission coefficient $S_{21}(f)$ for each frequency step. Figure III.30 presents the used channel sounding platform.

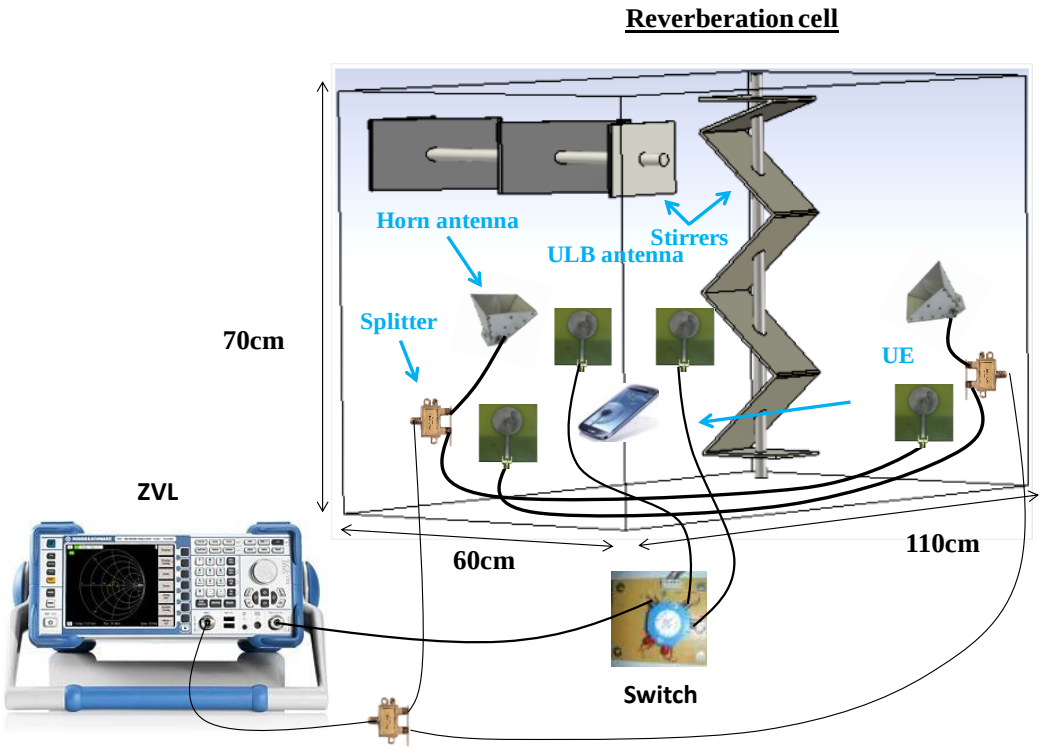

Figure III.30: Channel sounding platform

The measurement platform consists of a MSRC [13] (110x70x60 cm^3) described previously as shown in figure III.30. The stirring operation is performed by vertical and horizontal stirrers. Two receiving antenna are used in the test volume in order to perform channel sounding. In order to emulate a Rayleigh isotropic channel, each stirrer has to be illuminated by one antenna (SISO case). Then, as described on figure III.30, four transmitting antennas are needed for a MISO (2x1) or a MIMO (2x2) configuration.

3.3.1.2. Test plan

Several configurations have been tested with « stirrers in step by step mode» and «stirrers in continuous mode». Along this report, only two principles configuration are presented.

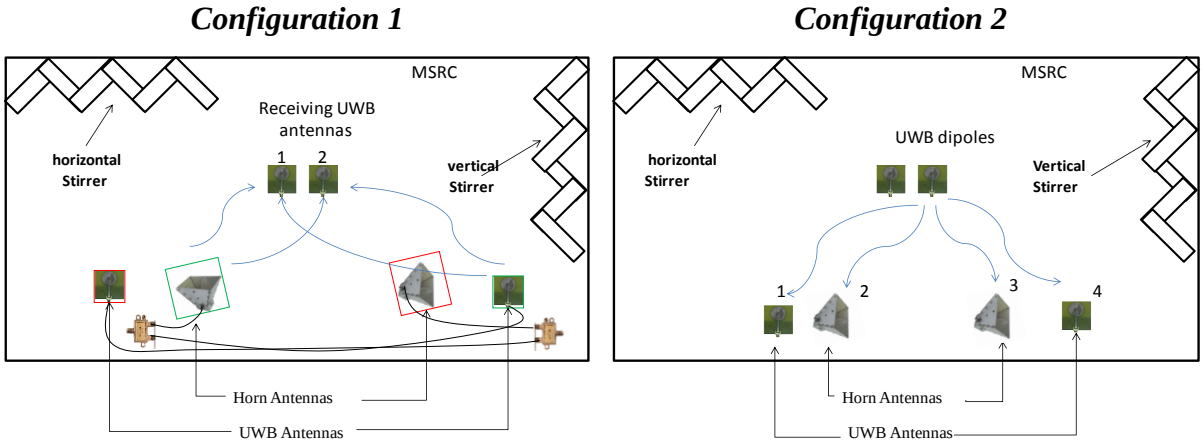

Figure III.31: Configurations used for channel sounding

As announced before the use of one antenna to illuminate one of the two stirrers not allows obtaining a Rayleigh isotropic channel.

The first configuration (*configuration 1*) aims to show that the use of two transmitting antennas (horn antenna illuminating the horizontal stirrer and a UWB dipole illuminating the vertical stirrer) are necessary, in order to emulate an isotropic propagation environment and to obtain a Rayleigh fading distribution.

The second configuration (*configuration 2*) is consists of four antennas that illuminate the stirrers and two receiving antennas. This configuration has been implemented to cheek that the MIMO channels are uncorrelated. As the propagation channel is reciprocal, the chamber is illuminated by the receiving antennas and the transmitted signal is received by the four transmitting antennas.

To analyze the impact of mobile terminals losses on the measured propagation channels, the experiments are made successively without and with LTE terminal. Table 6 summarizes the configurations tested.

	Stirrer in step by step mode		**Stirrer in continuous mode**
Configuration	1	2	1
Without mobile	Yes	Yes	Yes
With mobile	Yes	Yes	Yes

Table 6: Configurations tested during channel characterization

3.3.1.3. Channel sounding results

The channel sounding is performed with a reference antenna (UWB dipole) at central frequency of 2.595GHz for a bandwidth of 15MHz.

For the purposes of the statistics, 40*40 different stirrers' positions (rotation step of 9°) were chosen. The transmission coefficients are analysed to extract the channel parameter, such as: correlation coefficient, mean relative power, and power delay profile (PDP) (computed by applying the inverse Fourier transform to the transmission coefficients ($S_{21}(f)$), cumulative density function (CDF), and probability density.

The CDF's and probability density curves allow obtaining an idea concerning the channel type (Rayleigh, Rice, Nakagami…).

→Configuration 1 results « stirrers in step by step mode »

The measurement results are presented in table7 and in figures III.32 and III.33. The table 7 gives the values of the transmitted power and the correlation coefficient of the signals received by the two sounding antennas, and the delay spread of each channel.

	Without mobile		**With mobile**	
	Antenna1	Antenna2	Antenna1	Antenna2
$\langle \|S21\|^2 \rangle$ (dB)	-46.4258	-46.7222	-47.263	-47.4146
Standard_deviation(dB)	8.21	8.27	7.23	7.29
Correlation coeffievient	0.0441		0.0155	
τ_{rms}(ns)	370.35	389.7	334.06	323.85

Table7: characteristics parameters of the channel

From the table above, it can be observed that the mean transmitted power, and then the RMS delay spread decrease slightly when losses (due to the presence of the mobile) are introduced in the MSRC. Then, the influence of the device under test has to be carefully considered to emulate properly a frequency selective channel.

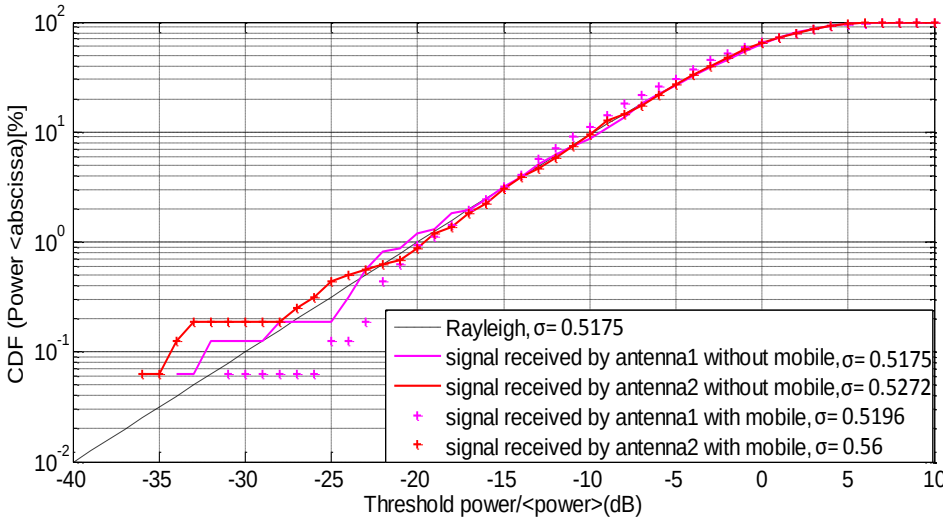

Figure III.32: Comparative study of cumulative probability density function with and without mobile

The figure III.32 presents CDF (Cumulative Density Function) curves of transmitted power for antenna 1 and antenna 2 (in presence and in absence of mobile). Each CDF is normalized to its own mean transmitted power. The figure shows that the obtained results are very close to that of the theoretical Rayleigh distribution. The figure III.33 shows the curves of the average normalized PDP in presence and absence of mobile versus time. The impulse response obtained inside MSRC follows an exponential law (exponential decay). When the mobile is introduced The PDP's curves fade faster. As observed in table 7, this can be explained by the fact that mobile brings more losses compared to empty chamber. The mean delay spread is around 380 ns for an empty MSRC (without mobile) and 328ns for a loaded MSRC (with mobile).

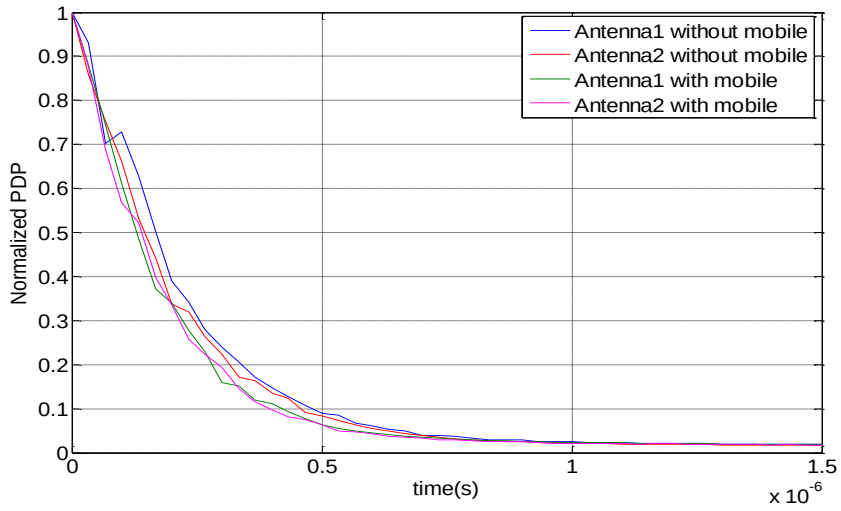

Figure III.33: Comparison of obtained PDP's with and without mobile

→ Configuration 2 results « stirrers in step by step mode »

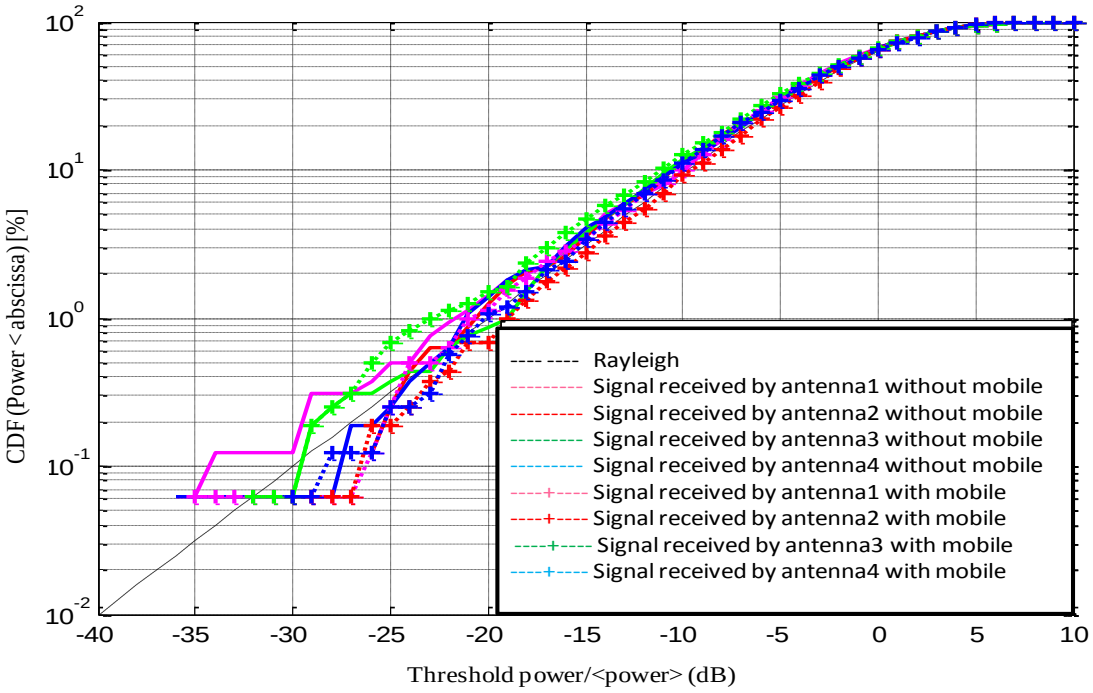

Figure III.34: Comparative study of cumulative probability density function with and without mobile

The measurements results (*configuration 2*) with « stirrers in step by step mode » are presented in table 8 and figures III.34. The average power values of signals received by the four received antennas (without and with mobile) are quasi-similar. As in configuration 1, the channel delay spread decrease in presence of mobile. The CDF curves (figure III.34) show that the emulated propagation environment still Rayleigh and isotropic.

	Without **Mobile**				With **Mobile**			
Antenna	1	2	3	4	1	2	3	4
$\langle \lvert S_{21} \rvert^2 \rangle$ **(dB)**	-47.04	-46.87	-48.85	-47.93	-47.45	-47.88	-49.04	-48.29
Standard_deviation(dB)	7.2	2.28	6.82	7.32	7.28	7.3	6.53	7.02
τ_{rms} **(ns)**	350.94	359.77	340.7	354.99	300.7	335.07	321.1	338.66

Table 8: characteristics parameters of the channel

The correlation coefficients between the four emulated propagation channels are shown in table 9. The correlation coefficients are very low; it can be conclude that the different channels are strongly uncorrelated.

<table>
<tr>
<td> 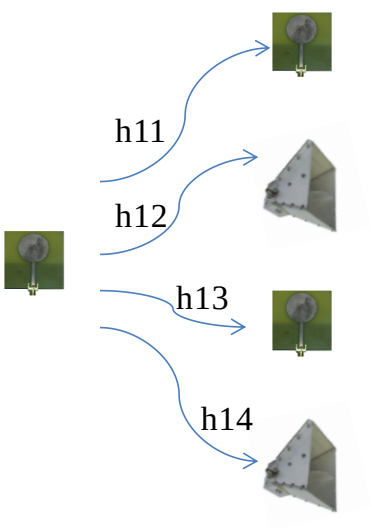
</td>
<td><u>Correlation coefficients without mobile</u>

$\begin{cases} h_{11}*h_{12}=0.0047 \\ h_{11}*h_{13}=0.0352 \\ h_{11}*h_{14}=0.0149 \\ h_{12}*h_{13}=0.037 \\ h_{12}*h_{14}=0.0244 \\ h_{13}*h_{14}=0.0419 \end{cases}$</td>
<td><u>Correlation coefficient with mobile</u>

$\begin{cases} h_{11}*h_{12}=0.0093 \\ h_{11}*h_{13}=0.0266 \\ h_{11}*h_{14}=0.0082 \\ h_{12}*h_{13}=0.028 \\ h_{12}*h_{14}=0.0142 \\ h_{13}*h_{14}=0.0321 \end{cases}$</td>
</tr>
<tr>
<td colspan="2">Vertical Horn : horn antenna illuminates the vertical stirrer
Horizontal Horn : horn antenna illuminates the horizontal stirrer</td>
<td>Vertical UWB : UWB antenna illuminates the vertical stirrer
Horizontal UWB : UWB antenna illuminates the horizontal stirrer</td>
</tr>
</table>

Table 9: Correlation coefficient without and with mobile

→ Configuration 1 results « stirrers in continuous mode »

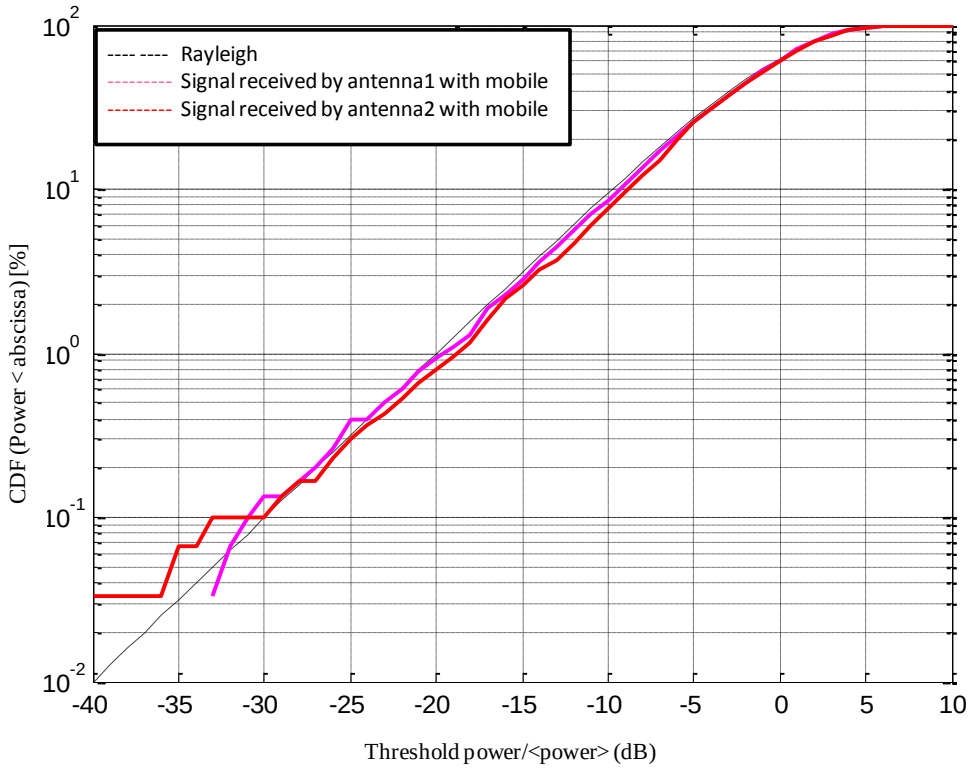

Figure III.35: Comparative study of cumulative probability density function with mobile

This paragraph aims to demonstrate that despite the fact that the two stirrers of the chamber rotate continuously, we obtain an environment statistically isotropic with a Rayleigh fading distribution. Only measurements with mobile are presented in figure III.35, since it has been shown that the presence of the mobile doesn't affect the Rayleigh distribution.

The channel sounding has allowed us to know the propagation channel emulated inside the MSRC. The mobile terminals measurements will be performed in a known propagation environment.

3.3.2. Real time active measurements of MIMO-LTE terminals

A MIMO system is characterized by the use of multiple antennas at transmitting and/or receiving side. MIMO technology has been introduced to improve performances and increase the communication systems throughput, particularly for data applications. Using the spatial diversity of the channel, it is possible to use effectively the radio resources (frequency spectrum occupied). For this, the new transmission technique is also accompanied by new measurement requirements. And is therefore the subject of several studies initiated by the standardization committees.

This section refers to MIMO OTA active measurements for 4G terminals in controlled multipath environment (MSRC) in order to evaluate its performance.

First, the hardware platform used and devices tested are presented. The second part is devoted to emulating realistic channels in the MSRC. The last part focuses on the experimental characterization of terminals. The key parameters associated and factors of merit are also described.

3.3.2.1. Implementation of MIMO-OTA measurements platform

a) Mono-cluster measurements platform

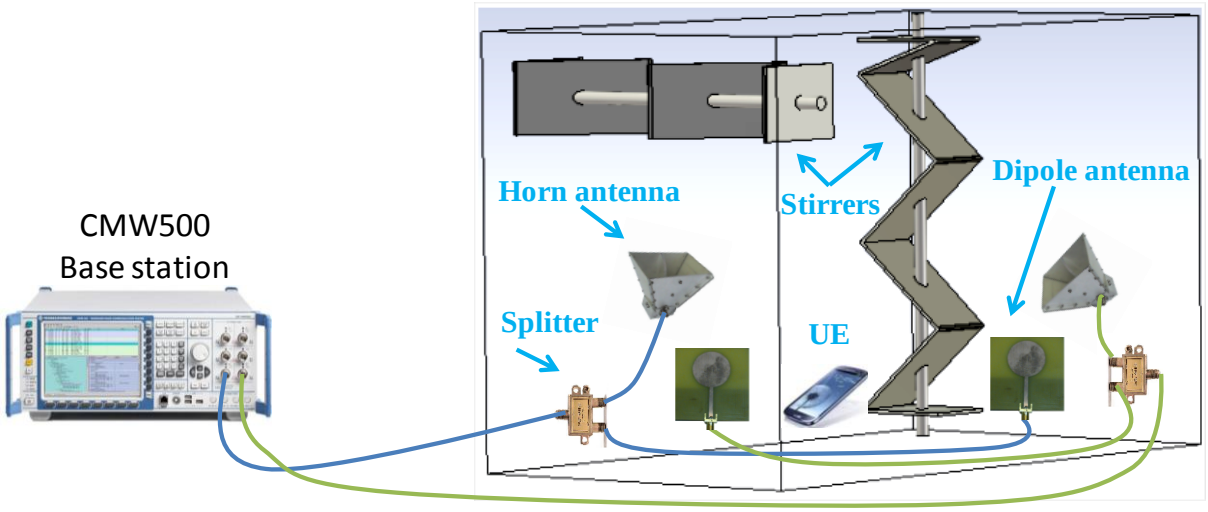

Figure III.36: Mono-cluster measurements platform (MIMO configuration)

The measurement platform consists of a MSRC described above, a CMW500 (Wideband Radio Communication Tester) from Rohde & Schwartz acting as MIMO-LTE base station emulator or eNodeB. The R&S CMW500 (figure III.36) is a wideband radio communication tester with several channels allowing to verify the characteristics of MIMO OTA terminals. In our case, only channel RF1COM and channel RF3COM are used. RF1COM is used both for transmission (downlink) and reception. RF3COM channel is only used for downlink (MIMO mode).

The chamber of measurements contains two antennas pairs. The first pair of antennas (horn and UWB dipole oriented respectively towards the horizontal and vertical stirrers) is connected to the RF1COM channel through a 1x2 power splitter. The second pair of antennas is connected to the channel RF3COM via a 1x2 splitter. The device under test (UE) located within the MSRC will interact in real time with the CMW500.

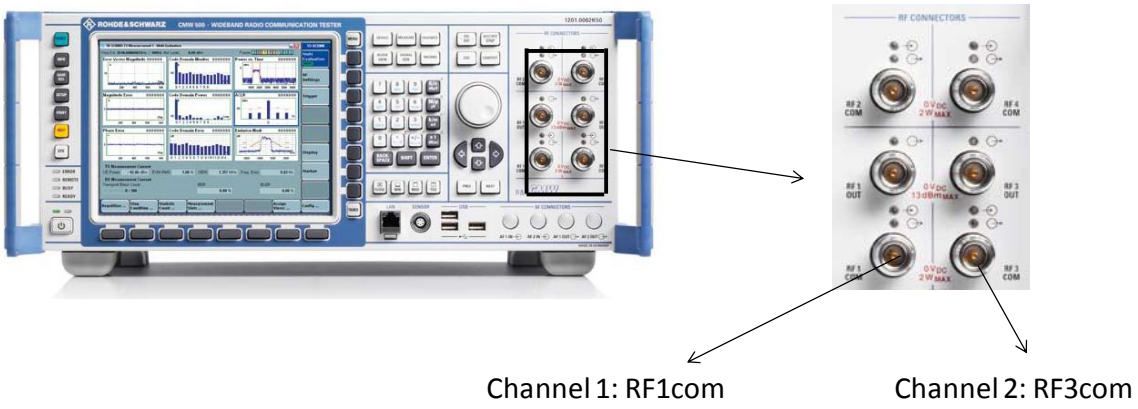

Figure III.37: R&S CMW500 Wideband Radio Communication Tester

To automate measurements, the set is controlled by a computer through a program developed in Matlab. The developed code allows simultaneous control of the CMW500 and stirrers, the platform configuration and the verification of communication between the terminal and the eNodeB emulator.

b) Multi-cluster measurements platform

A multi clusters channel method is implemented in the paragraph 3.2. This method aims to convolve the transmitted signal with channel models emulated in base band. In the following, a method that allows emulating multi clusters in real time is shown.

It is also possible to add between CMW 500 and MSRC a multi-cluster channel emulator (SPIRENT SR5500) (Figure III.38) to generate the arrival times of the macro channel paths.

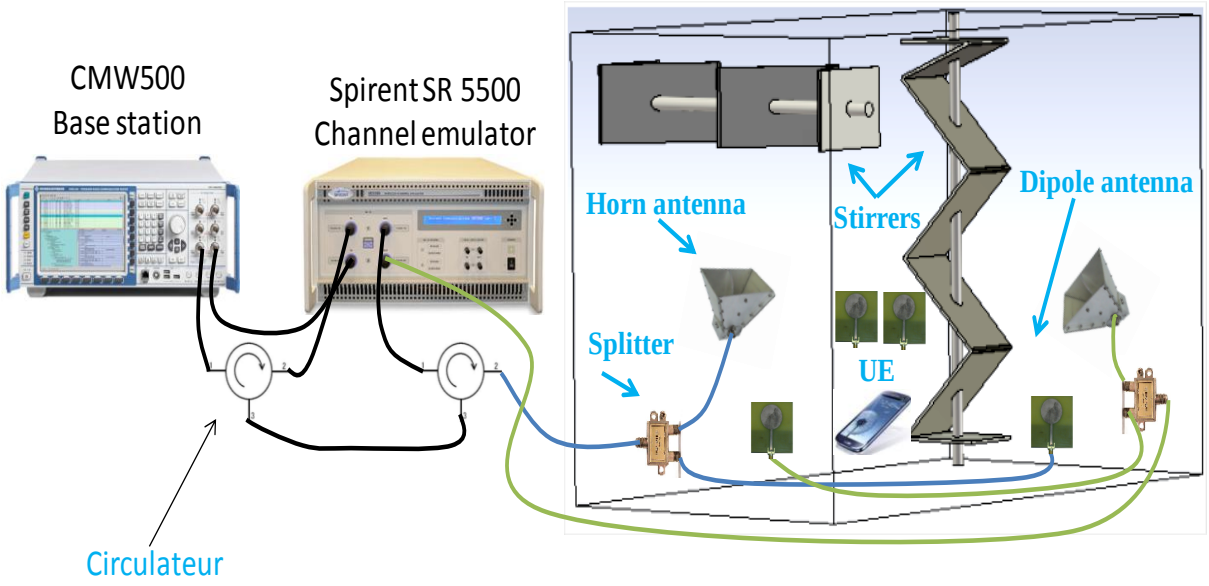

Figure III.38: Multi clusters measurements platform (configuration 2x2 MIMO)

The type of scenario that corresponds to the channel emulated by the platform can be shown in figure below:

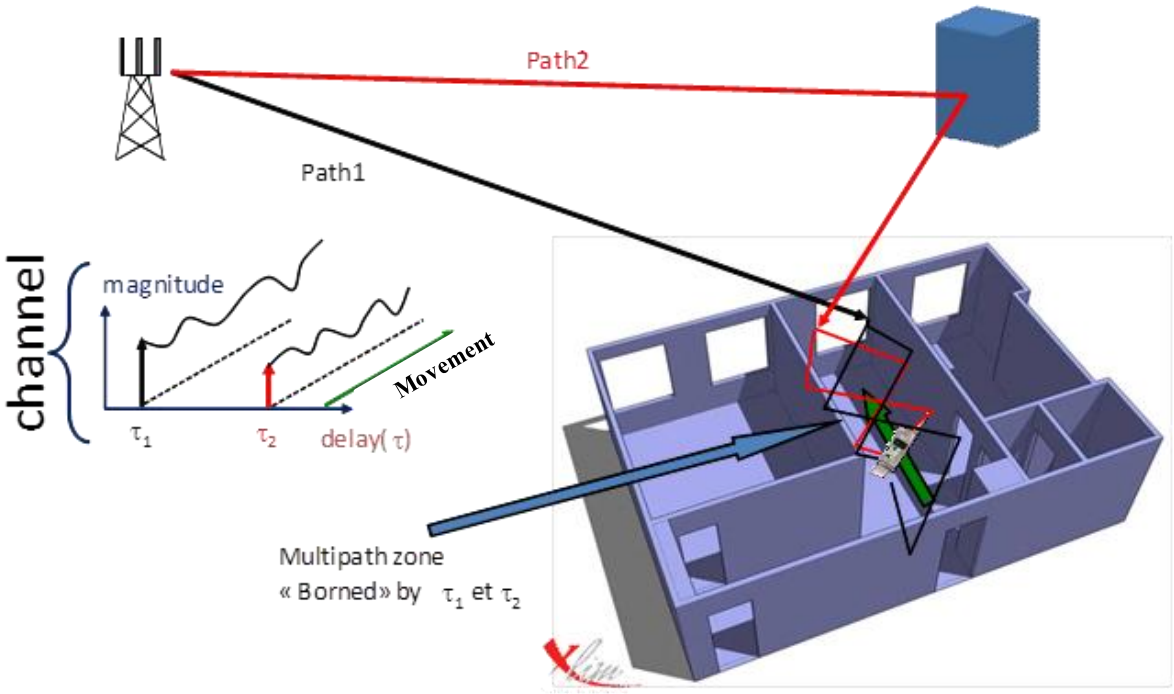

Figure III.39: example of emulated scenario

Overall, macro paths (also called clusters) illuminate the environment near the terminal (movement area of the terminal). These macros paths have different delays to be generated by the signal generator in the baseband (realization of an impulse response which to be convolved to the transmitted LTE signal).

The area near the terminal corresponds to a strongly multipath environment (micro path due to multiple reflections in this area). At each movement, these micro paths will recombine constructively or destructively at the terminal, creating variations in the amplitude and phase of the signal for each of the impulse response delay (generating fading effects on received power: "Rayleigh fading"). The stirrer's rotation in the reverberation chamber can artificially recreate the movement of the mobile by changing multipath environment for each rotation angle.

Realistically, every time is an average delay spread as a function of environment (intra-cluster delay spread). This delay spread is "visible" by the transmission system, if it has a sufficiently fine time resolution (that is to say, a relatively wide bandwidth).

c) 4G MIMO-LTE terminals tested

In this study, we investigated the characteristics of five MIMO-OTA LTE 4G mobile devices. Indeed, the LTE standard classify terminals into five categories (Table 10) [3GPP TS 136 306].

Categories		1	2	3	4	5
Bandwidth		1.4 à 20 MHz				
Modulation	Downlink	QPSK, 16QAM, 64QAM				
	Uplink	QPSK, 16QAM				QPSK, 16QAM, 64QAM
Throughput (Mb/s)	Downlink	10	50	100	150	300
	Uplinlk	5	25	50	50	75
Antennas Rx	MIMO 2x2	No	Yes			
	MIMO 2x2	No				Yes

Table 10: LTE terminals categories (3GPP TS 136 306 release 9)

3.3.2.2. Emulation of realistic channel inside MSRC

As explained above, the main source of disruption experienced by a signal as it propagates between the transmitter and the receiver, is the propagation channel. Indeed, because of the phenomena of multipath propagation, the signal suffers fading, frequency or even temporal offsets. Unlike conventional systems, MIMO systems take advantage of these types of propagation to improve its performance.

Several channel models have been developed by organizations like 3GPP, COST and CTIA 2100. The result of their work is synthesized in 3GPP TR 37.976 document. These channel models are likely to be used for testing MIMO-LTE terminals. However, several major issues (channel models used, measurements techniques or emulation of these channels) are not yet clear. The 3GPP proposes the Spatial Channel Model Extended (SCME) to model the broadband MIMO systems. It is actually a set of models allowing the simulation of channel propagation of several propagation environments.

Among the potential candidates for the final standardization, we chose to emulate the "Single Cluster" "SCME Urban micro-cell" and "SCME Urban macro-cell" models. These channel models are presented in Table 3.

"Single Cluster" model simulates a mono-cluster environment, "SCME Urban micro-cell" and "SCME Urban macro-cell" respectively emulates an urban macro-cell environment and urban microcell environment.

→Verification of emulated realistic channels

The emulation platform of single and multi-clusters channel that we have implemented is shown in Figure III.40. As the figure shows, the platform consists of a reverberation

chamber described in the first part of this report, a VNA, a channel emulator (Spirent SR5500) and a base station emulator (R&S CMW 500). The set is controlled by a computer through a Matlab implemented code.

In general, the principle of this method is to convolve the baseband signal to be transmitted with the channel models generated with the Spirent SR5500. The RF input Spirent SR5500 is connected to the RF output (port 1) of the VNA. The VNA is used here in order to verify the channel emulated by measuring the transfer function (S_{21}) (between transmission antenna connected to the RF output of Spirent SR5500 and the receiving antenna) of the MSRC.

In order to verify the proper functioning of the implemented emulation platform, a channel sounding was carried out at the frequency of 2.595GHz over a frequency band of 64MHz. This bandwidth is selected so as to achieve good temporal resolution to observe the entire emulated channel. A time spread intra-cluster 90 ns ± 5 ns is considered. As the reverberation chamber has inherently an important delay spread (of the order of several microseconds) which depends on its quality factor. Control of the delay spread was therefore carried out by charging the room with absorbing materials.

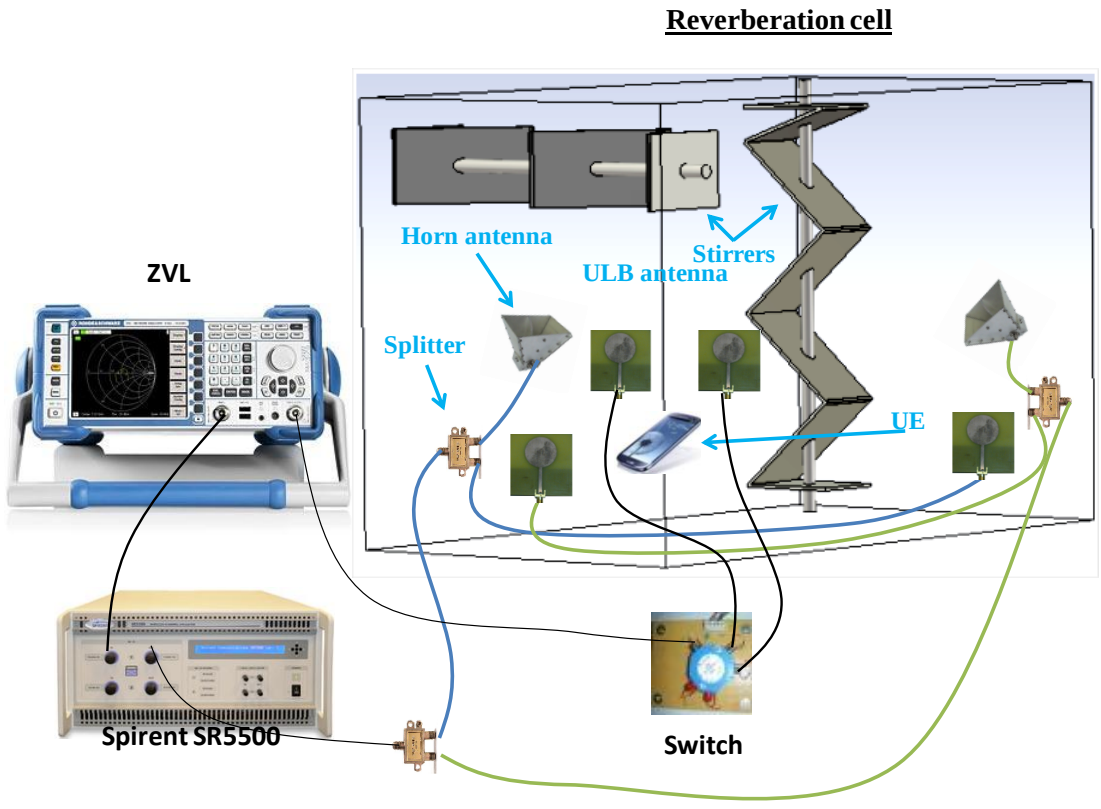

Figure III.40: XLIM channel emulation platform

At each stirrers step, the transmission coefficients between the transmission and reception are captured. Note that each change of position of the stirrer results in the generation of a new multi-path channel. The total number of positions stirrers is 1600. Figure III.41 shows the average impulse response or single-cluster channel emulated in the MSRC unloaded and loaded with an absorbent. Charging the MSRC, its quality factor and thus delay spread is changed.

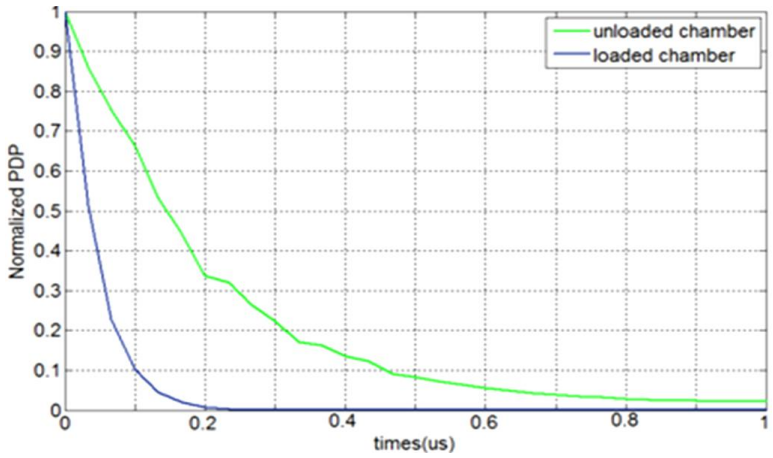

Figure III.41: Mono cluster channel emulated in XLIM MSRC

The implementation of this platform brings us to the same extent results shown in Figures III.24 and III.25, Which show the possibility of emulating realistic channel inside controlled channel (MSRC) with control of the intra-cluster delay spread in accordance with the 3GPP channel models.

After presenting the generation of single and multi-channel clusters, we are interested in the following paragraph to performance tests of LTE terminals.

3.3.2.3. Performance measurements of UE

a) Performance parameters and factors of merit

As CMW 500 allows performing measurements of performance parameters described in 3GPP TS 36521-1, sections 6 and 7. We used it to measure the figures of merit such as BLER, throughput, sensitivity, EVM and spectral flatness of the equalizer.

- Block error rate (BLER) expresses the loss of information that may be due to problems with bad blocks or disruptions on the system.

Throughput is the amount of information transmitted per unit time. It is obtained from the BLER [3GPP TR 37.976].

$$\text{Throughput (\%)} = 100 - \text{DL\_BLER}$$

$$\text{DL\_BLER (\%)} = (1-(\text{NACK+DTX})/(\text{ACK+NACK+DTX}))*100$$

With,

-ACK: percentage of packets transmitted and received by the EU.

-NACK: percentage of packets transmitted and not received by the EU.

-DTX: percentage of packets transmitted without response.

- **EVM** is representation of distortion of the amplitude and phase of the constellation diagram of characteristics of a digital modulation states. 3GPP recommends a maximum average EVM of 12.5% for 16QAM and 17.5% for QPSK or BPSK [3GPP TS 36521-1, Section 6].
- **The sensitivity** can be defined as the lowest received signal, which can be decoded by the device. The sensitivity level reference for a throughput ≥ 95% (BLER ≤ 5%) depending on the band and the duplex mode is given in [3GPP TS 36521-1, Section 7].

b) Methodologies and measurements tools

As stated above, the goal here is to evaluate experimentally the performance of MIMO-LTE terminals in controlled environment (MSRC). The picture above shows the implemented experimental setup. This test bed is compound from an emulator BS (R&S CMW500), a channel emulator (Spirent SR5500) and a mini MSRC with two mechanical stirrers (controlled by two motors) and four illumination antennas.

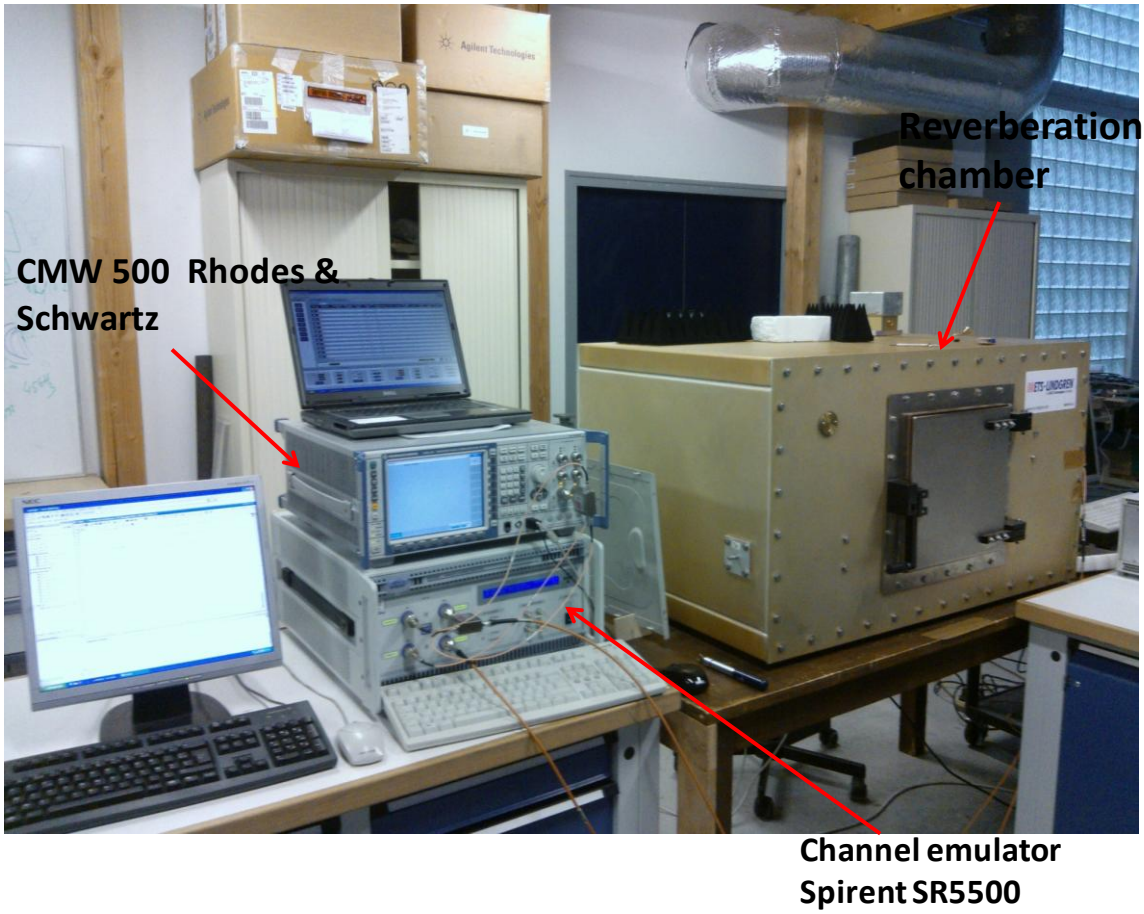

Figure III.42: Photo of the measurements platform used for MIMO-LTE terminals characterization

In the case of multi-cluster measurements, LTE signal generated by the CMW 500 is sent to the RF input of the SR5500. The output of the SR5500 is connected to the illumination antennas through a circulator and 1x2 power splitter. For The RF1COM channel (Figure III.37) is used for transmission and reception.

Terminal or UE is placed within the chamber in the test area (figure III.43) and communicates in real time with the CMW500. The UE is at the same level as receiving antennas used during channel sounding (figure III.43). The interest is to keep these antennas, and to ensure that we have the same type of propagation channel.

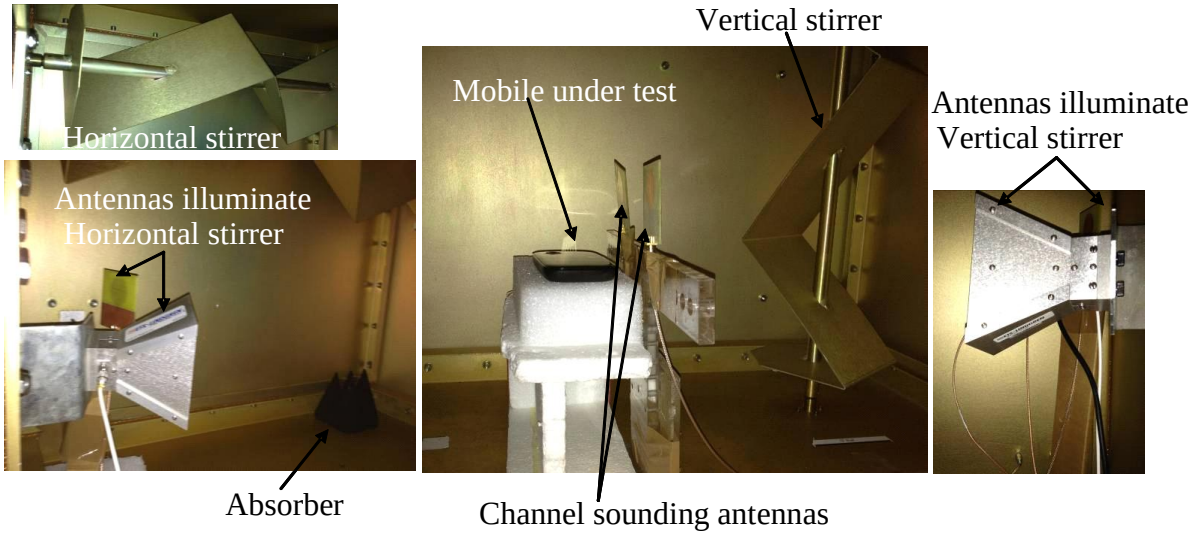

Figure III.43: localization of mobile under test (UE) inside reverberation chamber

In the framework of this work, we placed the CMW500 (emulator BS) in single-antenna configuration (SISO or "Standard Cell") and multi-antennas (MIMO or "Two RF ports"). Three types of multi-path channel are generated by the Spirent SR5500: mono-cluster, multi-cluster urban macro and multi-cluster urban micro. In each of these cases, the levels of BLER, the throughput, the received power by the UE, the EVM and spectral flatness of the equalizer are revealed.

These parameters are classified into two categories (depending on the types of measurements):

- **Tx measurements (Uplink)**, used for measuring the quality of the uplink transmission (signal transmitted by the UE). This type of measurement provides levels of:
  - EVM (EVM vs SC-FDMA symbol, EVM vs subcarrier) ;
  - Equalizer spectrum flatness that derives from the equalizer coefficients generated by the measure of EVM [3GPP TS 36521-1];
- **Rx measurements (Downlink),** measuring the quality of the downlink transmission. The measured parameters are:
  - BLER ;
  - Throughput ;
  - Power of the signal received by UE (RSRP or Reference Signal Received Power) ;

- Quality of reference signal received by the UE (RSRQ or Reference Signal Received Quality).

Indeed in Rx measurements, LTE terminal measures the RSRP, the RSRQ, ACK and NACK and transmits them in uplink to the BS. Throughputs measurements and BLER is achieved by counting the number of ACK and NACK.

According to the 3GPP standard, these measurements must meet certain criteria in terms of frequency, bandwidth, number of resource blocks (RBs), etc.. The operating band selected during these measurements is the band 7 with a bandwidth of 15MHz. Table 12 summarizes the parameters used to configure the BS emulator (CMW500). RMC channel (Reference Measurement Channels) defined by 3GPP is used.

Parameters		Unit	Value
Physical channel			
Connection mode of UE			Connection established
DL mode	SISO		Standard Cell
	MIMO		2 x 2 open loop spatial multiplexing
Duplex mode			FDD
Operating band (UL channel, DL channel)			LTE band 7 (21100, 3100)
Schedule type			Reference Measurement Channel (RMC)
DL Setting			
Bandwidth DL		MHz	15
Number of RBs DL			75
Start RB DL			Low
Modulation DL			QPSK
TBS Idx DL			5 (RMC 6712)
UL Setting			
Bandwidth UL		MHz	15
Number of RBs UL			75
Start RB UL			Low
Modulation UL			QPSK
TBS Idx UL			3 (RMC 4392)
Uplink TPC Pattern			Closed Loop
Closed-Loop Target Power		dBm	-10
PDSCH power offset relative to RS EPRE (Downlink power allocation)		dB	$\rho_A = 0$ $\rho_B = 0$
AWGN			OFF
DL power level (RS EPRE)		dBm / 15 kHz	
Number of subframes for FOM measurement			32000 TX measurement 8000000 RX measurement

Table 11: BS emulator parameters (CMW500)

➔ Measurements process :

- CMW 500 configuration with respect of parameters of table 11

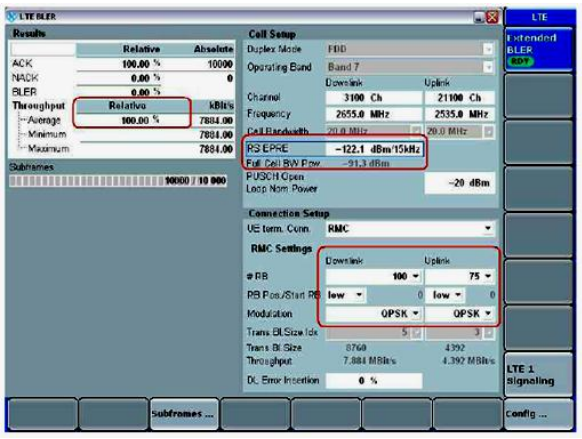

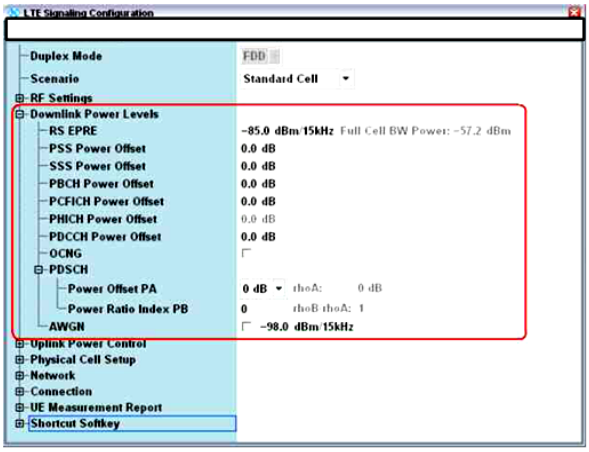

- Configuration of the channel emulator (SR5500) with respect of the parameters defined in Table 3 (Urban micro-cell or cell-Urban macro) for the generation of multi-cluster channels.

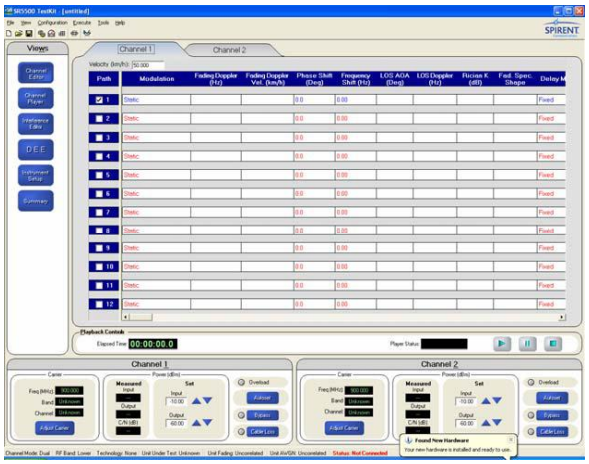

- Adjusting the average level of output power. The power level of transmission through RS EPRE (reference signal energy per resource element).

$$P_e = \text{RS EPRE} + 10*\log10(N\_RE)$$

With N_RE number of resource elements that is equal to (12*[number of RBs]).

- Localization of terminal under test inside reverberation chamber, in the position shown in figure III.41.
- Implementation of the connection :

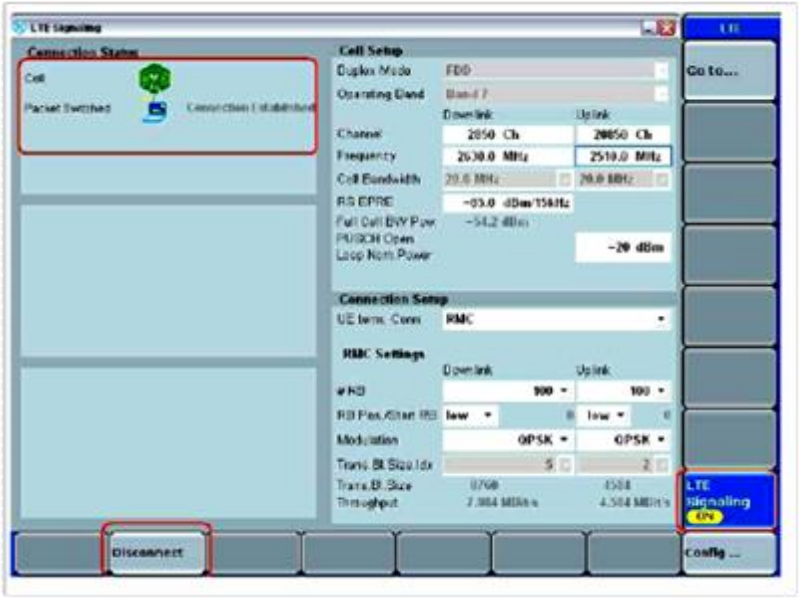

- if the mobile is attached to the BS, initiate measurements of figures of merit. Two types of test are performed:
  - ❖ Step by step stirring with a constant transmitting power of BS: at every stirrers step (1600 positions), 5000 sub frames are captured or 8000000 sub frames for measuring average throughput and average BLER. And 20 sub frames are captured, a total of 32000 sub frames for the average EVM measurements and spectrum flatness of the equalizer.
  - ❖ Continuous stirring with variable emission power of BS: 5 minutes of measurement are performed for each of the powers. The measurements are performed until the mobile can no longer be attached to the BS (disconnection of mobile). At each power, mean values of throughput, BLER and the average received power are identified.

c) Measurements Results

Terminals we used have a TX and two RX (receive diversity). And in MIMO mode that is means «Two RF ports» configuration, the CW500 supports only two Tx (transmit diversity) and one Rx. This amounts to the MIMO in downlink (figure III.44). On the uplink, this means one antenna for transmission at the mobile and one receiving antenna at BS side (figure III.44). Therefore, the performance of MIMO terminals (BLER and throughput) can only be measured in DL. So we will distinguish two types of MIMO according to CMW500 configuration.

- If CMW500 is in «Standard cell» mode (one transmit antenna), it is therefore SIMO mode. This mode will be referred in this document as DL-SISO.
- If CMW500 is in «Two RF output port» mode (two transmit antennas), it is full-MIMO mode. This mode will be referred in this document as DL-MIMO.

But the quality of signal transmitted by the UE is measured in UL (UL-SISO) with one transmission antenna and one receive antenna.

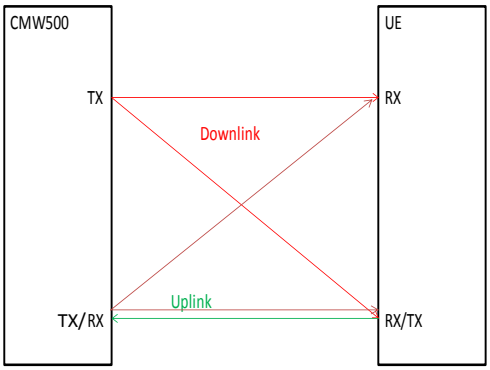

Figure III.44: MIMO-LTE configuration in Downlink with transmitting and receiving diversity

In the report the term SISO and MIMO refers respectively CMW500 mode «Standard cell» and «Two RF output port» mode (OL Spatial Multiplexing).

Table 12 summarizes the measurements and their durations for different terminals.

Tested mobiles												
			Mobile1		Mobile2		Mobile3		Mobile4		Mobile5	
			SISO	MIMO	SISO	MIMO	SISO	MIMO	SISO	MIMO	SISO	MIMO
Step by step stirring	Mono Cluster		✓	✓	✓	✓	X	X	X	X	X	X
	Time		5h	5h	5h	5h	-------	-------	-------	-------	-------	-------
	Multi Cluster	Urban Micro	✓	✓	✓	✓	X	X	X	X	X	X
		Time	5h	5h	5h	5h	-------	-------	-------	-------	-------	-------
		Urban Macro	✓	✓	✓	✓	X	X	X	X	X	X
		Time	5h	5h	5h	5h	-------	-------	-------	-------	-------	-------
Continuous stirring	Mono Cluster		✓	✓	✓	✓	✓	✓	✓	✓	✓	✓
	Durée		2h	2h	2h	2h	2h	2h	2h	2h	2h	2h
	Multi Cluster	Micro urbain	✓	✓	✓	✓	X	X	X	X	X	X
		time	2h	2h	2h	2h	-------	-------	-------	-------	-------	-------
		Macro urbain	✓	✓	✓	✓	X	X	X	X	X	X
		time	2h	2h	2h	2h	-------	-------	-------	-------	-------	-------

Table 12: list of performed measurements of mobile terminals

➔ **Measurements results: step by step stirring with constant transmitting power of BS**

The measurements are performed with three channels previously generated. Each channel has an intra cluster delay spread of 92.80 ns (for Mobile1), and 86.4 ns (for Mobile2). The transmit power of the RS EPRE base station is set to -72 dBm/15kHz. In each measurement cases of EVM in UL-SISO and BLER and throughput in DL (SISO & MIMO) are performed. DL-MIMO measurements are compared with measurements DL-SISO. Tables 13 and 14 summarize the average figures of merit measured in single-cluster channel, multi-clusters Urban Micro and multi-clusters urban Macro.

	Mono-cluster		Urban Micro		Urban Macro	
	SISO	MIMO	SISO	MIMO	SISO	MIMO
RSRP(dBm)	-81,09	-80,05	-81,53	-80,09	-82,04	-81,10
BLER (%)	0,001667	0,000486	0,000722	0,001021	0,002222	0,001069
Throughput (Mbits/s)	6,0409	12,0819	6,04096	12,0819	6,04087	12,0819
Throughput (%)	99,9983	99,9995	99,9993	99,999	99,9978	99,9989

Table 13: Comparison of factors of merit of Mobile1 in SISO and MIMO mode

	Mono-cluster		Urban Micro		Urban Macro	
	SISO	MIMO	SISO	MIMO	SISO	MIMO
RSRP(dBm)	-83,82	-83,42	-84,86	-83,93	-85,70	-85,14
BLER (%)	0,001194	0,000160	0,001111	0,000333	0,001014	0,000076
Throughputt (Mbits/s)	6,04093	12,082	6,04093	12,082	6,04094	12,082
Throughput (%)	99,9988	99,9998	99,9989	99,9997	99,999	99,9999

Table 14: Comparison of factors of merit of Mobile2 in SISO and MIMO mode

For the three emulated channels, the average power of signal received by the UE is almost identical. Even with a MIMO throughput twice higher, the level of BLER in SISO mode is higher than that of MIMO. This can be explained by the use of antenna diversity. For this, whatever the mode (SISO or MIMO) used BLER levels remain very low. Whatever generated channel, performance in terms of BLER and throughput remain similar. The same observation is done for the Mobile1 and the Mobile2. MIMO performances of Mobile2 are better.

	Mono-cluster		Urban Micro		Urban Macro	
	SISO	MIMO	SISO	MIMO	SISO	MIMO
EVM (%)	8,97	9,05	9,33	9,37	9,39	9,25
Standard deviation EVM (%)	6,0677	6,5947	7,3935	7,2773	7,4139	7,1508
SNR (dB)	20,94	20,87	20,61	20,56	20,55	20,68

Table 15: UL signal quality in mono cluster and multi clusters channel (Mobile1)

Quality of signal transmitted by the Mobile1 and the Mobile2, measured in terms of the mean EVM is reported in Tables 15 and 16. We must remember that the EVM is measured in UL (in SISO mode) and channel emulator is placed on the DL link (connected to the Tx ports of CMW500). So, the terms SISO, MIMO, Single-cluster, Urban Micro and Urban Macro (Tables 15 and 16) simply indicate the DL configurations for which the EVM is measured.

	Mono-cluster		Urban Micro		Urban Macro	
	SISO	MIMO	SISO	MIMO	SISO	MIMO
EVM (%)	9,99	10,15	9,45	9,84	9,37	9,68
Standard deviation EVM (%)	7,4597	6,2075	5,8738	6,5355	6,1365	6,3251
SNR (dB)	20,01	19,87	20,49	20,14	20,57	20,28

Table 16: UL signal quality in mono cluster and multi clusters channel (Mobile2)

The average values of EVM obtained for the six DL configurations are substantially identical. This shows the repeatability of measurements. Moreover, these values are lower than 17.5% (max value of EVM. Defined by the standard for QPSK [3GPP TS 36521-1]). The SNR is the inverse of the EVM.

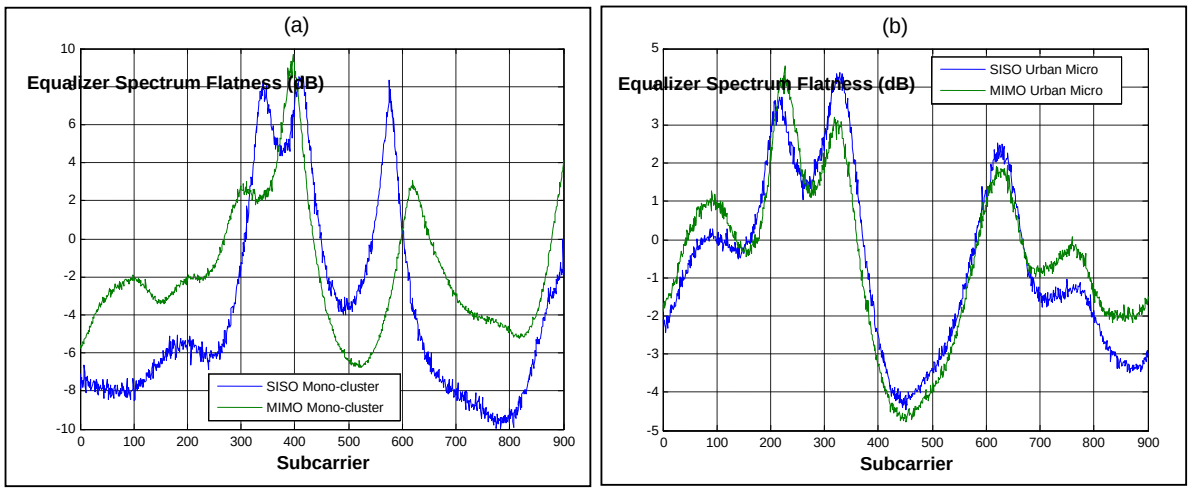

Figure III.45: Variation of amplitude of equalizer coefficients versus sub-carriers

In order to better realize the impact of the channel on the signal transmitted by the UE, an example of the equalizer spectrum flatness at one position of stirrers is given in Figure III.45 The curves in this figure show the variation of the amplitude coefficients of the equalizer versus sub-carriers at one stirring position. It is observed that some subcarriers are milder than others. This attenuation is between 10 and -10 dB for the mono-channel cluster, and between 5 and -5 dB for the micro-urban channel. Averaging over 1600 stirrer's positions, a variation of the amplitude of these coefficients that does not exceed 2 dB (Figure III.46) was obtained.

This is in agreement with the value recommended in the standard (the difference between maximum and minimum coefficient must not exceed 5dB) [3GPP TS 36521-1, Section 6].

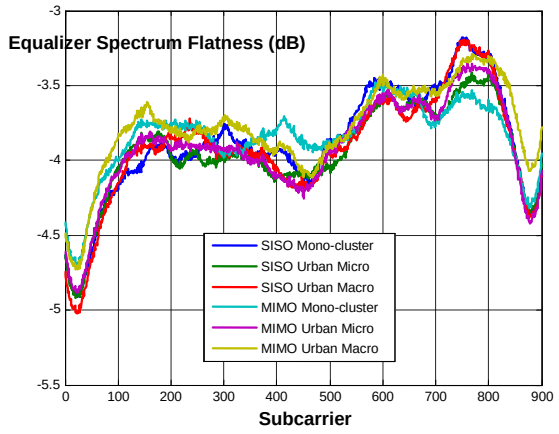

Figure II.46.a : Averaged amplitude coefficients of equalizer versus sub-carriers (Mobile1).

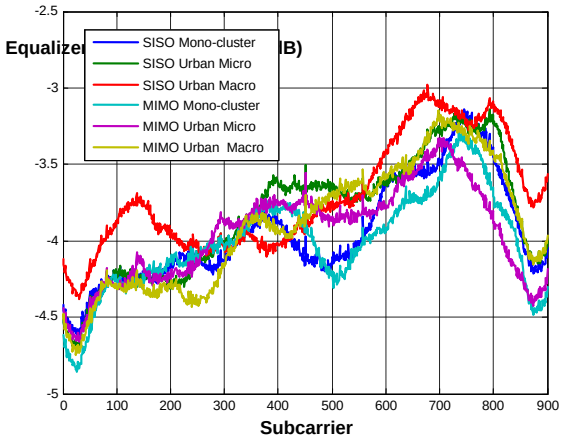

Figure III.46.b : Averaged amplitude coefficients of equalizer versus sub-carriers (Mobile2).

➔ **Sensitivity measurements results: continuous stirring with variable transmitting power of BS**

After characterizing the Mobile1 and Mobile2 at fixed transmit power of BS, the second set of measurements is to test the sensitivity of 4G terminals.

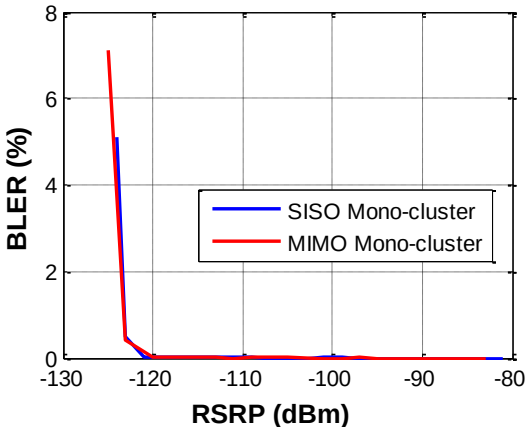

Figure 47.a: Comparison of SISO and MIMO BLER versus RSRP in mono-cluster channel (Mobile1).

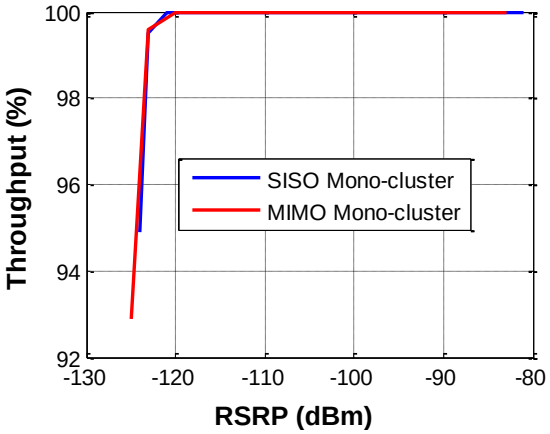

Figure 47.b: Comparison of SISO and MIMO Throughput (%) versus RSRP in mono-cluster channel (Mobile1).

These sensitivity tests are performed in continuous stirring and varying the transmission power of BS, in order to see the evolution of the throughput and BLER versus power received

at the UE. For each power step, 5 minutes of measurement (rotation of stirrers) are performed, about 300,000 Sub frames captured. The average values of throughput, BLER and the received power (RSRP) are identified. The theoretical throughput in SISO and MIMO modes are respectively 6.0410 Mbit/s and 12.082 Mbit/s. The measurement results are shown in Figures 46-52.

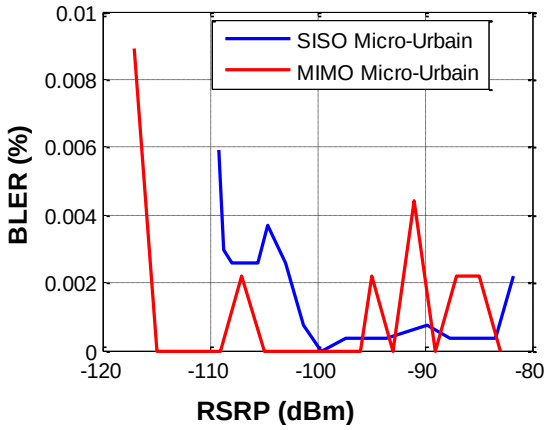

Figure 48.a: Comparison of SISO and MIMO BLER versus RSRP in mono-cluster channel (*Mobile1*)

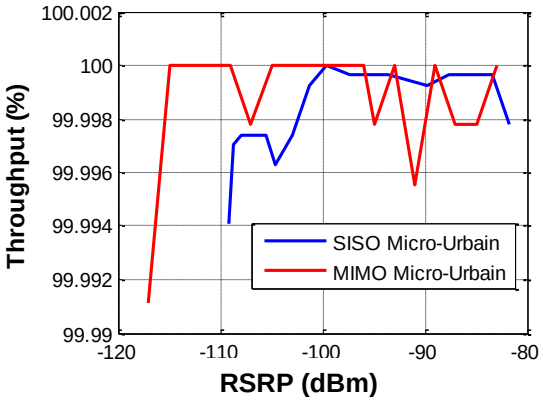

Figure 48.b: Comparison of SISO and MIMO Throughput (%) versus RSRP in mono-cluster channel (*Mobile2*)

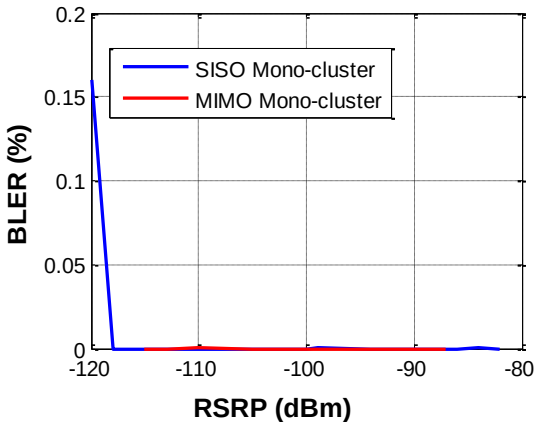

Figure 49.a: Comparison of SISO and MIMO BLER versus RSRP in mono-cluster channel (Mobile2)

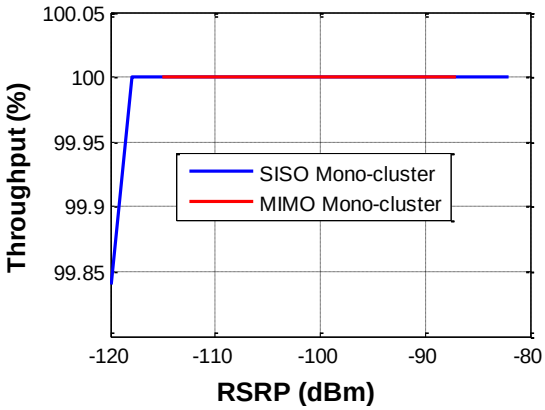

Figure 49.b: Comparison of SISO and MIMO Throughput (%) versus RSRP in mono-cluster channel (Mobile2)

The curves in figures 47-53.a, represent the evolution of SISO and MIMO BLER versus the average power of the received reference signal (RSRP). The curves in figures 47-53.b represent the evolution of the percentage of throughput in SISO and MIMO configuration versus RSRP. Performances of 4G router in mono cluster and multi-cluster channel are shown in Figures 48 and 49. In mono cluster channel the router sensitivity at 5% of BLER or at 95% of the throughput is -127 dBm. For other mobiles, the evolution curves of BLER or

throughput does not allow obtaining the sensitivity threshold at 5% of BLER. As mentioned above, the Measurements are made until the mobile is no longer able to attach to the BS. So the average power received by the UE, revealed at step before (last level of received power or the lowest value of the RSRP) will be the threshold sensitivity of the device under test (Table 17).

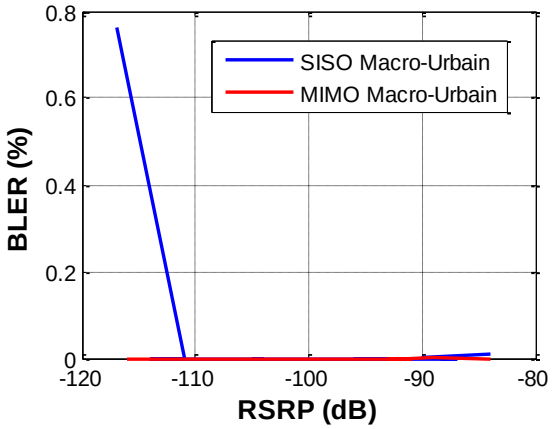

Figure 50.a: Comparison of SISO and MIMO BLER versus RSRP in mono-cluster channel (Mobile2)

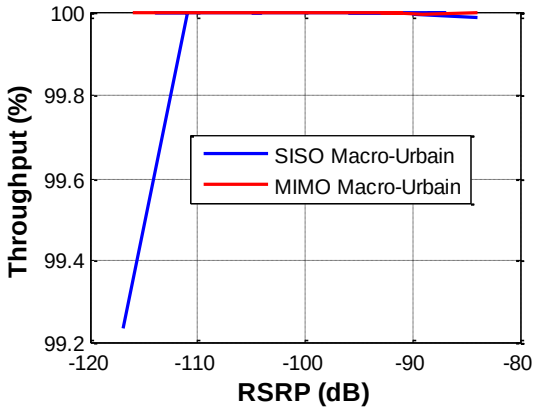

Figure 50.b: Comparison of SISO and MIMO Throughput (%) versus RSRP in mono-cluster channel (Mobile2)

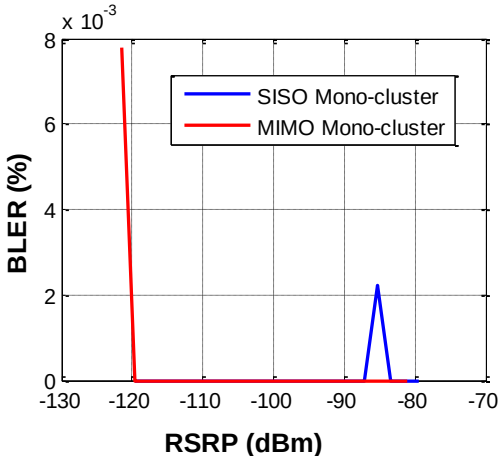

Figure 51.a: Comparison of SISO and MIMO BLER versus RSRP in mono-cluster channel *(Mobile3)*

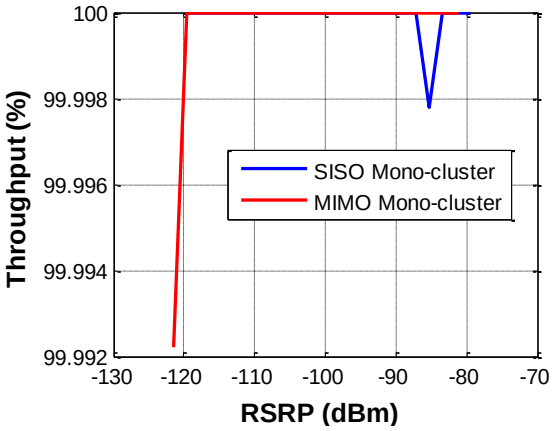

Figure 51.b: Comparison of SISO and MIMO Throughput (%) versus RSRP in mono-cluster channel *(Mobile3)*

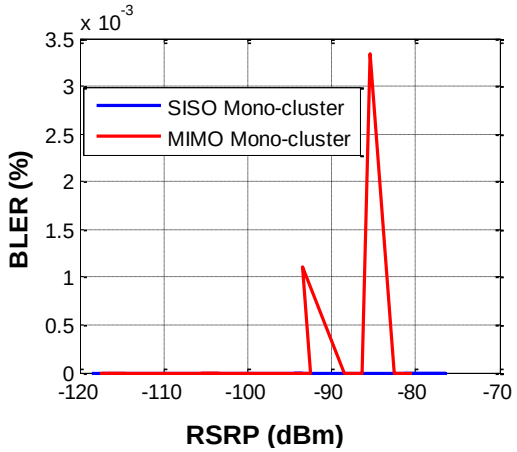

Figure 52.a: Comparison of SISO and MIMO BLER versus RSRP in mono-cluster channel *(Mobile4)*

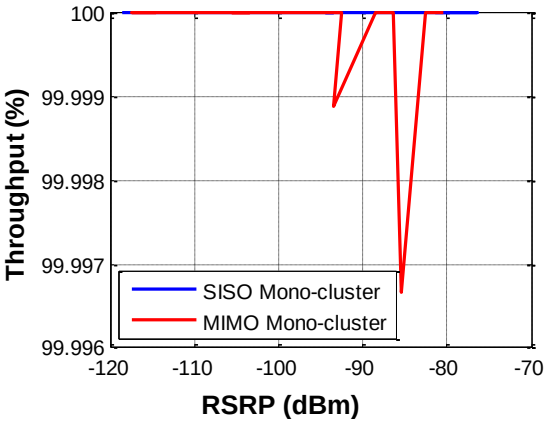

Figure 52.b: Comparison of SISO and MIMO Throughput (%) versus RSRP in mono-cluster channel *(Mobile4)*

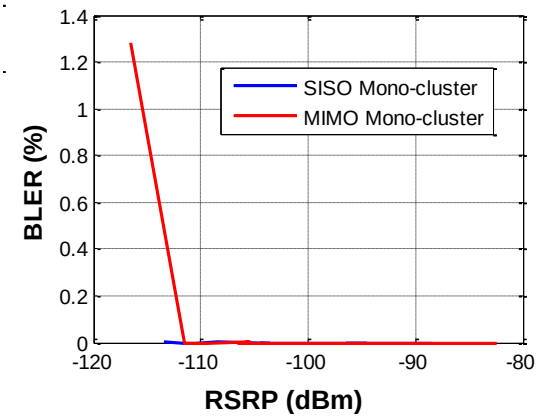

Figure 53.a: Comparison of SISO and MIMO BLER versus RSRP in mono-cluster channel *(Mobile5)*

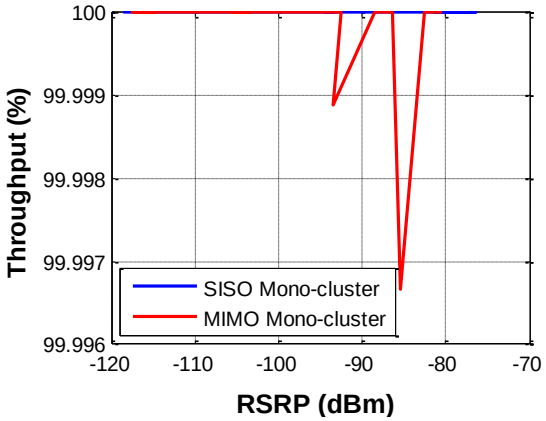

Figure 53.b: Comparison of SISO and MIMO Throughput (%) versus RSRP in mono-cluster channel *(Mobile5)*

Comparison of values in table 18 shows that the Mobile1 has better performance in terms of sensitivity in the case of single cluster channel. The sensitivity of each mobile in SISO and MIMO modes (mono cluster channel) is very close with a maximum deviation of 3 dB for the tablet and 1 dB for other mobiles. In the case of the Mobile1, the sensitivity in mono cluster channel is better than multi-cluster case. However, these values are consistent with the sensitivity value given in [3GPP TS 36521-1, Section 7].

		Mono -cluster		Urban Micro		Urban Macro	
		SISO	MIMO	SISO	MIMO	SISO	MIMO
Mobile1	RSRP	-124	-125	-109,21	-117	-112,48	-115,44
	RSSI	-95.25	-96.24	-71.24	-75.25	-82.98	-85.25
Mobile2	RSRP	-120	-119,47	-119	-113	-117	-116,65
	RSSI	-87.2	-86.24	-85.24	-81.24	-82.24	-86.24
Mobile3	RSRP	-119	-121				
	RSSI	-84.24	-91.24				
Mobile4	RSRP	-119	-118				
	RSSI	-83.24	-87.24				
Mobile5	RSRP	-114	-115				
	RSSI	-78.24	-80.24				

Table 17: Sensitivities of the different 4G mobiles

The comparison of values presented in table 17 shows, an identical result of measured sensitivities for MIMO and SISO mode in mono cluster case. This is due to the use of diversity combining, when the base station is configured in SISO mode. Another observation that can be made is the degradation of the sensitivity that is logical, when the channel delay spread is most important.

➔ **Sensitivity measurements results: comparison with TIS measurement performed in anechoic chamber**

In the following, a measurement of TIS in anechoic chamber equipped with SATIMO SG24 system for mono cluster case is made in order to compare it with the TIS measurement carried out in reverberation chamber (table17).

The SATIMO SG24 system illustrated in figure III.54 is an effective device capable of performing passive and active measurements to evaluate the performance of mobile communication terminals under test. This system is installed in an anechoic chamber of 4 meters wide, 4 meters long and 4 meters in height. The probes of the system are uniformly distributed every 15 degrees on a circular arc with a diameter of 2.4 meters.

Each probe allows measuring the electromagnetic field for both vertical and horizontal polarizations. This system allows making 3D measurements using a CMW500 wideband communication tester.

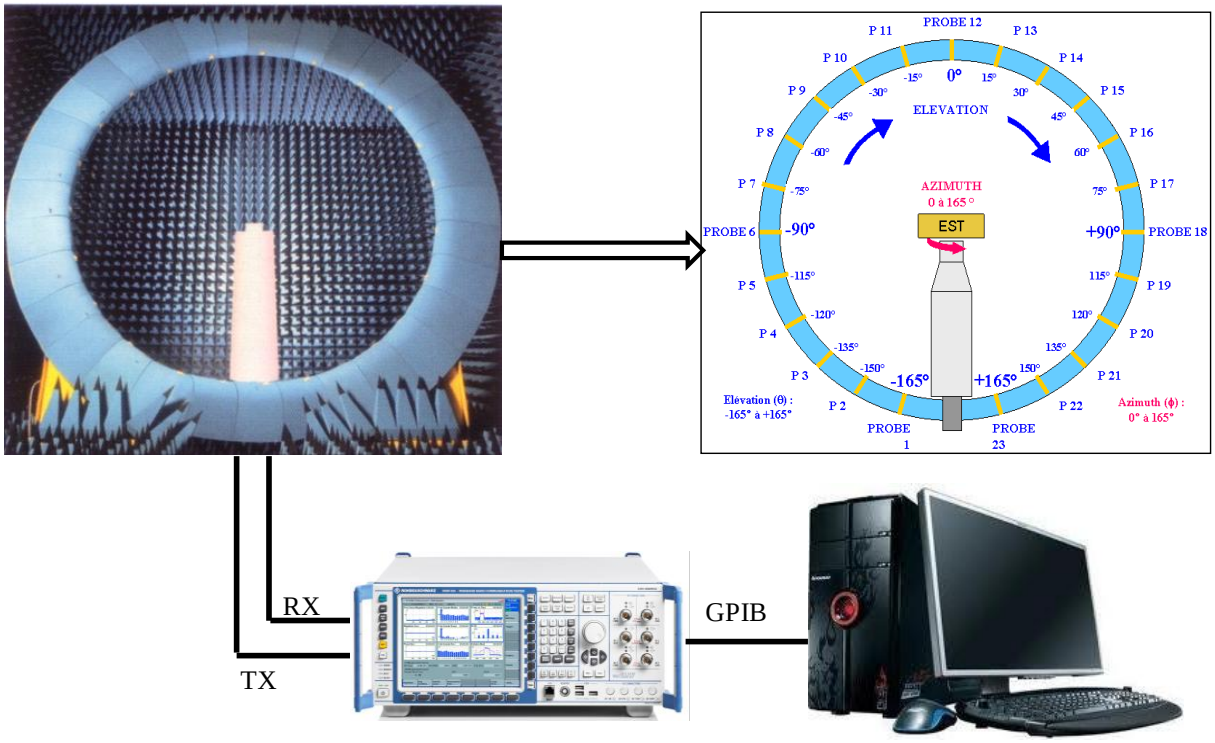

Figure III.54: 3D measurement test bed

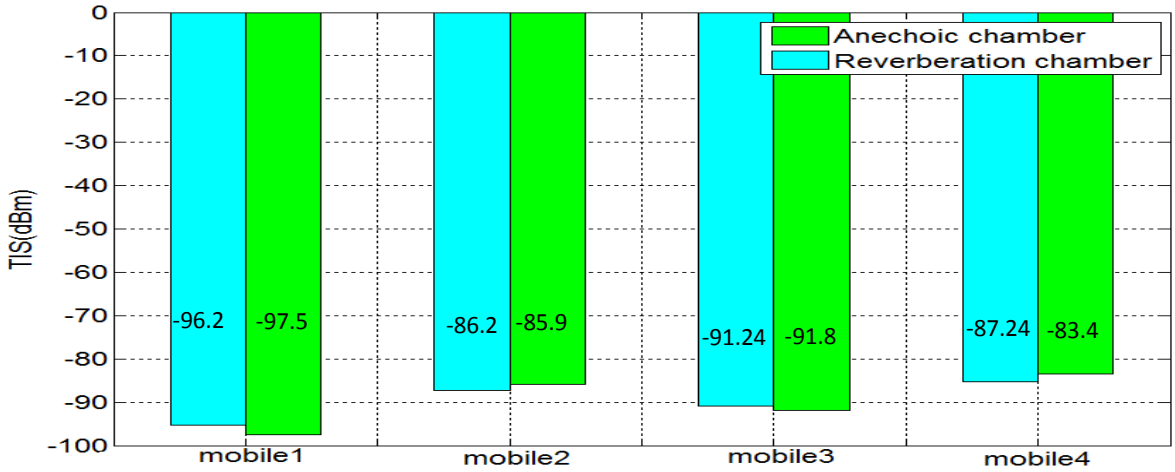

Figure III.55: comparison between measurements performed in RC chamber and AC for mono cluster case

The figure above shows that in mono cluster channel, the obtained results are similar. But this is not always the case. In fact, the received power varies in MSRC with stirring (fading phenomenon), so the TIS are calculated for an average received power. This is not the case in anechoic chamber (since received power stay constant). Here the antenna diversity and frequency diversity on the mobile make this power variation smoothed; so logically for a terminal with single antenna/single carrier we would have certainly a less good TIS due to the fading.

4. Conclusion

In the beginning of this work, the dependence of a 1x2 SIMO antenna diversity system on the RMS delay spread of a multi-path channel inside an RC has been studied. The results presented in this contribution demonstrate that the effective diversity gain (EDG) is in inverse variation to the channel RMS delay spread of the channel. This delay spread is varied by introducing different amounts of absorbing material inside the MSRC.
The presented work helps to understand the channel characteristics under which the active multi-antenna measurements have been performed in the RC.

Experiments presented in (IV.2) allowed us to perform a complete statistical characterization of the radio channel in the MSRC. From the data collected we were able to evaluate the cumulative density function and the correlation coefficient. We have shown that two illumination antennas (SISO case) or 4 illumination antennas (MIMO case) are required to obtain an isotropic environment Rayleigh within the MSRC. The same results are observed in the presence or absence of the mobile, stirrers in step by step mode or continuous mode (which minimizes the measurement time). For MIMO-LTE terminals measurements, configuration 2 with two illumination antennas (horn illuminating the horizontal stirrer and UWB dipole illuminating the vertical stirrer) will be useful for the SISO mode and the configuration with four illumination antennas will be useful for MIMO mode.

Concerning the last part of this chapter, a first measurement of MIMO-LTE total isotropic sensitivity (TIS) inside reverberation chamber for multi clusters channels is performed. A rapid measurement method (5 minutes for a fixed transmitted power, compare to 5 hours in step by step mode) based on continuous stirring that aims to measure sensitivity of MIMO-LTE terminal has been proposed . A comparison between TIS measurements in RC and in AC is made, but still not generalized due to the fading. This work is of particular interest for OTA characterization of MIMO-LTE terminals in MSRC, because it allows the implementation of a measurement platform that can assess the terminals sensitivity while respecting parameters defined by the 3GPP standard.

References

[1] Verdone, Roberto; Zanella, Alberto (Eds.), " Pervasive Mobile and Ambient Wireless Communications", COST Action 2100 Series: Signals and Communication Technology; ISBN 978-1-4471-2315-6.

[2] 3GPP TR 37.976, "Measurement of radiated performance for MIMO and multi-antenna reception for HSPA and LTE terminals (Release 10)", version 1.1.0.3GPP TR 37.976, "Measurement of radiated performance for MIMO and multi-antenna reception for HSPA and LTE terminals (Release 10)," version 1.1.0, May 2010.

[3] Sanchez-Heredia, J.D. ; Valenzuela-Valdes, J.F. ;Martinez-Gonzalez, A.M. ; Sanchez-Hernandez, D.A., "Emulation of MIMO Rician- Fading Environments With Mode-Stirred Reverberation Chambers", Antennas and Propagation, IEEE Transactions on Volume: 59 , Issue: 2, Publication Year: 2011 , Page(s): 654 – 660.

[4] Kildal, P.-S. ,"Overview of 6 Years o R&D on Characterizing Wireless Devices in Rayleigh Fading Using Reverberation Chambers", in International Workshop on Antenna Technology: Small and Smart Antennas Metamaterials and Applications, 2007. IWAT '07. Page(s): 162 – 165

[5] C. Orlenius, P.-S. Kildal, and G. Poilasne, "Measurement of total isotropic sensitivity and average fading sensitivity of CDMA phones in reverberation chamber," in Proc. IEEE AP-S Int. Symp., Washington, DC, Jul. 2005, pp. 3–8.

[6] N. Serafimov, P.-S. Kildal, and T. Bolin, "Comparison between radiation efficiencies of phone antennas and radiated power of mobile phones measured in anechoic chambers and reverberation chamber," in Proc. IEEE AP-S Int. Symp., San Antonio, TX, Jun. 2002, vol. 2, pp. 478– 481.

[7] Moctar Mouhamadou, Charles A. Tounou, Cyril Decroze, David Carsenat and Thierry Monediere ", Active measurements of antenna diversity performances using a specific test-bed, in several environments", International Journal of RF and Microwave Computer-Aided Engineering, Volume 20, Issue 3, May 2010, Pages: 264–271,

[8] A. Belhouji, C. Decroze, D. Carsenat, M. Mouhamadou, and T. Monediere, " Active measurements of a MIMO WiMAX- OFDM based system in reverberation chambers," Microwave and Optical Technology Letters, vol. 52, no. 10, pp. 2347–2352,2010.

[9] Xiaoming Chen ; Kildal, P.-S. ; Orlenius, C. ; Carlsson, J., "Channel Sounding of Loaded Reverberation Chamberfor Over-the-
Air Testing of Wireless Devices:Coherence Bandwidth Versus Average ModeBandwidth and Delay Spread", Antennas and Wireless Propagation Letters,IEEE Volume: 8, Publication Year: 2009 , Page(s): 678 - 681

[10] Holloway, C.L. ; Hill, D.A. ; Ladbury, J.M. ; Koepke, G., "Requirements for an effective reverberation chamber: unloaded or loaded", Electromagnetic Compatibility, IEEE Transactions on Volume: 48 , Issue: 1, Publication Year: 2006 , Page(s): 187 - 194

[11] Garcia-Fernandez, M.A. ; Arsalane, N. ; Mouhamadou, M. ;Carsenat, D. ; Decroze, C. ; Monediere, T. , " Analysis of antenna diversity performance dependence on multi-antenna

channel delay spreadin reverberation chamber", 6th European Conference on Antennas and Propagation (EUCAP), 2012, Page(s): 456 - 459

[12] Genender, E. ; Holloway, C.L. ; Remley, K.A. ; Ladbury, J.M. ;Koepke, G. ; Garbe, H., "Simulating the Multipath Channel With a Reverberation Chamber: Application To Bit Error Rate Measurements", IEEE Transactions On Electromagnetic Compatibility, Volume: 52 , Issue: 4 , 2010 , Page(s): 766 - 777

[13] ETS-Lindgren's, SMART 1000 Mini-Reverb Cell," http:// www.ets-lindgren.com/pdf/smart1000.pdf.

[14] M. Mouhamadou, Contribution au développement et à l'optimisation d'un démonstrateur d'antennes adaptatives, applications à un système de communications sans fil haut débit, Thèse de Doctorat, Université de Limoges, Septembre 2007

[15] A. Halder, A. Chatterjee, "Low-Cost Alternate EVM Test for Wireless Receiver System", Proceedings of the 23rd IEEE VLSI Test Symposium.

[16] G. Baudoin, Radio-communications Numériques/1, Principes, modélisation et simulation, Dunod, 2è edition, 2003.

[17] M. D. McKinley, K. A. Remley, M. Myslinski, J. S. Kenney, D. Schreurs, B.Nauwelaers, " EVM Calculation for Broadband Modulated Signals", 64th ARFTG Conf. Dig., Orlando, FL, pp. 45-52, Dec 2004.

[18] K. M. Gharaibeh, K. G. Gard, M. B. Steer, "Accurate Estimation of Digital Communication System Metrics- SNR, EVM and ρ in a Nonlinear Amplifier Environment",

[19] R. A. Shafik, M. S. Rahman, A. R. Islam, "On the Extended Relationships Among EVM, BER and SNR as Performance Metrics", 4th International Conference on Electrical and Computer Engineering, ICEC E 2006, 19-21 December 2006, Dhaka, Bangladesh

[20] K. Kagoshima, W. C. Y. Lee, K. Fujimoto, and T. Taga, "Essential Techniques in Mobile Antenna Systems Design," in Mobile Antenna Systems Handbook, 2nd ed., K. Fujimoto and J. R. James, Eds., Norwood, MA: Artech House, 2001, pp. 55-61.

[21] 3GPP TR 37.976, "Measurement of radiated performance for MIMO and multi-antenna reception for HSPA and LTE terminals (Release 10)," version 1.1.0, May 2010.

[22] V. Plicanic, "Antenna diversity studies and evaluation," M.S. thesis, Lund University, Lund, Sweden, May 2004.

[23] A. Paulraj, R. Nabar, and D. Gore, Introduction to Space-time Wireless Communication, Cambridge University Press, 2003.

[24] X. Chen, "Spatial Correlation and Ergodic Capacity of MIMO Channel in Reverberation Chamber," International Journal on Antennas and Propagation, 2011.

[25] O. Delangre, P. De Doncker, M. Lienard, and P. Degauque, "Delay spread and coherence bandwidth in reverberation chamber," Electronics Letters, vol. 44, no.5, pp. 328-329, Feb. 28 2008.

[26] X. Chen, P.S. Kildal, C. Orlenius, J. carlsson, "Channel sounding of loaded reverberation chamber for the over the air testing of wireless devices: coherence bandwidth versus average mode bandwidth and delay spread," Antennas and wireless Propagation Letters, IEEE, vol. 8, pp. 678-681.2009.

[27] M. Koubeissi, M. Mouhamadou, C. Decroze, D. Carsenat, and T. Monédière, "Triband Compact Antenna forMultistandard Terminals and User's Hand Effect," International Journal of Antennas and Propagation, pp. 1-7, Dec. 7 2009.

[28] M. Mouhamadou, C. A. Tounou, C. Decroze, D. Carsenat, and T. Monediere, "Active Measurements of Antenna Diversity Performances Using a Specific Test-Bed, in Several Environments," International Journal of RF and Microwave Computer-Aided Engineering, pp. 264-271, Nov. 23 2009.

[29] S. A. Chakra, "La Boucle Locale Radio et la Démodulation Directe de signaux larges bandes à 26GHz", Thèse de Doctorat, Télécom Paris, ENST, P.44.

[30] O. Akhdar, Conception d'une méthode de déconvolution pour l'estimation des angles d'arrivée sur une antenne. Application au sondage spatio-temporel du canal de propagation, Thèse de Doctorat, Université de Limoges, Octobre 2009.

[31] E. Genender, C.L. Holloway, K.A. Rembey, J.M Ladbury, G. Koepke, H. Garbe, "Simulating the multipath channel with a reverberation chamber: application to bit error rate measuremants," IEEE Transactions on Electromagnetique compatibility, vol. 52, pp. 766-777, 2010.

[32] H. Arslan, T. Yucek, "Delay spread estimation for wireless communication systems," The 8th IEEE Symposium on Computers and Communications (ISCC'2003), pp. 282-287, vol. 1, 2003.

[33] D. A. Hill, M. T. Ma, A. R. Ondrejka, B. F. Riddle, M. L. Crawford, and R. T. Johnk, "Aperture excitation of electrically large, lossy cavities," IEEE Transactions on Electromagnetic Compatibility, vol. 36, no. 3, pp. 169–178, 1994.

[34] X. Chen, P. S. Kildal, C. Orlenius, and J. Carlsson, "Channel sounding of loaded reverberation chamber for over-the-air testing of wireless devices: coherence bandwidth versus average mode bandwidth and delay spread," IEEE Antennas and Wireless Propagation Letters, vol. 8, Article ID 5072260, pp. 678–681, 2009.

[35] 3GPP TS 36.101, Evolved Universal Terrestrial Radio Access (E.UTRA); User Equipment (UE) radio transmission and reception (Release 9), version9.3.0, Mars 2010.

[36] 3GPP TR 37.976, Measurement of radiated performance for MIMO and multi-antenna reception for HSPA and LTE terminals (Release 10), version 1.1.0, May 2010.

[37] A. Diallo, C. Luxey, P. L. Thuc, R. Straj, and G. Kossiavas, "Diversity performance of multiantenna systems for UMTS cellular phones in different propagation environments," International Journal of Antennas and Propagation, vol. 2008, Article ID 836050, 10 pages, 2008.

[38] A. Pascual-Iserte, L. M. Ventura, and X. Nieto, "Residual carrier frequency offset estimation and correction in OFDM MIMO systems," in Proceedings of the 18th Annual IEEE International Symposium on Personal, Indoor and Mobile Radio Communications (PIMRC'07), pp. 1–5, Athens, Greece, September 2007.

[39] S. Blanch, J. Romeu, and I. Corbella, "Exact representation of antenna system diversity performance from input parameter description," Electronics Letters, vol. 39, no. 9, pp. 705 707, 2003.

[40] M. B. Knudsen and G. F. Pedersen, "Spherical outdoor to indoor power spectrum model at the mobile terminal," IEEE Journal on Selected Areas in Communications, vol. 20, no. 6, pp. 1156–1169, 2002.

[41] T. Bolin, A. Derneryd, G. Kristensson, V. Plicanic, and Z. Ying, "Two-antenna receive diversity performance in indoor environment," Electronics Letters, vol. 41, no. 22, pp. 1205–1206, 2005.

[42] R. G. Vaughan and J. B. Andersen, "Antenna diversity in mobile communication," IEEE Transactions on Vehicular Technology, vol. 36, no. 4, pp. 149–172, 1987.

[43] effective diversity gain and how to measure it in a reverberation chamber," Microwave and Optical Technology Letters, vol. 34, no. 1, pp. 56–59, 2002.

[44] T. Taga, "Analysis for mean effective gain of mobile antennas in land mobile radio environments," IEEE Transactions on Vehicular Technology, vol. 39, no. 2, pp. 117–131, 1990.

[45] A. Belhouji, C. Decroze, D. Carsenat, M. Mouhamadou, and T. Monediere, "Active measurements of a MIMO WiMAX OFDM based system in reverberation chambers," Microwave and Optical Technology Letters, vol. 52, no. 10, pp. 2347–2352, 2010.

[46] J. D. Sanchez-Heredia, J. F. Valenzuela-Vald`es, A.M.Martinez Gonzalez, and D. A. Sanchez-Hernandez, "Emulation of MIMO rician fading environments with mode-stirred reverberation chambers," IEEE Transactions on Antennas and Propagation, vol. 59, no. 2, pp. 654–660, 2011.

[47] http://www.ecanechoicchambers.com/.

[48] J. C. Lin and C. Y. Lin, "Noncoherent sequential PN code acquisition using sliding correlation in DS/SS," in Proceedings of the IEEE International Conference on Communications (ICC'00), vol. 1, pp. 341–345, New Orleans, La , USA, June 2000.

[49] M. Mouhamadou, M. Koubeissi, C. Tounou et al., "Multiband diversity antenna performances evaluation for multistandard compact wireless terminal," in Proceedings of the

3rd European Conference on Antennas and Propagation (EuCAP ’09), Berlin, Germany, March 2009.

[50] M. Mouhamadou, M. Koubeissi, C. Tounou et al., “Multiband diversity antenna performances evaluation for multistandard compact wireless terminal,” in Proceedings of the 3rd European Conference on Antennas and Propagation (EuCAP’09), Berlin, Germany, March 2009.

[51] R. A. Shafi, S. Rahman, and A. H. M. Razibul, “On the extended relationships among EVM, BER and SNR as performance metrics,” in Proceedings of the International Conference on Electrical and computer Engineering (ICECE ’06), Dhaka, Bangladesh, December 2006.

General Conclusions

The work presented in this thesis focused on the study and implementation of an analytical method to control the temporal spread of a channel emulated inside a reverberation chamber. And on experimental characterization for wireless communication system.

This first chapter provides an introduction to MIMO OTA standardization, and describes the different test methodologies under consideration by 3GPP/CTIA. Many different MIMO OTA test methods have been proposed, which vary widely in their propagation channel characteristics, size, and cost. In this chapter, it has been shown that the test methodology adopted in this thesis is the MIMO OTA test methodology based on MSRC. This choice is made for several reasons: the ability to emulate a variety of fading scenarios and the cost effectiveness.

This chapter have shown that the measurement methodologies based on MSRC are classified in two types of measurements. The first type is the passive measurement and the second is the active measurement. Regarding active measurements, two aspects will be distinguished not real-time active measurements, and real-time active measurements.

In the MSRC, the emulation of a channel model encounters two major problems: the first is the control of the delay spread and the second is the control of the spatial parameters. For the second, it can be solved by the emulation of an isotropic environment.

Our first contribution to us in this thesis is manifested in the implementation of a method able to control the delay spread of an emulated channel in the MSRC.
The channel delay spread is strongly linked to the quality factor of the chamber. The first to explore is to control this parameter experimentally, but this solution will be costly in terms of time. A second solution that will make the goal of the second chapter is to control this parameter analytically. This means to develop an analytical model allowing the estimation of the channel delay spread value.

The second chapter was dedicated to study the possibility of setting up an analytical Matlab© simulator able to estimate the value of the channel RMS delay spread in a reverberant room. The novelty brought by this simulator is that it was based on a circuit approach and takes in account the antenna, the stirrer, and losses effects.

The description of the circuit approach that has allowed the development of this simulator has been made. The challenge of this method was to calculate the coupling between the antenna and the mode excited in the metal cavity. For this reason a calculation method using the theorem of reciprocity and equivalence theorem has been developed.

The validation of the results obtained from Matlab simulator with CST simulations and measurements, has shown the performance of the developed simulator. The obtained results remain satisfactory.

The analytical simulator developed with Matlab allows having an idea about the average value of the RMS delay spread versus losses. The knowledge of this value will optimize the measurements campaigns time. And subsequently estimate the amount of losses to be introduced inside MSRC in order to obtain the desired channel RMS delay spread value.

In the beginning of this third chapter, the dependence of a 1x2 SIMO antenna diversity system on the RMS delay spread of a multi-path channel inside an RC has been studied. The results presented in this contribution demonstrate that the effective diversity gain (EDG) is in inverse variation to the channel RMS delay spread of the channel. This delay spread is varied by introducing different amounts of absorbing material inside the MSRC.
The presented work helps to understand the channel characteristics under which the active multi-antenna measurements have been performed in the RC.
Experiments presented in (III.2) allowed us to perform a complete statistical characterization of the radio channel in the MSRC. From the data collected we were able to evaluate the cumulative density function and the correlation coefficient. We have shown that two illumination antennas (SISO case) or 4 illumination antennas (MIMO case) are required to obtain an isotropic environment Rayleigh within the MSRC. The same results are observed in the presence or absence of the mobile, stirrers in step by step mode or continuous mode (which minimizes the measurement time). For MIMO-LTE terminals measurements, configuration 2 with two illumination antennas (horn illuminating the horizontal stirrer and UWB dipole illuminating the vertical stirrer) will be useful for the SISO mode and the configuration with four illumination antennas will be useful for MIMO mode. Concerning the last part of this chapter, a first measurement of MIMO-LTE total isotropic sensitivity (TIS) inside reverberation chamber for multi clusters channels is performed. A rapid measurement method (5 minutes for a fixed transmitted power, compare to 5 hours in step by step mode) based on continuous stirring that aims to measure sensitivity of MIMO-LTE terminal has been

proposed . A comparison between TIS measurements in RC and in AC is made, but still not generalized due to the fading. This work is of particular interest for OTA characterization of MIMO-LTE terminals in MSRC, because it allows the implementation of a measurement platform that can assess the terminals sensitivity while respecting parameters defined by the 3GPP standard.

Perspectives

- Active characterization of MIMO system in controlled channel (space/time).
- Management of angles of arrivals by using the inverse time principle.
- A new definition of TIS in MSRC linked to the standard deviation of RSRP variation will be investigated.

Appendix I: Electromagnetic analysis of MSRC

1. Modal representation of the electric field

Let us consider a perfectly conducting parallelepiped cavity, if we insert source inside the cavity, electric and magnetic fields that satisfy the Maxwell equations are established. Electric and magnetic fields meet the Maxwell's equations and boundary conditions of the cavity. These conditions require that the tangential components of the electric field and the normal component of the magnetic field are equal to zero on the walls. The unique solutions of Maxwell's equations satisfying the boundary conditions are called cavity modes.

If an object is inserted into the cavity, the boundary conditions are changed and a new spatial redistribution of electric and magnetic fields can be calculated. If we move the object, the electric and magnetic fields at any point are changed. Different realizations of these fields are obtained. It's then a reverberation chamber, which means a cavity where the field distribution can be changed easily and repeatedly.

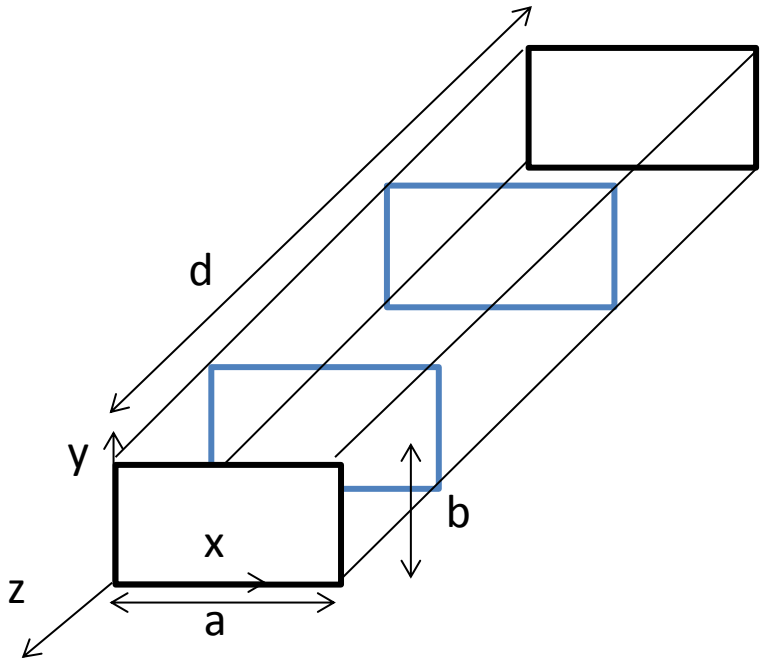

Figure AI.1: Rectangular wave guide

Let us look first at the case of a perfectly conducting cavity to present the theory of reverberation chambers.

To determine the electric and magnetic fields in closed rectangular cavity, we consider this cavity as a waveguide with a rectangular section oriented to z that should have shorted both ends with perfectly conducting walls (see figure AI.1). Modes of waveguide with rectangular section are classified into types, TEnm (transverse electric) modes and TMnm (transverse magnetic) modes. These are characterized respectively by a lack of the z component of the electric field (TE) or the magnetic field (TM). For the case of the TE mode, the expressions of electric (E) field and magnetic (H) field are given by [chapter I.32]:

$$E_x(x,y,z) = \frac{j\omega\mu k_y}{k_{c_{n,m}}^2} A\cos(k_x x)\sin(k_y y)e^{-j\beta_{nm}z} \qquad (A1.1)$$

$$E_y(x,y,z) = -\frac{j\omega\mu k_z}{k_{c_{n,m}}^2} A\sin(k_x x)\cos(k_y y)e^{-j\beta_{nm}z} \qquad (A1.2)$$

$$H_x(x,y,z) = \frac{j\beta_{nm}}{k_{c_{n,m}}^2} A\sin(k_x x)\cos(k_y y)e^{-j\beta_{nm}z} \qquad (A1.3)$$

$$H_y(x,y,z) = \frac{j\beta_{nm}}{k_{c_{n,m}}^2} A\cos(k_x x)\sin(k_y y)e^{-j\beta_{nm}z} \qquad (A1.4)$$

$$H_z(x,y,z) = A\cos(k_x x)\sin(k_y y)e^{-j\beta_{nm}z} \qquad (A1.5)$$

Where A is a constant, ω [rad.s^{-1}] is the pulsation, μ [H.m^{-1}] permeability of the propagation environment, and

$$k_x = \frac{n\pi}{a} \qquad n = 0,1,2,.... \qquad (A1.6)$$

$$k_y = \frac{m\pi}{b} \qquad m = 0,1,2,.... \qquad (A1.7)$$

$$k_{c_{nm}}^2 = \left(\frac{n\pi}{a}\right)^2 + \left(\frac{m\pi}{b}\right)^2 \qquad (A1.8)$$

$$\beta_{nm} = \sqrt{\omega^2\mu\varepsilon - \left(\frac{n\pi}{a}\right)^2 - \left(\frac{m\pi}{b}\right)^2} \qquad (A1.9)$$

Where a and b are respectively the dimensions along the x and y axis, ε [F.m^{-1}] is the permittivity of the propagation environment and m and n are not simultaneously zero. Modes in the wave guides propagate if their cutoff frequency is less than the operating frequency. Consider that TE10 (n=1, m=0) and close the waveguide at its two ends. Hz component can be written as superposition of two modes propagating in opposite directions (following the reflections on the walls closing the guide).

$$H_z(x,y,z) = A^{+}\cos(k_x x)e^{-j\beta_{10}z} + A^{-}\cos(k_x x)e^{+j\beta_{10}z} \qquad (A1.10)$$

By applying the boundary conditions, Hz must be zero at z=0 and z=d (where d is the dimension of the cavity in the z direction), using the following conditions (Hz =0 for z=0; and Hz =0 for z=d) we obtain $A^{+}= A^{-}$, therefore it can be written:

$$H_z(x,y,z=d) = A^{+}\cos(k_x x).(e^{-j\beta_{10}d} - e^{+j\beta_{10}d}) = 0 \qquad (A1.11)$$

The nontrivial solution of this equation is $\beta_{10}d=p\pi$, for p=1, 2, 3…; the result for p=1:

$$H_z = H_0\cos(k_x x).\sin\left(\frac{\pi z}{d}\right) \qquad (A1.12)$$

Where $H_0=-2jA^{+}$ is a new constant. Within a cavity, there are three parameters defining parameters: m, n, p. using previous equations, we obtain the other components of the field. The mode TE_{101} is given by:

$$H_x(x,y,z) = -\frac{a}{d}H_0\sin(k_x x).\cos(k_z z) \qquad (A1.13)$$

$$E_y(x,y,z) = -\frac{j\omega\mu a}{\pi}A\sin(k_x x)\sin(k_z z) \qquad (A1.14)$$

Where $k_z = \frac{p\pi}{d}$. Generally, there is a discrete infinity of modes satisfying Maxwell's equations and respecting the boundary conditions of the cavity. These modes exist at a specific frequency which explains the appellation of "resonant cavity". The resonance frequency of a mode is given by:

$$f_{c_{nmp}} = \frac{c}{2\pi}\sqrt{\left(\frac{n\pi}{a}\right)^2 + \left(\frac{m\pi}{b}\right)^2 + \left(\frac{p\pi}{d}\right)^2} \qquad (A1.15)$$

Finally, the density of modes D_n [modes/Hz], that means the number of modes present per Hz, is given by [33]:

$$D_n = \frac{8\pi abdf^2}{c^3} \qquad (A1.17)$$

And the total number of modes in a frequency band Δf is given by:

$$N_n \approx \frac{8\pi V f^2}{c^3}\Delta f \qquad (A1.18)$$

2. Stochastic modeling of the reverberation chamber

The quality factor is defined by [chapter I.34]:

$$Q = \omega \frac{U_s}{P_d} \qquad (A1.19)$$

Where U_s [J] is the electromagnetic energy stored is the chamber, ω is pulsation and P_d is the dissipated power. In steady state, the energy stored by the reverberation chamber is given by the integral of the energy density, w [$J.m^{-3}$] over the cavity volume, V [m^3]:

$$U_s = \int_v w dV \qquad (A1.20)$$

$$= \bar{w} V \qquad (A1.21)$$

And $\bar{w}$ is the spatially averaged power density, defined as

$$\bar{w} = \frac{1}{V}\int w dV \qquad (A1.22)$$

Through the assumption of ergodicity, this spatial average is equivalent to an average over all realizations (positions of mechanical stirrers), w=<w>. The most specific aspect of reverberation chambers appears here clearly since the energy density <w>is an average over all achievements of the channel. Finally, note that the average density of power flow $\langle S_c \rangle$ [$W.m^{-2}$] is given by:

$$\langle S_c \rangle = c \langle w \rangle \qquad (A1.23)$$

Where c is the speed of light.

To calculate the quality factor of a reverberation chamber, the mechanisms of power dissipation must be identified. There are four mechanisms [chapter I.33]: the power dissipated in the walls, in the objects in the chamber, in the load impedance of the receiving antenna, and the power loss optionally present in the apertures. The total power dissipated is the sum of the powers dissipated by each mechanism. Each mechanism of power dissipation can be associated to one quality factor Q_i and the global Q factor is given by [chapter I.34]:

$$Q^{-1} = Q_1^{-1} + Q_2^{-1} + Q_3^{-1} + Q_4^{-1} \qquad (A1.24)$$

Where Q_1, Q_2, Q_3, Q_4 are respectively the Q factors associated to each of the four mechanisms described above. The smallest Q_i factor, that means, the dominant mechanism in term of dissipation of power, will be the dominant value in the calculation of the global Q factor.

In most cases, the power dissipation due to the finite conductivity of walls is the dominant factor. In order to calculate the Q factor resulting from this loss power, we need to evaluate (A1.18), knowing that the dissipated power P_d, is the power dissipated in the walls. The stored energy U_s is the sum of the electric and magnetic energy. In one chamber, the electric and magnetic energy are equal [chapter I.35] and it can be write:

$$U_s = 2U_m \qquad (A1.25)$$

Where U_m is the magnetic energy. Therefore (I.18) is written

$$Q = \omega \frac{2U_m}{P_{wall}} \qquad (A1.26)$$

Where P_{wall} is the power dissipated by conduction in the walls. This power dissipation is due to the currents induced in the walls. Developing the calculation of magnetic energy and the power dissipated in the walls, we have [35]:

$$Q = 2\pi f \frac{2\frac{\mu}{4}\int_V \left|\vec{H}\right|^2 dV}{\frac{R_s}{2}\int_S \left|\vec{H}_t\right|^2 dS} \approx \frac{2V}{\delta S} \qquad (A1.27)$$

Where R_s is the surface resistance, H_t is the magnetic field tangent to the wall and δ is the skin depth. The integral in the numerator is proportional to volume although the exact value depends on mode type and the chamber size. Similarly, the integral in denominator is proportional to the surface walls.

This value of Q factor takes into account only the conduction losses in walls. An experimental method incorporating all the dissipation mechanisms, easy to use is introduced in the next section.

Appendix II: Reminders on digital communication systems

The general block diagram of a digital communication channel is shown in figure AII.1. According to this figure, before it was transmitted, the signal source is modulated. The modulation technique is to adjust the signal, typically in baseband, in propagation channel. It is an operation which consists in transmitting a modulated signal through an analog signal called carrier signal.

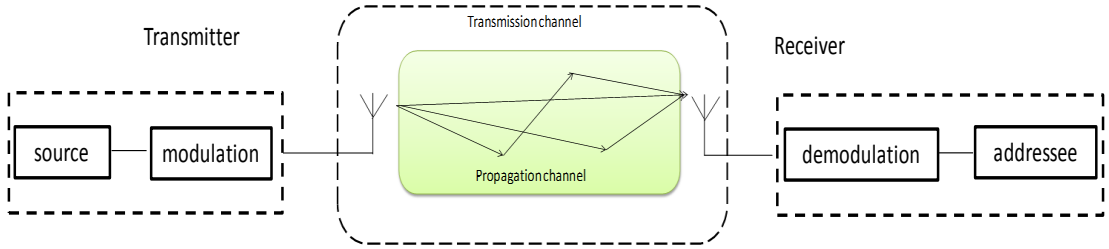

Figure AII.1: General block diagram of a digital transmission chain

The carrier is an electromagnetic wave that can be written in complex form:

$$S(t) = A \cdot \exp\left[j \cdot \left(\omega t + \phi_p \right) \right] = A \cdot \exp\left[j \cdot \left(2\pi F t + \phi_p \right) \right] \qquad (A2.1)$$

Or in a sinusoidal shape:

$$S(t) = A \cdot \cos\left(\omega t + \phi_p \right) = A \cdot \cos\left(2\pi F t + \phi_p \right) \qquad (A2.2)$$

With A the amplitude, ω the carrier pulsation and F is the frequency, ϕ_p is the phase at time origin.

Based on the equation (AIII.1), the modulated wave is equal to:

$$S_{Mod}(t) = A(t) \cdot \exp\left[j \cdot \left(\omega t + \phi_p + \phi_t \right) \right] = A(t) \cdot \exp\left[j \cdot \left(2\pi F t + \phi_p + \phi_t \right) \right] \qquad (A2.3)$$

At the reception, the process is reversed. The signal is first demodulated before being received by the receiver, the demodulation process being the inverse of the modulation.

1. Bit error probability, the probability of symbol error and frame error probability

In digital communications, the signal to be transmitted is presented in the form of data frames whose the total number is denoted N_T. Each frame is composed of o total number of symbols (Ns) and each symbol from k bits. The total bits per frame is Nb=kNs.

We denote by:

- Bit error rate (BER), is the ratio between the number of erroneous bits (nb_error) and the total number of transmitted bits (Nb), or:

$$TEB = \frac{nb\_error}{N_b} \qquad (A2.4)$$

- Symbol error rate (SER), is the ratio between the number of erroneous symbols (ns_error) and the total number of transmitted symbols (Ns):

$$SER = \frac{ns\_error}{N_s} \qquad (A2.5)$$

- Frame error rate (FER), is the ratio of erroneous frames (nt_error) to the total number of frames sent (N_T)

$$FER = \frac{nt\_error}{N_T} \qquad (A2.6)$$

These parameters added to the classical parameters (correlation coefficients, mean SNR, effective diversity gain) enable a more complete assessment of the antenna diversity.

2. Signal to noise ratio measurement

The signal to noise ratio (SNR) is a parameter of great importance for the study of digital communications and diversity. There are several channel estimation techniques, including the method of moments, the method of estimation by maximum likelihood (ML) and the calculation of the EVM . The latter was chosen to be implemented on the measurements test bed.

A. EVM calculation

EVM (Error Vector Magnitude) is the representation of amplitude and phase distortions over the constellation diagram of states characteristics of a digital modulation.

Figure (AII.2) represents a portion of digital communication chain with the signals transmitted (reference signals: S) and the signals received (distorted signals: Z). The in-phase signal components of transmitted and received signal are given by S_I and Z_I respectively. Their components in quadrature phase are S_Q and Z_Q.

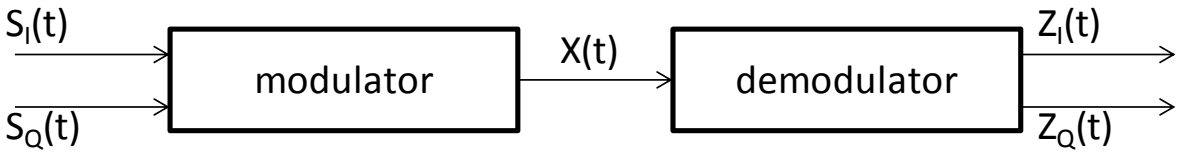

Figure AII.2: Representative scheme of the signals used for the calculation of the EVM

$S_I(k) = A(k) \cdot \cos(\phi_p + \phi_k)$, in-phase signal

$S_Q(k) = A(k) \cdot \sin(\phi_p + \phi_k)$, quadrature phase signal.

The signal at the output of the modulator is given:

$$X(t) = S_I(t)\cos(\omega t) - S_Q(t)\sin(\omega t) \qquad (A2.7)$$

The complex signals transmitted S (k) and received Z (k) are given by the equations:

$$\begin{cases} S(k) = S_I(k) + jS_q(k) \\ Z(k) = Z_I(k) + jZ_q(k) \end{cases} \qquad (A2.8)$$

In a polar diagram, the in-phase and quadrature phase signal components has a constellation shown in Figure (AII.3). This figure shows two consecutive constellations S (k) and S (k +1).

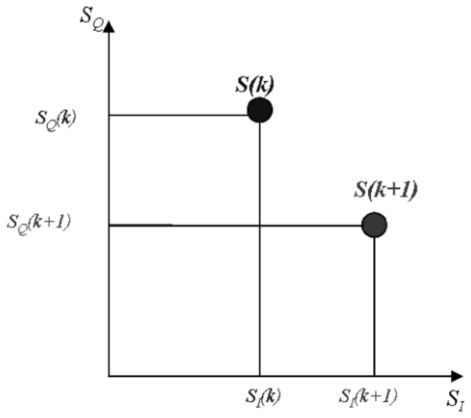

Figure AII.3: Signals constellation S*(k)* et *S(k+1)*

The received signal vector Noted Z (k) may be different from the transmitted vector S(k) due to interactions with the propagation channel, noise measuring instruments and the frequency difference associated with the transmitter local oscillators and receiver. Figure (AII.4) shows a case where the transmitted signal is different from the received signal.

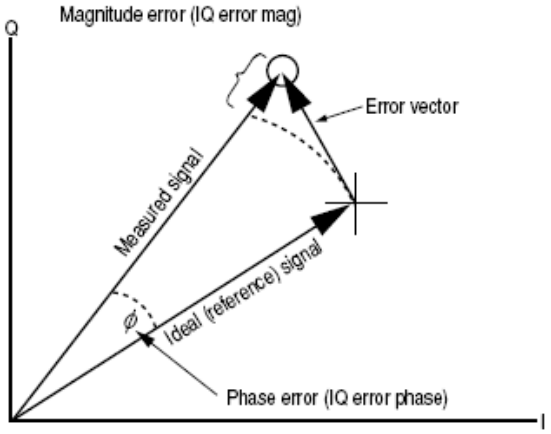

Figure AII.4: Constellation of transmitted and received symbols and the error between them.

The difference between the transmitted signal vector (ideal symbol or reference) and the received signal vector (distorted symbol) is the error vector. For one symbol, the EVM of the received signal is the modulus of the vector error. If, however, several Ns symbols are generated, the EVM is given as follows

$$EVM(rms) = \left[\frac{\frac{1}{N_s}\sum_{k=1}^{N_s} \left| Z(k) - S(k) \right|^2}{\frac{1}{N_s}\sum_{k=1}^{N_s} \left| S(k) \right|^2} \right]^{1/2} \qquad (A2.9)$$

B. Signal to noise ratio calculation

The effective diversity gain is calculated with the received SNR on the branches of diversity system and the reference system. It can also check the necessary condition for antenna diversity (difference of mean effective gain for example). It will be calculated from the EVM by the equation:

$$SNR_{dB} = 20 \cdot \log_{10}\left(\frac{1}{EVM}\right) \qquad (A2.10)$$

Publications in an international scientific review

Arsalane N., Mouhamadou M., Decroze C., Carsenat D., Garcia Fernandez M. A., Monédière T, "3GPP Channel Model Emulation with Analysis of MIMO-LTE Performances in Reverberation Chamber". International journal of antennas and Propagation (MIMO Over-The-Air Research, Development, and Testing special issue) Volume 2012 (2012), Article ID 239420 (2012) 8 pages.

Garcia Fernandez M. A., Decroze C., Carsenat D., **Arsalane N**., Andrieu G, "On the Relationship between Field Amplitude Distribution, Its Maxima Distribution, and Field Uniformity inside a Mode-Stirred Reverberation Chamber". International Journal of Antennas and Propagation 2012, ID 483287 (2012) 7 pages.

International communications with acts of reading

Garcia Fernandez M. A., **Arsalane N**., Mouhamadou M., Carsenat D., Decroze C., Monédière T, "Analysis of antenna diversity performance dependence on multi-antenna channel delay spread in reverberation chamber". Antennas and Propagation (EUCAP), 2012 6th European Conference - EuCAP 2012: the 6th European Conference on Antennas and Propagation, Congress Centre in, Tchèque, République (2012).

Arsalane N., Mouhamadou M., Decroze C., Carsenat D., Liebus S, "Total isotropic sensitivitry (TIS) and throughput measurements for MIMO-LTE terminals on reverberant cell". IC 1004 - IC1004 - 7th MC Meeting and joint workshop with FP7 Greenets on University of technology Ilemenau, Allemagne (2013).

International communications without acts of reading

Sanchez D., **Arsalane N.,**Garcia Fernandez M. A., Mouhamadou M., Carsenat D., Decroze C. "Validation of 3GPP SCME channel models emulated in mode-stirred reverberation chambers", 3GPP TSG-RAN WG4 #63, Tchèque, République (2012).

Sanchez D., **Arsalane N.,** Garcia Fernandez M. A., Mouhamadou M., Carsenat D., Decroze C. "Validation of 3GPP SCME channel models emulated in mode-stirred reverberation chambers", CTIA Certification Program Working Group, Contribution, France (2012).

Thesis abstract

This thesis is part of the field of the characterization of wireless communication systems using antennas diversity. Indeed, such systems allow fighting against the signals fading, when the terminal is inside a strong multipath environment. The issue of such research is: to study the association of multiple antennas at transmitting and/or receiving sides to improve the link budget, and the capacity of wireless systems, (decrease of BER (Bit Error Rate), increase of throughput …). This thesis takes an interest to the electromagnetic aspect, and signal processing. In order to understand the involved phenomena, and to characterize the terminal performance, it should be placed in a controlled multipath propagation environment in time, and in space. This brings us to find measurement methodologies able to reproduce models of realistic propagation channels. As part of this thesis the method used is the reverberation chamber. In this thesis we are interested in the time aspect. Reverberation chamber (RC) is considered as a useful tool to emulate rich multipath environments. In this contribution, this device is employed to emulate multi clusters channel models (cluster is defined as a group of multipath), and evaluate performance of wireless communication systems. This evaluation is performed with real time and not-real time measurements. It remains to note that among the objectives set out in this PhD thesis is to obtain electromagnetic simulation model of the reverberation chamber based on circuit approach, in order to determine the channel transfer function versus losses quantities.

Résumé de thèse

Cette thèse s'inscrit dans le domaine de la caractérisation des systèmes de communication sans fil utilisant la diversité des antennes. En effet, ces systèmes permettent de lutter contre les évanouissements des signaux, lorsque le terminal est placé dans un environnement riche en multi-trajets. L'objectif d'une telle recherche est: d'étudier l'association de plusieurs antennes à l'émission et / ou la réception pour améliorer le bilan de liaison, et la capacité des systèmes sans fil, (diminution de BER (Bit Error Rate), augmentation de débit ...). Cette thèse s'intéresse à l'aspect électromagnétique et traitement du signal. Afin de comprendre les phénomènes mis en jeu, et de caractériser les performances du terminal, il doit être placé dans un environnement de propagation multi-trajets contrôlable dans le temps et dans l'espace.

Cela nous amène à trouver des méthodes de mesures capables de reproduire des modèles de canaux de propagation réalistes. Dans le cadre de cette thèse la méthode utilisée est la chambre réverbérante. Dans cette thèse, nous nous intéressons à l'aspect temporel. La chambre réverbérante (RC) est considérée comme un outil utile pour émuler des environnements riches en multi-trajets. Dans cette contribution, ce dispositif est utilisé pour émuler des modèles canaux multi-trajets, et évaluer la performance des systèmes de communication sans fil. Cette évaluation est effectuée avec des mesures en temps réel et non temps réel. Parmi les objectifs de cette thèse est d'obtenir un modèle de simulation électromagnétique de la chambre réverbérante basé sur une approche circuit, afin de déterminer la fonction de transfert de canal en fonction des pertes.